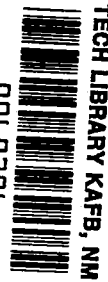# NASA CONTRACTOR REPORT

NASA CR-1519

N·A·S·A· CR-15

$c. 1$

AN APPLICATION OF THEORY TO AXIAL COMPRESSOR NOISE

by J. B. Ollerhead and C. L. Munch

Prepared by
WYLE LABORATORIES
Huntsville, Ala.
for Langley Research Center

NATIONAL AERONAUTICS AND SPACE ADMINISTRATION • WASHINGTON, D. C. • APRIL 1970

AN APPLICATION OF THEORY TO AXIAL COMPRESSOR NOISE

By J. B. Ollerhead and C. L. Munch

✓ *CCM 70*

Distribution of this report is provided in the interest of information exchange. Responsibility for the contents resides in the author or organization that prepared it.

add e:

Issued by Originator as Report WR 69-15

omit

Prepared under Contract No. NAS 1-8278 by

M. e. WYLE LABORATORIES
Huntsville, Ala.

for Langley Research Center

NATIONAL AERONAUTICS AND SPACE ADMINISTRATION

CONTENTS

TABLES

SYMBOLS

a	section lift curve slope
a_0	speed of sound
b	normal half distance between adjacent blade wake centerlines
c	mean blade chord
d	axial row separation
k	summation index, mode number
l	blade length
m	sound harmonic number
m	compressor mass flow
n	loading harmonic number
p	pressure
r	distance
t	time
u	axial flow velocity
u_c	centerline wake velocity defect
v	circumferential flow velocity
v	mean swirl component
w	velocity perturbation
x	tensor coordinate
y	source coordinate; wake ordinate

A	compressor annulus area
A_E	nozzle exit area
B	number of blades
C	sound harmonic amplitude
C_D	blade profile drag coefficient
C_L	list coefficient
C_Q	torque coefficient
C_T	thrust coefficient
D	drag force
DI	directivity index
F	aerodynamic in-plane forces
$J_g(z)$	Bessel function of order g and argument z
L	lift force
M	Mach number
P	power
PR	modal rotor or stator sound power
Q	mass source strength; torque
R	mean rotor blade radius
S	lift response function
T	thrust
T_{ij}	stress tensor
U	mean flow velocity

V	number of vanes, flow velocity
V_T	blade tip velocity
W	defined in equations (55) and (56)
Y	wake half-width
ΔP_T	total pressure rise
ΔP	static pressure rise
α	blade/vane angle
β	wake swirl angle
ϵ	phase angle
ζ	nondimensional flow velocity Fourier coefficient
η	wake velocity Fourier coefficient
θ	angle from fan axis to field point, blade pitch
λ	nondimensional swirl velocity
λ	wavelength
λ	nondimensional mean swirl
μ	nondimensional axial flow velocity
ν	nondimensional flow velocity
ν	nondimensional flow velocity (mean)
ρ	density fluctuation
σ	solidity (total blade area/ annulus area)
ϕ	inflow angle
ψ	rotational angle

ω	frequency
Ω	rotational speed

Subscripts:

m	harmonic number
0	zeroth harmonic
i,j	tensor notation
r	rotor
v̇	inlet guide vane
s	stator
o	outlet
i	inlet
E	nozzle exit conditions
b	blade
k	modal order
R	real part
I	imaginary part

ACKNOWLEDGEMENT

AN APPLICATION OF THEORY TO
AXIAL COMPRESSOR NOISE

By J.B. Ollerhead and C.L. Munch
Wyle Laboratories Research Staff
Payne Division, Rockville, Maryland 20852

SUMMARY

The theoretical solutions for the discrete frequency noise radiation by compressors and fans developed in a previous study are reviewed and programmed for computer solution. A method is developed to predict both steady and unsteady compressor airloads which generate the noise and which are required as input to the acoustic theory. Comparisons of theory and experiment show encouraging agreement, at least for the first harmonic noise and the potential of the method for design applications is demonstrated.

1.0 INTRODUCTION

As turbine powered aircraft increase in size, so too does the associated noise problem. Noise is rapidly becoming one of the major considerations in aircraft design and for this reason it is very desirable to have at hand methods by which the acoustic characteristics of a projected engine can be predicted from its design features. Unfortunately, accurate noise prediction methods do not yet exist despite the fact that the relative insensitivity of the hearing mechanism makes sound pressure level estimates with a one hundred percent error relatively accurate.

The noise of a turbine engine contains two major components, exhaust noise and rotating machinery noise, where the latter is generated by compressors, fans, and turbines[†]. Jet exhaust noise dramatically appeared as a social intruder with the introduction of commercial jet transport aircraft in the early fifties. Research into methods of reducing jet noise has continued at a steady pace since that time but following Lighthill's analytical explanations of the major observed features of jet noise, little has been accomplished in the way of theoretical advance. The main reasons for this without doubt lie in the great difficulties of specifying the turbulent properties of the exhaust flow.

[†] Throughout this report the terms "compressor" and "fan" tend to be used interchangeably since acoustically there is little difference between them.

In the days of the pure turbojet engine, compressor noise received little attention since, despite its characteristic whine, it was by no means objectionable when compared with the broadband sound of the high velocity exhaust. However, the introduction of by-pass flow engines, in which part of the total flow passes through secondary fan stages, with correspondingly lower exhaust velocities, shifted the emphasis to those harmonic components of the noise generated by the fans and compressors. Fan noise is particularly significant when the aircraft is on landing approach at fairly low altitudes and with the exhaust flow velocity relatively low.

In principle, fan noise, although at first sight somewhat more complicated than jet noise, should be easier to analyze. This is because all the features of the source, i.e., its geometry, motion and force inputs, should be specifiable with some accuracy. To show that this is indeed the case is the intention of this report. In a previous study (ref. 1) Lowson developed closed form solutions for various components of fan noise radiation. The results of this analysis yielded new insight into the acoustic effects of various design and operational parameters. A limited number of practical applications of the theory indicated its promising potential as a prediction technique, which was particularly interesting in view of the fact that until now it has been common practice to use entirely empirical methods for compressor noise estimation.

This report describes a subsequent study which has been made to further examine the accuracy of the theoretical results through comparisons with experimental data, both model and full scale. The results have been encouraging and suggest that the very complex noise generation process can be simulated by a relatively simple mathematical model. In the following sections the basic theory is reviewed with emphasis on the problem of practical application, aerodynamic input terms are developed, the accuracy of the analytical model is demonstrated through correlation with experiment and parameter studies are presented which illustrate how the theory can be utilized in a typical design application.

2.0 THEORY

2.1 Compressor Noise Generation

The present study is basically an application of Lowson's theoretical results to practical compressor and fan configurations. For the sake of completeness, however, a brief review of the analysis of reference 1 is included here. The development of the equations is followed in a simplified manner; for a rigorous treatment, the reader is referred to reference 1.

The simplest form of compressor, from an acoustic standpoint, is an isolated rotor operating in free air, namely a propeller. The fundamental mechanism of propeller noise generation has been understood since the work of Gutin (ref. 2) gave a theoretical solution for the sound radiated by the steady thrust and torque forces acting on the blades. It was shown that due to their rotary motion these forces generate noise at all harmonics of the blade passage frequency ΩB. The noise arises merely because the point of action of the forces undergo oscillatory motion with respect to the observer. In present notation, the sound pressure amplitude of the mth sound harmonic is

$$C_m = \frac{mB^2\Omega}{2\pi a_0 r} \left\{ T_0 \cos\theta - \frac{F_0}{M} \right\} J_{mB} \; (mBM \sin\theta) \tag{1}$$

(note that T_0 and F_0 are the thrust and in-plane forces per blade)

which has a finite value for all m. Figure 1 shows the calculated first harmonic sound pressure level variations around a typical 4-blade propeller and a 40-blade fan under the action of the steady forces only. The contributions of the thrust and drag terms are indicated independently. The rotational Mach number in this case is $M = 0.5$. The noteworthy features of this comparison are in the propeller case, the double lobed pattern with a predominance of rearwards radiated noise (i.e., in the downstream hemisphere), and the greatly increased sideways radiation in the case of the fan. The latter is purely a result of blade number; the higher the number of blades, the greater the sideways radiation.

However, not too much importance should be attached to these results for the case of the isolated fan is a long way removed from the realistic situation of an axial flow compressor where the fan is mounted inside a duct in close proximity to surfaces which interfere with the flow. In this case the fan operates in an unsteady flow environment, both the fan and other surfaces radiate noise which then couples into the acoustic modes of the duct, and finally the duct radiates the sound into the free air. The problems of duct propagation and radiation were treated extensively by Tyler and Sofrin (ref. 3) in 1961 and by Morfey (ref. 14) and their analytical results explained many of the observed directional characteristics of compressor noise (e.g., ref. 4). However, it was shown by Lowson (ref. 1) that many of the effects formerly attributed to the duct could be explained in fact by generation rather than by propagation effects. For this reason we will proceed directly to the problem of noise generation by the fan.

Figure 2 illustrates a typical compressor or fan configuration which will be explained in some detail in section 2.2. Air is drawn into the system through a circular intake and passes into the annular duct which contains the fan elements. It first passes through a row of stationary inlet guide vanes, undergoing in the process circumferential acceleration in a direction opposite to the motion of the rotor which is located immediately downstream. The rotor compresses the flow and imparts swirl in the direction of the rotation. Finally the air passes through another stationary row of blades, or stators, which "straighten" the flow, removing the circumferential velocity components. Many variations of this configuration are used in practice and the only element common to all axial compressors and fans is the rotor. Most primary compressors in aircraft turbine engines have many rotor/stator stages and may or may not have inlet guide vanes. The configuration illustrated is typical of aft-fan stages although it is becoming common practice to eliminate the row of inlet guide vanes.

Whatever the configuration, at the root of the compressor noise problem lie the viscous wakes which stream from the blades of both rotor and stator alike. Because of these wakes, subsequent blade rows encounter highly non-uniform flow patterns. This causes noise to be generated by several mechanisms as discussed below.

The foundation for Lowson's analysis is the basic acoustic equation derived by Lighthill (ref. 5). In tensor notation this is

$$\frac{\partial^2 \rho}{\partial t^2} - a_0^2 \frac{\partial^2 \rho}{\partial x_i^2} = \frac{\partial Q}{\partial t} - \frac{\partial F_i}{\partial x_i} + \frac{\partial^2 T_{ij}}{\partial x_i \partial x_j} \tag{2}$$

The left hand side of this equation is the acoustic wave equation in three dimensions and the three terms on the right hand side are forcing functions corresponding to various types of acoustic source all of which can be present in a compressor. The first term, $\partial Q / \partial t$, is the effect of mass fluctuations and represents a monopole source. In the compressor, monopole sound is generated by the fluctuating flow velocities which effectively become mass flow variations through the rotor and stator rows. The second term, $\partial F_i / \partial x_i$, represents a dipole source which introduces the effects of aerodynamic pressures acting on the airfoil surfaces. These are largely lift fluctuations, the origins of which are treated in section 2.2. The final term, $\partial^2 T_{ij} / \partial x_i \partial x_j$, involves many effects, predominant among which is the sound radiation by turbulence. There is a certainty that both steady and fluctuating stress fields around the airfoils generate a significant amount of sound directly as quadrupole sources (ref. 6). Although these would become most important at transonic tip velocities, they have been ignored in reference 1 and the present study. The results obtained tend to justify this omission.

Of the other two sources the dipole noise due to force fluctuations is the more important. Lowson (ref. 1) showed that for typical fan configurations, the acoustic power generated by mass fluctuations would be between 15 and 25 dB less than that due to force fluctuations. Based on theoretical arguments, the following expression was obtained (ref. 1) for the ratio between monopole and dipole acoustic power for a single compressor mode

$$10 \log_{10} \left(\frac{\text{Mass Source Power}}{\text{Force Source Power}} \right) = 36.5 - 20 \log_{10} V_T \qquad (3)$$

which simply says that only at tip velocities of less than about 70 feet per second are the mass sources more significant than for the force terms. Accordingly, although in reference 1 theoretical results were derived for both mass and force sources, only the force terms have been considered in the present work. Restricting the right hand side of equation (3) to the dipole term only, its solution can be written

$$\rho = - \frac{1}{4\pi a_0^2} \frac{\partial}{\partial x_i} \int \left[\frac{F_i}{r} \right] d\underset{\sim}{y} \qquad (4)$$

where the integration is performed over the entire source region (e.g., the compressor face). It is most important to note that the contents of the square brackets must be evaluated at the appropriate retarded time. This takes account of the fact that it takes finite time for the sound to propagate to the point where the density fluctuation ρ is observed. The value of the retarded time can thus vary over an extended source region. Now a fan blade can be represented acoustically by a set of rotating forces. In the simplest case two forces per blade are sufficient, corresponding to the thrust and drag forces acting at a single point along the blade radius. This is the model adopted by Gutin where the forces are steady. Considering now only one of these forces, the thrust component, but giving it a harmonically varying amplitude so that

$$T = T_n \cos (n \psi)$$

equation (4) can be integrated over a one revolution interval (ref. 7) to yield the result for the observed sound pressure amplitude, in a form corresponding to equation (1), the Gutin equation:

$$C_m = \frac{mB^2 \Omega}{4\pi a_0 r} \left\{ T_n \cos \theta \right\} \left\{ J_{mB-\lambda} (mBM \sin \theta) + (-1)^{\lambda} J_{mB+\lambda} (mBM \sin \theta) \right\} \qquad (5)$$

It should be noted that when $n = 0$, i.e., when the thrust is steady, equation (5) becomes identical to the thrust term of the Gutin equation. The important thing to note about equation (5) is that a value of C_m can be calculated for any value of m, i.e., any loading harmonic contributes to any sound harmonic. This is simply a manifestation of the Doppler effect. As the sinusoidal source approaches the observer, an increase of frequency is heard; as it moves away, away, a decrease is heard. The net result is a periodic modulation of the observed frequency, giving a signal which has a Fourier spectrum consisting of an infinite number of harmonic components.

5

Turning to the case of the compressor rotor, only certain values of n can exist. To understand this it is sufficient to consider a single rotor/stator pair and to acknowledge that when a rotor blade passes close to a stator blade it experiences a force fluctuation. If there are V stator vanes then any single rotor blade encounters V force fluctuations during the course of one revolution. If the fluctuations are all identical, then the blade airload cycle can be represented by a Fourier series having a fundamental frequency of $V\Omega$. In other words, only the harmonics corresponding to integral multiple of V (i.e., m = kV) can be present (where k is any positive integer). Thus, summing equation (5) over all these harmonics we obtain an equation of the form

$$C_m = \frac{mB^2\Omega}{2\pi a_0 r} \sum_{k=-\infty}^{+\infty} T_k \cos\theta \cdot J_{mB-kV}(mBM\sin\theta) \qquad (6)$$

Note that, as in the case of a propeller, only harmonics of the blade passage frequency can be radiated. This is because pressure fluctuations at any fixed point in the compressor plane pass through a complete cycle between the passage of successive blades. Thus the source only contains harmonics of $B\Omega$. The complex radiation patterns which will be discussed shortly are functions of the phase variations of these harmonics over the distributed source.

The components of the sound pressure C_m attributable to the different loading harmonics k have been distinguished as "modes" of the acoustic field with the parameter (mB-kV) referred to as "modal order." This is because of the analogy with Tyler and Sofrin's duct modes which indeed is a good one as far as the effects are concerned. Tyler and Sofrin (ref. 3) showed the importance of the same modal order parameter to duct propagation and found that, in general, only a limited number of modes propagate, high values of mB-kV corresponding to modes which rapidly decay along the duct. In the same way, only a few low numerical values of mB-kV need be retained in the summation of equation (6) as we shall shortly see.

Just as the fluctuating forces on the rotor blades generate noise, so too do those acting on the stator blades. However, in this case, the source is a stationary dipole field with rotating phase patterns caused by the motion of the blade/vane interaction positions. Because of this phase rotation, the theoretical result for the stator radiation is remarkably similar to that for the rotor, the significant difference being that any sound harmonic (m) is generated only by load fluctuations of the same frequency (T_m). This can be explained by the lack of any Doppler effect for the stationary blades. The stator equation which is equivalent to equation (6) for the rotor would be

$$C_m = \frac{mBV\Omega}{2\pi a_0 r} T_m \cos\theta \sum_{k=-\infty}^{+\infty} J_{mB-kV}(mBM\sin\theta) \qquad (7)$$

where the obvious difference is the presence here of the thrust term outside the summation. The summation remains to take account of the source phase effects which, of course, are highly dependent on the numbers of blades and vanes. It is most important to realize, however, that now k is not related to any load harmonic but is merely a summation parameter which cannot

be described in any better way than a mode number. In the stator case, the vane loading harmonics are related to the fundamental frequency at which the rotor blades pass by rather than to any spatial variable.

At this point, it is only necessary to present the complete, rigorous solutions for the rotor and stator noise radiation due to aerodynamic forces. These are, from reference 1:

$$C_m = \frac{i\,mB^2\Omega}{2\pi\,a_0\,r} \sum_{k=-\infty}^{+\infty} (-i)^{mB-kV} \left\{ T_k \cos\theta - \frac{F_k}{M}\left(1 - \frac{kV}{mB}\right)\right\} J_{mB-kV}\,(mBM \sin\theta) \qquad (8)$$

for the rotor, and

$$C_m = \frac{i\,mBV\Omega}{2\pi\,a_0\,r} \sum_{k=-\infty}^{+\infty} (-i)^{mB-kv} \left\{ T_m \cos\theta - \frac{F_m}{M}\left(1 - \frac{kV}{mB}\right)\right\} J_{mB-kV}\,(mBM \sin\theta) \qquad (9)$$

for the stator.

As before, these equations represent the acoustic field due to point fluctuating thrust and in-plane forces acting on the blades and vanes of a stationary compressor. These form the basis for all the work reported here and although the effects of forward speed were discussed in reference 1, effort has been concentrated on the case of the stationary engine, for which detailed experimental data is available. It should be noted however that it is a relatively straightforward matter to accommodate the effects of flight velocity.

In order to apply equations (8) and (9) to practical compressor configurations, it has been necessary to make a number of simplifying assumptions. Predominant among the acoustic assumptions are

      1)   representation of each blade or vane by a pair of point forces,

      2)   neglect of a variety of phase variations,

      3)   neglect of finite flow velocity in the vicinity of the blade rows, and

      4)   neglect of duct effects.

In practice, of course, the blade forces are caused by distributed pressure acting over their entire surfaces and the use of point forces can only be an approximation. However, this step has proven successful for both propellers and helicopter rotors (ref. 7) where extensive spatial pressure distributions have been replaced by a single force.

In a previous study of helicopter noise (ref. 7), one of the most difficult practical problems was that of the phase relationships between the various loading harmonics and the various acoustic modes. It was found that any attempt to take into account the detailed in-phase and

out-of-phase components resulted in violent fluctuations of the results depending upon field point (i.e., observer) position and the precise number of airload harmonics admitted. This is the result of very significant concellation effects which can occur in highly localized regions. Such variations do not occur in practice and sound pressure level surveys made around compressors show fairly smooth and continuous intensity changes. The reasons for this are that (a) the noise is generated by distributed pressure fluctuations rather than by point forces which cause a "smearing" of source phase angle due to random pressure variations over the surface and small retarded time differences, (b) flow irregularities cause departures from purely harmonic variations, and (c) propagation effects such as scattering cause redistributions of sound energy at significant distances from the source, in particular, large "dips" in the radiation patterns are rapidly "filled in." In the present study, as before, the phase problem has been eliminated by ignoring all phase terms in both the acoustic and the aerodynamic expressions and simply adding intensities due to different modal contributions. This is, of course, equivalent to assuming uncorrelated sources, i.e., sources having random phase relationships.

The effects of finite duct flow velocities have not been considered since until the axial flow Mach number approaches unity, they are not thought to be especially significant. The two main effects are to effectively lengthen the upstream duct length and to introduce refraction due to velocity variations across the duct. Although account of such phenomena could be incorporated, it does not seem justifiable at the present time in the light of the rather large number of assumptions made in other areas.

The duct mode coupling effects have already been briefly discussed and further discussion is deferred until section 4.4.

In the next section, methods for estimating the magnitudes of both the steady and fluctuating forces are presented. Additional assumptions regarding the nature of the flow processes are discussed therein.

2.2 Blade Airload Prediction

Expressions presented in the previous section give the acoustic field around a compressor as functions of its basic design and operating parameters and the equivalent harmonically fluctuating point forces which act upon the blades. In this section, the aerodynamic features of an axial flow compressor which are important to its acoustic features are discussed. A simplified analysis is presented which is used in subsequent sections to define the force inputs to the acoustic equations. This analysis is based on incompressible, inviscid flow theory which is adequate for low speed flow.

2.2.1 <u>Basic design principles</u>. — The main purpose of an axial flow compressor is, as the name implies, to increase the pressure in a fluid flow. The simplest compressor configuration is that of a single fan, or rotor, installed in a pipeline as shown in figure 3. The blades are attached radially to the hub and rotate to impart energy to the flow. Consider a cylindrical section of radius R, thickness dR, concentric with the axis, into or out of which there is no flow. This cylinder can be developed into a plane to give a plane "cascade" flow, which is

different for different radii. If u and v are the axial and circumferential flow velocity components (the latter being measured positive in the direction of rotation) the axial mass flow through the section is

$$\dot{m} = 2\pi R \rho u \, dR \tag{10}$$

Denoting conditions upstream and downstream of the fan by the subscripts i (inlet) and o (outlet), respectively, for mass continuity:

$$u_0 = u_i \tag{11}$$

However, the cross flow component is increased by the fan from v_i to v_0. For the rotor,

$$\text{torque} = \text{mass flow rate} \times \text{change in swirl}$$

i.e.,

$$Q_r = \dot{m} R (v_0 - v_i) \tag{12}$$

where swirl is defined as the product of the tangential velocity and radius (v is subsequently referred to as the "swirl velocity"). The rotor power required is therefore

$$P_r = \dot{m} \Omega R (v_0 - v_i) \tag{13}$$

Assuming unit efficiency, this can be equated to the power added to the flow which is the product of the volume flow rate and the total pressure rise. That is,

$$\dot{m} \Omega R (v_0 - v_i) = \dot{m} (\Delta P_T)/\rho$$

or

$$\Delta P_T = \rho \Omega R (v_0 - v_i) \tag{14}$$

By Bernoulli's equation the total pressure rise is the sum of the dynamic and static pressure increments:

$$\Delta P_T = \frac{1}{2} \rho (v_0^2 - v_i^2) + \Delta P \tag{15}$$

Therefore, the static pressure rise across the rotor at station R is

9

$$\Delta P = \rho \left(v_0 - v_i\right)\left(\Omega R - \frac{v_0 + v_i}{2}\right)$$

$$\Delta P = \rho \left(v_0 - v_i\right)\left(\Omega R - v\right) \tag{16}$$

where v is the mean swirl velocity in the rotor plane.

In general, it is desirable to maximize the static pressure rise component of the rotor because this can always be converted to velocity head with little loss through an appropriate contraction. The converse is difficult to achieve since subsonic flow diffusion is inevitably accompanied by pressure losses associated with flow separations and turbulence. If the fan is being used as a flow accelerator, as it is in the case of an aircraft engine, the swirl component at the outlet is of not value; it merely represents a loss of energy. Consequency, it is common to find a set of stationary flow straightening vanes, or stator, downstream of the fan whose function it is to recover the swirl energy as static pressure. As figure 4 shows, the space between each pair of stator vanes is effectively a diffuser which removes the swirl component and reduces the resultant flow velocity from $(v_0{}^2 + u^2)^{\frac{1}{2}}$ to u. Neglecting the viscous losses which are associated with this process in reality the pressure rise denoted by equation (14) is then completely converted to static pressure by a rotor/stator combination.

The maximum value of v_i obtainable in practice is, of course, limited by the rotational velocity of the rotor. One common method of increasing the total pressure rise obtainable by a single stage fan is to introduce negative swirl upstream of the rotor (v_i) by the use of inlet guide vanes. The additional losses incurred by first reducing and then increasing the static pressure are more than compensated by the additional total pressure rise across the system.

Thus, it is more meaningful for the present purposes to consider the general case of an axial compressor stage consisting of inlet guide vanes, rotor and stator. Typical aircraft engine compressors generally consist of multiple rotor/stator stages in series which incrementally achieve a high overall pressure ratio. However, the fan or bypass flow is normally driven by a single stage unit.

2.2.2 Fan performance analysis. — It can be shown (e.g., Betz, ref. 8, p. 155) that the maximum total pressure rise achievable in a fan of finite blade length is roughly proportional to the square of the ratio of hub radius/tip radius. For this reason, it is common practice to use a large hub, which enables the fan to be conveniently approximated by a thin annulus in which the blade length is small compared to the mean radius.

The assumed fan system geometry is shown in figure 2. The duct cross sectional area is constant at all three rows (IGV, rotor and stator). The static pressure rise applied by the fan stage is dissipated by accelerating the flow through the exhaust nozzle which has a smaller cross-sectional area.

The basic fan design parameters are

Duct area   A
Mean radius   R
Rotational speed Ω
Nozzle area A_E

(Note that R is now the average blade radius.)

	IGV	Rotor	Stator
Number of blades	V_v	B	V_s
Solidity	σ_v	σ_r	σ_s
Blade pitch	θ_v	θ_r	θ_s

It is assumed that the blades are sufficiently short so that forces calculated for the mid-section can be assumed uniform over the blade length. "Solidity" is the ratio of the total blade area to the duct cross-sectional area (where blade length = duct thickness). Thus, for example,

$$\sigma_r = \frac{Bc\ell}{A} = \frac{Bc}{2\pi R}$$

where c = mean blade chord, and ℓ = blade length. Figure 5 shows the rotor blade flow velocity diagram where all velocities have been non-dimensionalized on the mean blade velcoity ΩR. The non-dimensionalized coefficients are listed in Table I.

The angle ϕ is the effective inflow angle so that the blade angle of attack α is obtained by subtracting the inflow angle from the geometric blade pitch setting θ. The blade lift L_b acts in a normal direction to the inflow so that the axial thrust component T_b and in-plane force component F_b are given by

$$\left.\begin{aligned} T_b &\cong L_b \cos \phi \\[2ex] F_b &= \frac{Q}{RB} = L_b \sin \phi \end{aligned}\right\} \tag{17}$$

In these expressions the blade drag force, which acts in a parallel direction to the inflow, has been ignored. This is justified because the drag is very small compared with the lift and because at typical compressor inflow angles the thrust and in-plane force components are of the same order.

TABLE I

NON-DIMENSIONAL VELOCITY COEFFICIENTS

	Dimensional	Non-dimensional
Axial flow velocity	u	μ
Rotor inlet swirl velocity	v_i	λ_i
Rotor outlet swirl velocity	v_0	λ_0
Mean rotor swirl velocity	$\bar{v}$	$\bar{\lambda}$

From equations (17, (12), and (14),

$$\tan \phi = \frac{F_b}{T_b} = \frac{Q}{RA \, \Delta P} = \frac{\mu}{\Omega R - \bar{v}} = \frac{\mu}{1 = \bar{\lambda}} \tag{18}$$

So that, as shown in figure 5, the in-plane flow component is proportional to $(1 - \bar{\lambda})$ and the resultant inflow to $[\mu^2 + (1 - \lambda)^2]^{\frac{1}{2}}$.

Applying isolated airfoil blade element theory to a single rotor blade

$$L_b = \frac{1}{2} \rho \, (\Omega R)^2 \, [\mu^2 + (1 - \bar{\lambda})^2] \, C_L \, C_r \tag{19}$$

Now the lift coefficient C_L is the product of the lift curve slope, and the angle of attack, i.e., $C_L = a \, \alpha = a \, (\theta - \phi)$, and

$$\cos \phi = \frac{1 - \bar{\lambda}}{\sqrt{\mu^2 + (1 - \bar{\lambda})^2}} \tag{20}$$

Also, since the blade angle of attack α is always a small angle

$$\alpha \approx \sin (\theta - \phi) = \sin \theta \cos \phi - \cos \theta \sin \phi \tag{21}$$

whence from equation (17),

$$T = B \, L_b \cos \phi = \frac{1}{2} \rho A \, (\Omega R)^2 \, a \, \sigma_r \, (1 - \bar{\lambda}) \left\{ (1 - \bar{\lambda}) \sin \theta - \mu \cos \theta \right\} \tag{22}$$

Equation (18) can be rewritten

$$T = \rho A (\Omega R)^2 (\lambda_0 - \lambda_i)(1 - \bar{\lambda}) \tag{23}$$

Equating equations (22) and (23)

$$(\lambda_0 - \lambda_i) - \frac{a \, \sigma_r}{2} [(1 - \bar{\lambda}) \sin \theta - \mu \cos \theta] \tag{24}$$

Assuming now that the stator always recovers 100 percent of the static pressure

$$\Delta P_T = \frac{1}{2} \rho V_E^2 \tag{25}$$

where V_E = nozzle exit velocity

$$V_E = \mu \Omega R \left(\frac{A}{A_E} \right) \tag{26}$$

Equating equations (14) and (26) we obtain

$$\mu^2 = 2 \left(\frac{A}{A_E} \right)^2 (\lambda_0 - \lambda_i) \tag{27}$$

Assuming no swirl upstream of the inlet guide vanes, the torque on the guide vane row is, similarly,

$$\dot{m} \, v_i = \rho A (\Omega R)^2 \mu \lambda_i = \frac{1}{2} \rho A (\Omega R)^2 \, \sigma_v \, C_{L_v} \tag{28}$$

whence

$$\lambda_i = \frac{\sigma_v \, C_{L_v}}{2 \mu} \tag{29}$$

where C_{L_v} = IGV lift coefficient which is constant for a given IGV pitch setting.

Equations (24), (26), (27) and (29) can be combined to give the following cubic in μ:

$$\left(1 + \frac{\sigma_r \, a}{4} \right) \mu^3 + \sigma_r \, a \left(\frac{A}{A_E} \right)^2 (\mu^2 \cos \theta - \mu \sin \theta) + \frac{C_{L_v} \, \sigma_v \, \sigma_r \, a}{2} \left(\frac{A}{A_E} \right)^2 = 0 \tag{30}$$

which can be solved numerically for the axial flow ratio μ.

13

Equation (30) shows that μ is constant for a particular fan design and it follows from equations (29), (17), and (24) that so also are λ_i, λ_0, and λ. This, of course, is one result of the inviscid flow assumption. Within this constraint, once these parameters have been calculated for a given fan, all results can be dimensionalized by scaling flow velocities as the rotor speed and airloads as the square of rotor speed. That these relationships are in fact good approximations is indicated by figure 6 which shows experimental data for three fans. Specifyin overall rotor thurst and torque coefficients as

$$C_T = \frac{T}{\frac{1}{2}\,\rho\,A\,(\Omega R)^2}$$

$$C_Q = \frac{Q}{\frac{1}{2}\,\rho A\,(\Omega R)^2 R} \tag{31}$$

it can be deduced from equations (23) and (12) that

$$C_T = 2\,(\lambda_0 - \lambda_i)\,(1 - \bar{\lambda}) \tag{32}$$

$$C_Q = 2\,\mu\,(\lambda_0 - \lambda_i) \tag{33}$$

The equations presented up to this point can be used to estimate the steady thrust and in-plane forces acting on all blades. In the next section the fluctuating force problem is treated.

2.2.3 Fluctuating blade forces. — Compressor blades operate in a non-steady flow environment due to the proximity of other blades. Kemp and Sears (refs. 9 and 10) showed that two fundamental mechanisms cause blade lift fluctuations; potential flow interactions between blade rows and wake impingement. In the former case, the bound vortex associated with each blade induces flow perturbations at blades in both preceding and following rows. In the latter, each blade passes through an endless series of wakes shed by the blades in the preceding rows. Of the two problems, that of the viscous wake is the most significant (and, fortunately, is the easier to tackle). This is because the induced field of a vortex decays as the inverse of distance whereas wake velocities decrease approximately as the inverse square of distance. Kemp and Sears (ref. 10) found that the two effects were equally significant at row spacings corresponding to approximately one tenth of the blade chord dimension. Since it is common practice in modern compressors to separate rows by at least a chord length, the potential flow interactions are probably an order of magnitude less important than the viscous ones. In the analysis that follows, which is similar to that of Kemp and Sears, the following assumptions are made:

14

1) The flow is inviscid and incompressible with the viscous wakes being represented by inviscid shear flows.

2) Isolated two-dimensional thin airfoil theory can be used to define mean blade loadings.

3) Wake data for single airfoils in a free stream can be used to approximate the wakes behind compressor cascades.

The validity of these assumptions will be discussed at a later point in the report.

2.2.3.1 Rotor forces. — During its motion around the annular duct the rotor blade passes through a periodically varying flow field because of the velocity reductions occurring in the wakes of the inlet guide vanes (fig. 7). This is equivalent to a periodic variation of the blade angle of attack α which can therefore be expressed as a Fourier series:

$$\alpha = \alpha_0 + \sum_{k=1}^{\infty} \alpha_k \cos (kV\psi) \tag{34}$$

The sine terms have been dropped by appropriate choice of a zero reference for ψ. If we assume that the principle of linear superposition holds in this case, we can write

$$L_b = L_{b_0} + \sum_{k=1}^{\infty} L_{b_k} \cos (kV\psi + \epsilon_k) \tag{35}$$

where L_{b_k} is the kth harmonic blade lift in response to the kth angle of attack harmonic and ϵ_k is a phase angle.

In point of fact the notion of angle of attack loses some of its meaning when the spatial extent of the velocity perturbations is small compared with the blade dimensions (such as illustrated in figure 7). Sears (ref. 11) analyzed the problem of a wing entering a sinusoidal gust. For an upwash variation of the form

$$w = w' \cos \omega \left(t - \frac{x}{U} \right) \tag{36}$$

he showed that the lift per unit span has the form

$$L = \frac{1}{2} \rho c U w' S \left(\frac{\omega c}{U} \right) \cos (\omega t + \epsilon) \tag{37}$$

15

The lift response function S (ωc/U) accounts for the tendency of the airfoil to "filter" the effect of the velocity fluctuations so that these effects become increasingly attenuated with frequency. Lowson (ref. 1) showed that for most practical applications, Sears' exact expression for the lift response function could be represented by an approximation of the form (note that there is a typographical error in reference 1)

$$\left| S\left(\frac{\omega c}{U}\right) \right| = \left(\frac{U}{\pi \omega c}\right)^{\frac{1}{2}}$$

(38)

(Note also that a phase angle has been omitted; see ref. 1.)

Since in equation (37), a small upwash velocity w is equivalent to an angle of attack increase of w/U, the equation could be rewritten for the compressor case,

$$L_k = \frac{1}{2} \rho c U^2 \alpha_k \left(\frac{U}{\pi k V \Omega c}\right)^{\frac{1}{2}}$$

(39)

where it must be remembered that α_k is an "effective angle of attack" harmonic related to localized upwash variations.

It is convenient to express the compressor flow velocity fluctuations as a proportion of the free stream velocity, V. Using the Fourier representation and non-dimensionalizing

$$\frac{\Delta V}{V} = \delta_0 + \sum_k \delta_k \cos (k V \psi)$$

where again the phase angle can be dropped without loss of generality.

Referring now to the blade velocity diagram, figure 8, it can be seen that the change of angle of attack $\Delta \alpha$ due to a (non-dimensional) velocity decrement Δv

$$\Delta \alpha = - \Delta \phi = \Delta v \frac{\sin (X + \phi)}{\mu^2 + (1 - \bar{\lambda})^2}$$

(40)

$$\Delta \alpha = \frac{\Delta v}{v} \frac{\mu}{[\mu^2 + (1 - \lambda)^2]^{\frac{1}{2}}}$$

(41)

In the notation of equation (34) $\Delta \alpha$ can be expressed

$$\Delta \alpha = \sum_{k=1}^{\infty} \alpha_k \cos (kV \psi)$$

16

Noting that the ratio $\Delta v / v$ is equivalent to $\Delta V / v$, the corresponding lift harmonic L_k acting on the blade is obtained by substituting $U^2 = (\Omega R)^2 [\mu^2 + (1 - \lambda)^2]$ into equation (39)

$$L_{b_k} = \frac{1}{2} \rho \, \sigma_r \, A \, (\Omega R)^2 \, [\mu^2 + (1 - \lambda)^2] \, a \, \Delta \, \alpha_k \left\{ \frac{R \, [\mu^2 + (1 - \lambda)^2]^{\frac{1}{2}}}{\pi \, k \, c \, V} \right\}^{\frac{1}{2}}$$

$$= \frac{1}{2} \rho \, \sigma_r \, A \, (\Omega R)^2 \, a \, \delta_k \, \mu \left\{ \frac{R [\mu^2 + (1 - \lambda)^2]^{\frac{1}{2}}}{\pi \, k \, c \, V} \right\}^{\frac{1}{2}} \tag{42}$$

The lift force can then be resolved into its thrust and in-plane force components according to equation (17).

2.2.3.2 Stator forces. — Figure 9 shows the equivalent wake geometry and vector diagrams for a stator blade. A similar analysis can be followed to show that, for a stator blade

$$L_{b_k} = \frac{1}{2} \rho \, \sigma_v \, A \, (\Omega R)^2 \, a \, \delta_k \, \mu \left\{ \frac{R \, \mu^2 + (1 - \lambda_0/2)^2]^{\frac{1}{2}}}{\pi \, k \, c \, B} \right\}^{\frac{1}{2}} \tag{43}$$

which is almost identical in form to that for a rotor blade.

As in the work of Kemp and Sears, use is made here of the empirical wake relationships presented by Silverstein, et al. (ref. 12) who collapsed experimental wake data obtained from isolated airfoils. They showed that the wake half-width, as indicated in figure 10 may be expressed by the formula

$$\frac{y}{c} = 0.68 \sqrt{C_D \left(\frac{x}{c} - 0.6 \right)} \tag{44}$$

The notation is that of the present report where C_D is the airfoil profile drag coefficient, and x is measured, in the direction of flow, from the 1/4-chord point. Also from the results of Silverstein, et al. (ref. 12), it can be deduced that the centerline velocity defect μ_c is given by

$$\frac{\mu_c}{U} = \frac{1.21 \, C_D^{\frac{1}{2}}}{\frac{x}{c} - 0.45} \tag{45}$$

17

where u is the free stream velocity. Finally, the velocity defect profile across the wake can be approximated by

$$\frac{\mu}{\mu_c} = \cos^2\left(\frac{\pi y}{2Y}\right) \tag{46}$$

Equations (45) and (46) define the velocity profile across the wake at any distance behind the airfoil. However, we require this information in the form of a Fourier series so that the profile must be written

$$\frac{\mu}{\mu_c} = \eta_0 + \sum_k \cos\left(\frac{k\pi y}{b}\right) \, dy \tag{47}$$

where

$$\eta_k = \frac{1}{b} \int_{-b}^{+b} \left(\frac{\mu}{\mu_c}\right) \cos\left(\frac{k\pi y}{b}\right) \, dy$$

(The sine term can again be discarded because of wake symmetry about y = 0.)

Now, since the velocity defect μ/μ_c is zero outside the wake limits $- Y < \mu/\mu_c < Y$, the integration limits can be changed to $\bullet$ y. Substitution of equation (46) gives

$$\eta_k = \frac{1}{b} \int_{-Y}^{Y} \cos^2\left(\frac{\pi y}{2Y}\right) \cos\left(\frac{k\pi y}{b}\right) \, dy$$

$$= \frac{\sin(k\pi Y/b)}{\pi k \left[1 - \left(\frac{kY}{b}\right)^2\right]} \tag{48}$$

Since $\mu/U = \mu/\mu_c \cdot \mu_c/U$, equations (45) and (48) can be combined to give the following for the harmonic coefficient δ_k of equation (48).

$$\delta_k = \frac{1.21 \, C_D^{\frac{1}{2}}}{\frac{x}{c} - 0.45} \, \frac{\sin(k\pi Y/b)}{\pi k \left[1 - (kY/b)^2\right]} \tag{49}$$

18

Note that for the rotor force fluctuations due to the IGV wake (fig. 7),

$$\frac{x}{c} = \frac{d}{c} \frac{\sqrt{\mu^2 + \lambda_i^2}}{\mu}$$

$$b = \frac{\pi R}{V_v} \frac{\mu}{\sqrt{\mu^2 + \lambda_i^2}}$$

and for the stator forces due to the rotor wake

$$\frac{x}{c} = \frac{d}{c} \frac{\sqrt{\mu^2 + (1-\lambda_0)^2}}{\mu}$$

$$b = \frac{\pi R}{B} \frac{\mu}{\sqrt{\mu^2 + (1-\lambda_0)^2}}$$

2.2.4 <u>Summary of airload theory</u>. — The analysis followed in sections 2.2.1 through 2.2.3 yielded various relationships which may be used to estimate both the steady and fluctuating airloads acting upon both rotor and stator blades. These methods have in fact been used for all the ensuing acoustic analyses. However, it is extremely difficult to specify how the results are used since they depend entirely upon the specific application and the basic aerodynamic data available. However, for convenience the most useful equations are repeated.

    a)   total pressure rise across rotor

$$\Delta P_T = \rho (\Omega R)(\lambda_0 - \lambda_i) \tag{14}$$

    b)   static pressure rise across rotor

$$\Delta P = \rho (\Omega R)^2 (\lambda_0 - \lambda_i)(1 - \bar{\lambda}) \tag{16}$$

    c)   axial velocity ratio

$$\mu = \frac{A}{A_E} \sqrt{2(\lambda_0 - \lambda_i)} \tag{27}$$

19

d) rotor inflow angle

$$\tan \phi = \frac{\mu}{1 - \bar{\lambda}} \tag{18}$$

e) rotor thrust coefficient

$$C_T = 2 (\lambda_0 - \lambda_i) (1 - \bar{\lambda}) \tag{32}$$

f) rotor torque coefficient

$$C_Q = 2 \mu (\lambda_0 - \lambda_i) \tag{33}$$

g) non-dimensional velocity defect harmonic

$$\delta_k = \frac{1.21 \, C_D^{\frac{1}{2}}}{\frac{x}{c} - 0.45} \, \frac{\sin (k \pi Y/b)}{\pi k \,[1 - (k Y/b)^2]} \tag{49}$$

where $y = 0.68 c$ \hfill (44)

h) blade lift harmonic (for rotor)

$$L_{b_k} = \frac{1}{2} \rho \, \sigma_r \, A \, (\Omega R)^2 \, a \, \delta_k \, \mu \left\{ \frac{R \,[\mu^2 + (1 - \lambda)^2]^{\frac{1}{2}}}{\pi k c V} \right\}^{\frac{1}{2}} \tag{42}$$

for stator

$$L_{b_k} = \frac{1}{2} \rho \, \sigma_s \, A \, (\Omega R)^2 \, a \, \delta_k \, \mu \left\{ \frac{R \,[\mu^2 + (1 - \lambda_0/2)^2]^{\frac{1}{2}}}{\pi k c B} \right\}^{\frac{1}{2}} \tag{43}$$

This list is by no means exhaustive but is useful for defining a starting point for a particular analysis.

3.0 COMPUTATIONAL METHODS

Equations (8) and (9) have been programmed in FORTRAN for digital computer solution. These equations have been somewhat modified for use in the program and the modified equations, as well as other associated relationships, are discussed in the following sections. In this section the discussion is confined to general aspects of the numerical procedures followed. This is intended to serve as an introduction to readers who may wish to develop their own digital computer program.

During the development and use of these computer programs it became apparent that with the exception of the Bessel function calculation the arithemetical labor involved in calculating the sound pressure level at a single field point is not in general too excessive for manual computation. To make hand computation a realistic proposition, therefore, tables of Bessel functions necessary to this calculation have been prepared and have been published as a separate appendix to this report (ref. 15). The calculation method is designed to provide the engine designer a simple tool with which to make preliminary estimates of fan noise radiation. For detailed calculations of the sound field the computerized method is considered to be the only practical approach.

3.1 Mathematical Aspects

The basic relationships for the compressor noise radiation are equations (8) and (9) and these have been programmed for simultaneous solutions. They may be rewritten:

$$C_{mks} = \frac{V_s T_m}{2\pi R r} \left\{ mBM \cos \theta - (mB - k V_s) \left(\frac{F}{T}\right)_s \right\} J_{mB-kV_s} (mBM \sin \theta)$$

$$= \frac{V_s T_m}{2\pi R r} \ P_{mks} \tag{50}$$

$$C_{mkr} = \frac{B T_k}{2\pi R r} \left\{ mBM \cos \theta - (mB - k V_v) \left(\frac{F}{T}\right)_r \right\} J_{mB-kV_v} (mBM \sin \theta)$$

$$= \frac{B T_k}{2\pi R r} \ P_{mkr} \tag{51}$$

where V_v = number of vanes on the upstream stator (IGV), and V_s = number of vanes on the the downstream stator.

Yet another phase term $(-i)^{mB(1-kV/mB)}$ has been neglected in equations (50) and (51) for similar reasons to those discussed in section 1, since it was felt their inclusion introduced unnecessary complexity. Further, in summing the sound pressure values of equations (50) and (51) over all modes, the procedure is one of taking the "sum of the squares" of the values, in effect, assuming random phase relationships between the different modes.

Advantages accrue from the simultaneous computation of equations (50) and (51) due to the use of the recurrence relations. Values of $J_n(x)$ are obtained using the recurrence relation

$$J_{n-1}(x) + J_{n+1}(x) = \frac{2n}{x} J_n(x) \tag{52}$$

$$J_{n-1}(x) = \frac{2n}{x} J_n(x) - J_{n+1}(x) \tag{53}$$

for the calculation of the Bessel function $J_n(x)$. For this method all orders from $n = 0$ up to the desired order $n = N$ are calculated for a given argument, (x), value. Thus, since the Bessel function argument is the same in equations (50) and (51), if the larger of the two values $|mB - k V_v|$ or $|mB - k V_s|$ is used for N, then Bessel function values will be available for both equations. A detailed discussion of the recursion method is given in Appendix A. The time saving resulting from this approach becomes especially important when summing equations (50) and (51) over all k modes where the argument does not change.

The sound power radiated by the compressor is found by integrating the sound intensity over a sphere containing the source as center which, recognizing that the compressor noise field is symmetric about the centerline axis of the compressor, becomes

$$W = \int_0^\pi 2\pi \, s \, r I \, d\theta \tag{54}$$

where s is the radius of the circle at angle θ and spherical radius r. Then the relations describing rotor and stator sound power in each mode k is given by:

$$PR_{mks} = V_s^2 \, T_m^2 \, W_{mks}$$

$$W_{mks}{}^* = \frac{1}{4\pi R^2 a_0 \rho_0} \int_0^\pi (P_{mks})^2 \sin\theta \, d\theta \tag{55}$$

---

* Note that here the rms values of P_{mks} and P_{mkr} are used.

$$PR_{mkr} = B^2 \ T_k^2 \ W_{mkr}$$

$$W_{mkr}^* = \frac{1}{4\pi R^2 a_0 \ \rho_0} \int_0^\pi (P_{mkr})^2 \ \sin\theta \ d\theta \tag{56}$$

and the total power (sum of all modes k) is given as:

$$W_{ms} = V_s^2 \ T_m^2 \ \sum_{k=-\infty}^{+\infty} PR_{mks}$$

$$W_{mr} = B^2 \ \sum_{k=-\infty}^{+\infty} PR_{mks} \ T_k^2$$

$$W_{mT} = W_{ms} + W_{mr} \tag{57}$$

The directivity index, which represents the sound level radiated in a particular direction relative to the sound level that would be generated in the same direction by a spherically radiating source, is given by the relation:

$$DI = \frac{\text{Actual sound pressure of azimuth}}{\text{Sound pressure at azimuth } \theta \text{ by equivalent spherical source}}$$

Thus, for the rotor, stator, and their total, the directivity indices are the equations:

$$D_{ms} = \frac{V_s^2 \ T_m^2 \ \sum_{k=-\infty}^{+\infty} (P_{mks})^2}{2\pi R^2 \ \rho_0 \ a_0 \ W_{ms}} \tag{58}$$

$$D_{mr} = \frac{B^2 \ \sum_{k=-\infty}^{+\infty} (P_{mkr})^2 \ T_k^2}{2\pi R^2 \ \rho_0 \ a_0 \ W_{mr}} \tag{59}$$

---

* Note that here the rms values of P_{mks} and P_{mkr} are used.

23

$$DI_{mT} = \frac{W_{mr} \, DI_{mr} + W_{ms} \, DI_{ms}}{W_{mT}} \qquad (60)$$

These, then, are the equations used in the computer program to calculate the sound power level and sound pressure level due to a particular IGV/rotor/stator configuration.

3.2 Computer Program

The program shown in schematic flow form in figure 11 calculates the sound power generated by the rotor, the stator, and their total, and lists for each sound harmonic m, directivity indices for each. The airloading data, in the form of Fourier harmonic amplitudes, either measured or calculated are required for input.

While the summation of equation (57), for instance, theoretically extends from $-\infty$ to $+\infty$ on k, in actual practice, the summation range of k is very limited. As pointed out by Lowson (ref. 1) for a given rotor/stator or stator/rotor configuration, there are a definite number of modes whose contribution is significant to the total, all others being ignorable. This is primarily the effect of the Bessel function term in equations (50) and (51) where incremental changes in k produce large changes in the order value. Once the value of the order $|mB - kV|$ gets very far from zero, the function value rapidly approaches zero resulting in insignificant modes. The range of significant k was given by Lowson as the inequality:

$$\frac{mB}{V} (1 - M \sin \theta) \leq k \leq \frac{mB}{V} (1 + M \sin \theta) \qquad (61)$$

This means, then, that for the rotor only those loading harmonics in the range established by equation (61) need be included in the computation. For the stator, of course, the number of loading harmonics required is equal to the number of sound harmonics being calculated since only the mth loading harmonic contributed to the mth sound harmonic. For the stator the limitation of equation (61) applies to the modal summation only.

It may be noted from equation (61) that for tip speeds less than Mach 1.0, the lower limit on k does not go below zero; however, for M greater than 1, k can be negative. This brings up the problem of how to treat negative harmonics of thrust loading (i.e., T_{-k} in equation (51)). The manner of describing the Fourier expansion of the fluctuating forces answers this question. From section 5.1 of reference 1 the fluctuating thrust is represented by the Fourier expansion:

$$T = \sum_{k=-\infty}^{+\infty} T_k \exp (-i \lambda \Omega t) \qquad (62)$$

24

where

$$T_k = T_{kR} + i\,T_{kI}$$

$$T_{-k} = T_{kR} - i\,T_{kI} = T_k^{\ *} \tag{63}$$

Now, since equations (50) and (51) compute the absolute magnitude of the sound pressure (C_{mkr} or C_{mks}) only the absolute magnitude, rather than the complex magnitude, of the force loadings need to be considered. In that case, equation (63) becomes

$$\left|T_k\right| = (T_{kR}^2 + T_{kI}^2)^{\frac{1}{2}} = \left|T_{-k}\right| \tag{64}$$

Thus, for negative loading harmonics (i.e., negative k), the value of thrust loading used is equal to the corresponding positive harmonic loading (i.e., $T_{-k} = T_k$). In general, however, negative modes when they occur in the real case are almost always insignificant because, in that case, the order of the Bessel function term in equations (50) and (51) is mB + kV, hence the value of the bessel function is negligible compared to the higher order modes where the Bessel function order is mB − kV.

The computation proceeds as indicated in the figure 11 flow diagram producing the output shown in figure 12. The integration indicated in equations (56) and (57) is performed using the trapezoidal integration method and as a result the accuracy is highly dependent upon the interval chosen for θ. For reasonable results, the increment should not exceed about one or two degrees.

The sound pressure level is calculated at each field point by direct evaluation of equations (50) and (51), thus accuracy is not a function of the interval chosen for θ. If, then, minimum compute-time is a requirement and only sound pressure level is needed, the increment selected for θ may take on any value up to 180 degrees remembering that if the increment is greater than 1 or 2 degrees the sound power levels and directivity indices will be in error.

3.3 Hand Calculation Method

For the purposes of calculating the sound pressure level generated by the rotor and stator of a compressor at one or two field points, a practical hand calculation method has been developed. This is made possible by the fact that in most cases the number of significant modes k is very limited, often being only a single mode. This allows a designer to determine the expected noise level of his designs in certain critical directions, thus easily enabling noise considerations to be a part of the design process.

25

The required compressor parameters are:

m	sound harmonic number
B	number of rotor blades
V_v	number of inlet guide vanes (or upstream stator vanes)
M	rotational Mach number
θ	field point azimuth location relative to the engine axis (0° in front of engine)
V_s	number of downstream stator vanes
$\tan \phi_r$	rotor inflow angle = $(F/T)_r$
$\tan \phi_s$	stator inflow angle = $(F/T)_s$
R	rotor and stator radius
r_1	radial distance to field point

Referring now to equations (50) and (51), the procedure for the calculation is as follows:

1) List all required parameter values including radial distance, r_1, and azimuth location θ.

2) Determine the range of "k":

$$k_{min} = \frac{mB}{V_v} (1 - M \sin \theta)$$

$$k_{max} = \frac{mB}{V_v} (1 + M \sin \theta) \qquad \text{rotor}$$

$$k_{min} = \frac{mB}{V_s} (1 - M \sin \theta)$$

$$k_{max} = \frac{mB}{V_s} (1 + M \sin \theta) \qquad \text{stator}$$

3) Calculate the required force harmonics using the equations of section 2.2.4.

$$\text{rotor:} \qquad T_{k_{min}} \text{ to } T_{k_{max}}$$

$$\text{stator:} \qquad T_1 \text{ to } T_m$$

26

4) Calculate the constant terms:

rotor: $\dfrac{B}{2\pi R r_1}$; mBM cos θ; mBM sin θ; (F/T)$_r$

stator: $\dfrac{V_s T_m}{2\pi R r_1}$; mBM cos θ; mBM sin θ; (F/T)$_s$

5) For each value of "k" calculate:

rotor: $20\log_{10}\left\{\dfrac{B\,T_k}{2\pi R r}\left[mBM\cos\theta - (mB - kV_v)\left(\dfrac{F}{T}\right)_s\right]\right\}$

stator: $20\log_{10}\left\{\dfrac{V_s T_m}{2\pi R r}\left[mBM\cos\theta - (mB - kV_s)\left(\dfrac{F}{T}\right)_s\right]\right\}$

6) From the table of Bessel functions determine the value of:

rotor: $10\log_{10}\left|J_{|mB-kV_v|}(mBM\sin\theta)\right|$

stator: $10\log_{10}\left|J_{|mB-kV_s|}(mBM\sin\theta)\right|$

and multiply by 2 to obtain $20\log_{10}\left|J_{|mB-kV|}(mBM\sin\theta)\right|$

7) For each value of "k" add the two previously calculated terms to obtain the modal sound pressure:

$$20\log_{10} C_{mkr} = 20\log_{10}\left\{\dfrac{B\,T_k}{2\pi R r}\left[mBM\cos\theta - (mB-kV_v)\left(\dfrac{F}{T}\right)_r\right]\right\}$$

$$+\; 20\log_{10}\left|J_{|mB-kV_v|}(mBM\sin\theta)\right|$$

$$20\log_{10} C_{mks} = 20\log_{10}\left\{\dfrac{V_s T_m}{2\pi R r}\left[mBM\cos\theta - (mB-kV_s)\left(\dfrac{F}{T}\right)_s\right]\right\}$$

$$+\; 20\log_{10}\left|J_{|mB-kV_s|}(mBM\sin\theta)\right|$$

27

8) Convert to sound pressure level by adding 127.5 dB to the calculated values of $20 \log_{10} C_{mkr}$ and $20 \log_{10} C_{mks}$.

9) For the rotor and for the stator, add logarithmically the modal sound pressure levels to obtain the total sound pressure level, C_{ms} and C_{mr}:

$$C_{ms} = 10 \log_{10} \sum_{k=k_{min}}^{k_{max}} \text{antilog}\left(\frac{SPL_{mks}}{10}\right)$$

$$C_{mr} = 10 \log_{10} \sum_{k=k_{min}}^{k_{max}} \text{antilog}\left(\frac{SPL_{mkr}}{10}\right)$$

10) Add logarithmically the values of C_{ms} and C_{mr} to obtain the total sound pressure level, C_{mt} and the given field point.

$$C_{mT} = 10 \log_{10} \left\{ \text{antilog}\left(\frac{C_{ms}}{10}\right) + \text{antilog}\left(\frac{C_{mr}}{10}\right) \right\}$$

An example of this calculation procedure is given in Appendix B.

3.4 Empirical Approximations for Modal Acoustic Power

Lowson (ref. 1) showed that the total acoustic power in the rotor or stator mode of order mB–kV is given by the approximate relationship:

$$W_{m,k} \approx \frac{1}{8\pi a_0 \rho_0 R^2} \left\{ |mB - kV|^2 F_k^2 \widehat{D} + (mBM)^2 T_k \widehat{T} \right\} \tag{65}$$

where

$$\widehat{D} = \sum_{r=0}^{+\infty} \frac{(-1)^r (mBM)^{2|mB-kV| + 2r}}{r!\,(2|mB-kV| + r)!\,(2|mB-kV| + 2r + 1)} \tag{66}$$

and

$$\widehat{T} = \sum_{r=0}^{+\infty} \frac{(-1)^r (mBM)^{2|mB-kV| + 2r}}{r!\,(2|mB-kV| + r)!\,(2|mB-kV| + 2r + 1)(2|mB-kV| + 2r + 3)} \tag{67}$$

28

The quantities $\hat{T}$ and $\hat{D}$ were numerically evaluated by computer for a number of values of (mB–kV) and the results are shown as the various broken lines in figure 13. For the purposes of illustration, a third quantity, $|mB-kV|\ \hat{D} + (mBM)^2\ \hat{T}$ has also been plotted in figure 13. This represents the term inside the brackets when $D_k = T_k$ (note that k here is an appropriate harmonic number) which is typical for a compressor.

Unfortunately the series given above are badly conditioned and their calculation leads to excessive computer time for practical purposes. Consequently, empirical approximations to these functions have been derived which should be accurate to within 2 dB and adequate for design purposes. These approximations are:

$$\hat{D} = \frac{1}{2mBM}\left\{\frac{\left\{M\left(1 - \frac{kV}{mB}\right)\right\}^{-1.8\,|mB-kV|}}{\frac{11}{|mB-kV|} + \left\{M\left(1 - \frac{kV}{mB}\right)\right\}^{-1.8\,|mB-kV|}}\right\} \tag{68}$$

and

$$\hat{T} = \frac{1}{4mBM}\left\{\frac{\left\{M\left(1 - \frac{kV}{mB}\right)\right\}^{1.8\,|mB-kV|}}{\frac{11}{|mB-kV|} + \left\{M\left(1 - \frac{kV}{mB}\right)\right\}^{-1.8\,|mB-kV|}}\right\} \tag{69}$$

These approximations are shown as the continuous curves in figure 13. At high values of (mB–kV) these tend to the asymptotic solutions given by Lowson (ref. 1):

$$\hat{D} = \frac{1}{2mBM}$$

$$\hat{T} = \frac{1}{4mBM} \tag{70}$$

Although these relationships have not been used in the present study they do provide very convenient and simple predictions of overall acoustic power for design purposes.

4.0 RESULTS

4.1 Some Basic Features of the Analytical Results

Before proceeding to the main results of the study it is worthwhile to pause and re-examine some of the general features of the basic equations (8) and (9) as applied to typical compressor configurations. For a detailed study the reader is referred to reference 1.

For both rotor and stator alike, the directional character of the radiated sound, and the relative importance of different acoustic modes, are accounted for by the common portion of the equations which is

$$\left\{ T_k \cos \theta - \frac{F_k}{M} \left(1 - \frac{kV}{mB} \right) \right\} J_{mB-kV} (mBM \sin \theta) \tag{71}$$

Both factors in this expression have characteristic directionalities. The directivity corresponding to the first can be rewritten:

$$G(\theta) = 10 \log_{10} \left\{ T_k \cos \theta - \frac{F_k}{M} \left(1 - \frac{kV}{mB} \right) \right\}^2 \tag{72}$$

which only differs from the Gutin form (see eq. 1) by the multiplier $1 - kV/mB$. Equation (72) is plotted for $T_k = D_k = 1$ (remember that $T/D = 1$ is typical of compressor rotors), $M = 0.5$ and various values of kV/mB in figure 14. Note that equation (72) is antisymmetrical about $kV = mB$ so that

$$G\left(\theta, \frac{kV}{mB} \right) = G\left(180° - \theta, 2 - \frac{kV}{mB} \right) \tag{73}$$

Thus each curve in figure 14 is labeled with two values of kV/mB. For the lower value, corresponding to $kV < mB$, the axis pointing toward the top of the page is the forward axis of the fan, i.e., the thrust line. For the higher value (in parentheses), corresponding to $kV > mB$, the axis is reversed so that the top of the page becomes the downstream side of the fan. The bold curve in figure 13 represents the limiting solution when $kV = mB$. This has two lobes and is perfectly symmetrical about $\theta = 90°$. In this case, inspection of equation (72) shows that the in-plane forces do not generate any noise. This condition is known as the "siren" mode (having zero modal order $kV - mB$) where the distributed sources are all in phase. This is easiest to visualize for the case when $V = B$, i.e., an equal number of rotor and stator blades. Here each blade passes a vane at the same instant so all force fluctuations occur simultaneously and the compressor face acts almost like a piston source (having force rather than mass fluctuations). This configuration was always believed to be undesirable because of this "siren" effect but in fact Lowson showed that it does not generate the maximum acoustic power and furthermore the sound is radiated in a predominantly axial direction which is quite desirable from a community noise standpoint.

For all values of kV/mB less than unity (including negative ones) the curves are asymmetrical about $\theta = 90°$ and show an increased radiation in an aft direction. In the range $0.5 < kV/mB < 1.0$ the pattern retains two lobes but the depression occurs at acute values of θ. In fact this is equivalent ot the propeller noise condition (eq. 1) where the in-plane force contribution is of the same order. When kV/mB is less than 0.5 the second lobe disappears and for kB/mB<< 1 the radiation tends to a spherical pattern as the influence of thrust becomes negligible.

When kV > mB the entire plot "flips over" and identical patterns arise, this time with more noise radiated forward than aft. This indicates an obviously important design feature, that the ratio of the number of blades and vanes governs the direction of predominant radiation.

Thus the first factor of equation (72) controls the relation between forward and aft radiated sound. The second term, which is symmetrical about $\theta = 90°$, governs the detailed lobed structure of the radiation pattern and accounts for the phase cancellation effects occurring across the compressor.

In most practical cases both B and V are large numbers so that successive values of the Bessel function order are separated by large differences. For example, taking typical values $B = 40$, $V = 30$, $M - 0.5$ we see that the order mB-kV can take values . . . -50, -20, 10, 40, 70 . . . with arguments in the range 0 to 20 for m = 1. For the second harmonic, m = 2, mB - kV = . . . -40, -10, 30, 50 . . . with arguments between 0 and 40. Since Bessel functions of the first kind are symmetrical about order zero, it is only necessary to inspect positive orders and figure 15 shows J_0, J_{10}, and J_{20} plotted (in intensity form, i.e., $10 \log_{10} J^2$) against argument up to a value of 40. Since the functions oscillate about zero, the logarithmic intensity profiles exhibit periodic troughs whose frequency decreases with order. The important feature is that higher order functions appear and become significant at higher argument values. Thus in the example cited above, the first harmonic m = 1, whose argument range (corresponding to $\theta = 0$ through 90°) is $0 < mBM \sin\theta < 20$ will be largely dependent on the k = 1 mode, the k = 2 mode only appearing as $\theta \to 90°$. The second harmonic with $0 < mBM \sin\theta < 40$ will receive contributions from the k = 1,2 and possibly 3 modes depending on the value of the respective airload harmonics.

Figure 16 which is reproduced from reference 1 gives a very clear illustration of the Bessel function effect. This is an array of directivity plots corresponding to increasing argument across the page from left to right and increasing order down the page. In physical terms, the argument increases with harmonic number, number of blades, and tip speed (all of which cause an increase of frequency) and the order with modal order (which tends to increase as the difference between the number of blades and vanes diverges. The clear message associated with this figure is that the number of lobes in the pattern increases with frequency and that sideways directivity is emphasized by increasing modal order.

One of Lowson's most significant findings was the existence of a source "cutoff" effect. Analytically this is tied to the behavior of the Bessel functions; physically, to the phase velocity of the blade/vane interactions. Essentially the consequence is that a tip speeds lower than some critical value, radiation efficiences rapidly diminish. In fact these critical values correspond almost exactly to Tyler and Sofrin's duct cutoff frequencies, which prompted Lowson's conclusion

that the presence of a hardwalled duct is of little consequence. The decay effects would be observed even if the duct were not there. Another related effect is that only a limited number of acoustic modes contribute to any particular sound harmonic, since the frequency lies in the inefficient radiation range of the remainder. It was shown in reference 1 that the number of contributing modes is given by the approximation

$$\frac{mB}{V} \; (1 - M\sin\theta) \leq \; k \; \leq \frac{mB}{V} \; (1 + M\sin\theta)$$

a criterion which has been used in the computations of the present study.

4.2 Comparison of Theory and Experiment

The main objective of this study is to determine how well the analytical model described in previous sections predicts the noise radiation of real compressors. For this purpose, noise data from three fan systems have been used, including a small research compressor and two full scale aft-fan engines. Unfortunately only a few basic flow measurements were made in each case and no data was available on the unsteady aerodynamic effects which are so important to the noise problem. Consequently it has been necessary to use the methods described in section 2.2 to estimate the necessary force input to the acoustic calculations. The research compressor data was obtained by Crigler and Copeland (ref. 4) at the Langley Research Center anechoic facility using a single IGV/rotor stage with a total thrust in the order of 100 lb. The full scale data, supplied by the Rolls Royce Company, was obtained out of doors around research engine test stands. These fans, designated Aft Fan 1 and Aft Fan 2 for present purposes, have estimated maximum thrusts of approximately 1000 and 5000 lbs, respectively. Of the three sets of data, that of Crigler and Copeland, being measured under accurately controlled laboratory conditions is considered to be the most reliable. The estimated design parameters of significance to the noise problem are listed in table II for each of the three fans. The correlation between theoretican and experimental results in each case will now be discussed in turn.

Crigler and Copeland's research compressor was manufactured from components taken from a multi-stage aircraft engine compressor. It consisted of a single stage comprising inlet guide vanes and a rotor mounted inside a faired duct. The inlet duct was of the order of three rotor diameters in length, and the outlet duct was extended to remove the exhaust flow from the test area. The blade assemblies were modified to enable the axial spacing between the IGV's and rotor blades to be varied and also the number of inlet guide vanes could be varied from 31 to 53 to 62. The number of rotor blades was fixed at 53. The entire unit, including an electric motor and dirve assembly, was mounted inside an anechoic chamber. A microphone attached to a rotating boom was used to measure sound pressure levels in the quadrant from $\theta = 0$ to $\theta = 90°$ on a 12 ft diameter circle centered on the duct inlet. The first harmonic sound components were extracted by passing the microphone output through a one-third octave harmonic filter encompassing the harmonic frequency.

The data are compared with theoretical results obtained using the fan parameters of table II in figures 17 through 23. Figures 17 through 19 show the directivity patterns only, and for

TABLE II

ESTIMATED COMPRESSOR PARAMETERS FOR
THREE EXPERIMENTAL UNITS

	Research Fan	Aft-Fan 1	Aft-Fan 2
Approximate gross thrust, T (lb)	100	1000	5000
Mean duct CSA at rotor, A (ft^2)	0.556	2.33	6.78
Mean blade radius, R (ft)	0.531	0.793	1.79
Contraction ratio, A/A_E	1.88	1.605	1.97
Nondimensional IGV-rotor separation	1.035[+]	1.3	2.1
Nondimensional rotor-stator separation	- -	1.3	1.5
Number of IGV's, V_v	31, 53, 62	43	5[*]
IGV chord (ft)	0.0584	0.194	0.335
Number of rotor blades, B	53	31	43
Rotor blade chord (ft)	0.0584	0.242	0.3
Number of stator vanes, V_s	- -	50	50
Stator vane chord (ft)	- -	0.183	0.32
Rotor inlet swirl ratio, λ_i	0	0.14	0
Axial flow ratio, μ	0.422	0.477	0.645[++]

[+]   Could be varied

[++] Varied slightly with RPM, significantly below 2500 RPM

[*]   Faired supports only

convenience, two sets of data are plotted back to back on each figure. Each plot has been normalized with respect to the maximum sound pressure level. For various reasons similar to those discussed in section 2.1, the pronounced lobes in the theoretical radiation patterns will not be so exaggerated in practice. This is because various propagational and spatial source effects tend to round out the profiles "filling in" the holes and reducing the peaks. Directional features become more obscured with increasing distance from the source. Taking this into account it appears that, with a few notable exceptions, the analytical results in figures 17 to 19 are fair representations of the measured directivity patterns. The main exceptions are evident in figure 19 (a), in the vicinity of 80 - 90 degrees on figure 17, and 0 - 20 degrees in figures 18 and 19. In each of these cases the disagreement appears as an underestimation of sound pressure level in the theoretical result. Whereas this might be partially explained by the "filling in" effect, it is more probably attributable to noise radiation by other components of the test set-up not accounted for in theory. In figure 19 (a) the additional sideways radiation could well be generated by the inlet guide vanes themselves due to potential flow interference from the rotor. This effect, which would in any case only arise for very small row spacings, has not been accounted for in the theory.

Figure 20 compares the measured and calculated absolute first harmonic sound pressure levels for the three sets of inlet guide vanes (62, 53, and 31 vanes) which a rotor/IGV chordal spacing of 1.035 lengths (i.e., for almost zero clearance between rows). Except for the locations mentioned above, the measured and calculated levels are in good agreement, the only exception being the 31 inlet-guide vane case where again the theoretical levels are a little low.

The effect of inlet-guide-vane/rotor separation is shown for the three inlet-guide-vane configurations in figures 21 to 23. These results indicate that the wake theory used takes adequate account of the row separation effect.

Particular note should be taken of figure 22 which corresponds to the case when the number of guide vanes and rotor blades are equal. This is the only situation in which axial radiation is predicted (see section 1.0) a fact which appears to be well supported by experiment.

The results obtained for the Crigler and Copeland fan, although confined to the first harmonic radiation, are considered to be encouraging. In particular, Lowson's conclusions regarding the hardwall duct seem to be justified, for in this case, the inlet duct was considerably longer than typical aircraft inlets, being three diameters, or more than 20 wavelengths, (at the higher RPM's) long. It is of interest to compare the present theoretical results with the radiation pattern predicted by Crigler and Copeland who used Tyler and Sofrin's radiation theory (see ref. 4, figs. 11 through 13). Whereas the Tyler and Sofrin results predict only the broadest features of the directivity pattern (in some cases only) the present theory without recourse to consideration of duct effects, predicts both overall sound pressure levels and directivity with some accuracy. It is interesting to contemplate what could be achieved if both source and duct effects were included simultaneously.

The full scale data included in this study was measured out of doors and run with the engine mounted horizontally a few feet above the ground. Both units were aft fan, by-pass stages driven by "slave" turbine engines. Attempts were made to screen the slave engine inlet noise

34

rom the microphones. The first two fan noise harmonics were measured, again using third-octave filters.

Turning to the first and smaller of these units, Aft Fan 1, theoretical results were computed using the input parameters listed in table III. These are compared with the experimental data in figures 24 through 26 for the first harmonics. Figure 24 corresponds to the design operating condition of the engine. Agreement in all three cases if fairly good although the validity of the comparison is uncertain. No information is available on background noise levels and the fan noise cannot be separated from the noise of the slave engine. Furthermore, the effects of sound reflection, refraction, and scattering, which are not accounted for theoretically, could be most significant.

Figures 27 and 28 show the results for the second and larger of the full scale fans, Aft-Fan 2. In this case the noise was measured on a line parallel to, and 100 ft from the engine axis. Because of the larger distances, the propagation effects mentioned above may be expected to be even more serious. Even so the agreement between the analytical and experimental results may be considered fair.

Attempts to correlate measured and calculated higher harmonic noise levels yeilded calculated levels which were of the order of 5-10 dB lower than experiment. It is possible that the simple theory used to predict the fluctuating blade airload is inadequate on the higher frequencies and further work is required to resolve this question.

4.3 Design Study

Having demonstrated the apparent accuracy of the compressor noise theory a short study has been made to illustrate its potential usefulness for design applications. Many of the basic design requirements for low noise, such as low tip speed and large spacings between blade rows, are well known but the present theory can now be used to attach quantitative significance to such measures. One of the problems in a design situation is of course that variables can rarely be varied independently. For example reduction of tip speed must be accompanied by other changes if a loss of performance is to be avoided. The methods described in section 2.2 have therefore been used as the basis for a realistic and consistent design analysis so that the full aerodynamic and acoustic consequences of parameter variations can be accounted for. The opportunity is also taken to examine in some detail the acoustic characteristics of compressors.

4.3.1 Baseline Case. — It was shown in section 2.2.2 that for incompressible inviscid flow, flow velocities through the fan are proportional to the rotor tip speed and that aerodynamic forces are proportional to the square of the tip speed. It is thus a fairly straightforward matter to study the effect of rotor tip speed on the noise radiation for a given fan system based upon these assumptions. In this and subsequent studies, a fan stage consisting of IGV's, rotor and stator, as illustrated in figure 2, has been adopted as a "design" or "baseline" case. The assumed design parameters are given in table III.

TABLE III

DESIGN PARAMETERS FOR BASELINE FAN STAGE

Gross static thrust, T	10,000 lb
Cross sectional area of duct, A (constant for each blade row)	10 ft^2
Mean blade radius, R	2 ft
Contraction ratio, A/A_E	2
Mean blade rotational Mach Number, M	0.7
Nondimensional row separation, d/c	1.0
Mean rotor swirl, λ	0.05
Number of rotor blades, B	40
Number of inlet guide vanes, V_v	35*
Number of stator vanes, V_s	47*

* These are numbers required to maintain given performance assuming equal
  blade chords and lift coefficients for all blades and vanes.

The methods described in section 2.2 were used to calculate the aerodynamic loadings
which are included in figure 29 as the solid curves marked "baseline". The total rotor thrust
is 9500 lb which indicates that 5 percent of the pressure rise across the rotor is dynamic, i.e.,
due to an increase in resultant velocity. As previously discussed, only when the mean rotor
swirl is zero does the rotor carry the total system thrust. It will be noted in figure 29 that the
first harmonic rotor blade thrust amplitude is less than 2 percent of the steady thrust per blade
and the higher harmonics fall off at a fairly high rate.

Figure 30 shows the first harmonic noise radiation pattern calculated for this case. The
vertical line represents the rotor axis, forward toward the top of the page, and the radiation
is, of course, symmetrical about this axis. The heavy line in figure 30 gives the total sound
pressure level, due to both rotor and stator noise on a 100 ft radius. In order to illustrate the
origins of this rather complex pattern, the constituent modes of significance are also indicated.
It can be seen that in the forward sector, the rotor and stator contribute approximately equally,
whereas in the aft sector the field is dominated by the rotor. The main reason for this can be
found in the discussion of section 4.1. The rotor noise results from the interaction with the
wakes from the 35 inlet guide vanes. Considering only the k = 1 mode, $kV/mB = 35/40 = 0.875$,

so that this mode may be expected to radiate slightly more noise aft then forward. The $k=1$ modal plot shows that this is indeed the case although the difference is only of the order of 2 dB. Turning now to the stator, which has 47 blades; its noise is the result of interactions with 40 rotor blade wakes so that, again for the $k=1$ mode, $kV/mB = 47/40 = 1.175$. Consequently the stator will radiate more noise in a forward direction. Figure 30 shows that the difference is around 7 dB. Consequently although the rotor and stator contributions are almost equal near to the forward axis, the stator noise is around 9 dB less than the rotor noise near $\theta = 100°$ only. The greatly increased sideways radiation of the second mode, relative to the first, as indicated by figure 30 can be clearly seen. For the stator (where now in eq. 61 $V = V_s$) only the first mode makes any contribution throughout the angular range.

The close similarity between the $k=1$ modal patterns for both rotor and stator simply result because the Bessel function orders ($|mB - kV_v|$) and ($|mB - kV_s|$) are not substantially different (5 and 7). Note that there is no radiation along the axis, either forward or aft. This only occurs in fact for "siren" modes, i.e., when $mB = kV$. That this should be so is fairly easy to understand physically since in this case the latter case the axis is surrounded by a ring of equal phase sources which will obviously be heard on the axis. When $kV \neq mB$ all sources are effectively out of phase with the phase angle passing through an integral number of cycles around the ring of sources. In such cases the radiation always cancels on the axis.

Figure 31 shows the equivalent results for the second harmonic sound field ($m = 2$) although now the picture is somewhat more complicated. To simplify the plot, as far as is possible, the rotor and stator radiation modes are drawn on opposite sides of the centerline. The continuous curve is the same in each case and represents the total sound pressure level on the 100 ft radius due to the complete fan stage. This time there are six significant modes altogether, corresponding to $k = 1, 2,$ and 3 for both rotor and stator. That roughly twice as many modes contribute to the second harmonics as to the first should of course be expected for the criterion given as equation (61) where m is now 2. Probably the most striking feature of figure 31 is that the rotor and stator are just about equally important around the azimuth. The differences this time are much more detailed and relative contributions change every few degrees.

4.3.2 Effect of RPM. — Figure 32 shows the acoustic effects of running this same fan at different RPM's. The curves in this figure show the first harmonic sound pressure level variation on the 100 ft radius for different rotor blade rotational Mach numbers in the range $0.4 \leq M \leq 0.9$. In evaluating these curves it must be remembered that the thrust (and other forces) is proportional to M^2 and the frequency to M.

The obvious features of these results are that as rotational Mach numbers increase

- overall sound power increases,
- the number of radiation lobes increases, and
- there is a dramatic increase in sideways radiation at high Mach numbers.

37

There is little point in plotting sound pressure level against Mach number for any radial position because the result will depend strongly upon the particular position chosen. Lowson showed in reference 1 that sound power output is approximately proportional to M^5, a result which agreed with available experimental data, and which may be expected to apply here also. The very substantial increase of sideways radiation for $M = 0.8$ and 0.9 is the consequence of additional modes entering the efficient radiation range as phase velocities increase.

4.3.3 Effect of Design Changes when Constant Performance is Maintained. — Although figure 32 illustrates very effectively the significant effect of blade rotational speed on noise output it does not give much indication of the potential of RPM control as a noise reduction procedure since reductions of tip speed are accompanied by very substantial reductions of performance. Consequently, blade speed changes have been included in an analysis of the acoustic effects of varying a number of design parameters, while maintaining constant system thrust. Naturally an infinite variety of such changes are possible and it has been necessary for present purposes to restrict the study to a number of very modest variations.

In order to isolate individual effects as far as possible, parmeters were varied one at a time about a set of baseline values, which are those listed in table III. The parameters varied were

- rotational Mach number, M
- number of rotor blades, B
- mean rotor swirl, λ
- row separation, d/c
- number of IGV's, stator vanes, V_v, V_s

To avoid changes of performance during parameter variations, blade chord changes were made, commensurate with constant lift coefficient. The relative numbers of IGV's, rotor blades and stator vanes were controlled by adopting the same chord dimensions for each. The nearest integral number was selected for each row which gave a lift coefficient closest to the design value. The parameter variations and the associated changes in the dependent variables are listed in table IV. It should be noted that to vary the number of IGV's and stator vanes to specific values, the chord dimensions had to lift free to vary.

4.3.3.1 Effect of Tip Speed (or Rotational Mach Number M). — For direct comparison with the results discussed above and shown in figure 32, the first design variation examined was that of rotational speed, this time maintaining constant performance. Before examining the acoustic results however, it is as well to look at some of the aerodynamic changes introduced. The major ones, indicated in table IV that when increasing the rotational Mach number from 0.4 to 0.9,

a) The number of inlet guide vanes changes from 27 to 39; this is to maintain the mean rotor swirl at the same percentage of the blade rotational speed,

TABLE IV

VARIABLES IN CONSTANT PERFORMANCE PARAMETER STUDY

Independent Variables				Dependent Variables							
M	B	λ	d/c	V_v	V_s	C (ft)	tan ϕ_R	Tan ϕ_s	T_o	$T1_R$ (lb per blade)	$T1_S$
0.7	40	0.05	1.0	35	47	0.476	0.615	1.492	237.5	3.808	2.419
0.4	.	.	.	27	30	1.196	1.077	0.933	"	5.878	8.895
0.5	.	.	.	30	35	0.843	0.862	1.137	"	5.230	5.293
0.6	.	.	.	33	41	0.622	0.718	1.324	"	4.487	3.444
0.8	.	.	.	37	54	0.375	0.538	1.641	"	3.239	1.770
0.9	.	.	.	38	63	0.302	0.479	1.771	"	2.733	1.327
1.0	.	.	.	39	72	0.249	0.431	1.882	"	2.307	1.043
.	20	.	.	18	24	0.952	0.615	1.492	475	5.389	3.350
.	30	.	.	26	35	0.635	0.615	1.492	316	4.392	2.812
.	50	.	.	44	59	0.381	0.615	1.492	190	3.412	2.149
.	60	.	.	53	71	0.317	0.615	1.492	158.3	3.113	1.959
.	.	0.1	.	30	55	0.458	0.65	1.323	225	2.970	2.512
.	.	0.2	.	19	73	0.423	0.731	1.079	200	1.519	2.575
.	.	0.3	.	6	95	0.389	0.835	0.911	175	0.395	2.496
.	.	.	1.2	35	47	0.476	0.615	1.492	237.5	3.397	2.133
.	.	.	1.5	"	"	"	"	"	"	2.939	1.833
.	.	.	3.0	"	"	"	"	"	"	1.912	1.090
.	.	.	6.0	"	"	"	"	"	"	1.201	0.585
.	.	.	11.0	"	"	"	"	"	"	0.758	0.269
.	.	.	.	20*	20*	0.836/1.123[+]	"	"	"	3.808	3.697
.	.	.	.	35*	35*	0.478/0.642[+]	"	"	"	3.808	2.797
.	.	.	.	60*	60*	0.279/0.374[+]	"	"	"	3.808	2.138

*Specified.

+IGV Chord/stator chord (rotor blade chord = 0.476 ft.)

b)   The number of outlet guide vanes (i.e., stator vanes) increases from 30 to 72 in order to remove the increasing rotor outlet swirl component,

c)   The blade chord reduces from 1.197 ft to 0.249 ft to maintain equal thrust at the same lift coefficient,

d)   The rotor inflow angle (ϕ_r) reduces from 1.077 to 0.431 so that the torque thrust/ratio reduces (conversely the stator inflow angle (ϕ_s) more than doubles from 0.933 to 1.881), and

e)   The harmonic blade airloads change substantially as shown in figure 33; the low harmonic amplitudes decreasing with Mach number, the higher harmonics increasing. This is mainly the result of changes in chord and swirl velocities.

Figure 34 shows the acoustic effects of these design changes on the first sound harmonic. At first sight this is similar to figure 32 which shows the effect of merely changing the RPM of the "baseline" fan stage.

However, closer examination reveals that the sound pressure variations are not as great when constant thrust is maintained. The sideways radiation ($\theta = 90°$) is greatest when $M = 0.9$, as before, but is only 13 dB less when $M = 0.4$ (as opposed to approximately 43 dB previously). Furthermore, the $M = 0.4$ case gave more sideline noise than the intermediate values investigated. In fact there is remarkably little variation between the results for $M = 0.5$ through 0.8 except in the detailed lobal structure of the patterns.

Particularly noteworthy in the $M = 0.9$ curve is its near symmetry about $\theta = 90°$. This is the result of the closeness between the numbers of rotor blades and inlet guide vanes (40 and 39, respectively). As seen previously the pattern becomes perfectly symmetrical when $mB = kV$.

4.3.3.2 Effect of Number of Rotor Blades. — Although the effects of five variations of rotor blades were investigated, only three are shown in figure 35 for clarity. The three curves correspond to $B = 20$, 40, and 60. The main aerodynamic result of changing blade number is of course to reduce the chord dimension since the solidity remains approximately constant for constant lift coefficient. Due to the design constraints imposed, changes of rotor blade number are accompanied by changes in the number of inlet guide vanes and stator vanes, again mainly due to the changes of chord length. The effects are summarized in table IV. Figure 35 clearly indicates that changing the number of blades has very little effect on the first harmonic noise output.

4.3.3.3 Effect of IGV and Stator Vane Number. — Much more dramatic effects may be observed in figure 36 which shows the effect upon the first harmonic noise of changing either V_v or V_s. The plots show the noise radiated by either the rotor or stator which, under the conditions imposed, are acoustically equivalent. The main reason for the significant changes here is that the number of rotor blades is unvarying and similar results would have been seen in figure 35 if B had been varied for constant V_v and V_s. The sideways shift in emphasis for $V = 60$ can be seen in figure 36 together with a general reduction in sound power.

4.3.3.4 Effect of Mean Rotor Swirl. — As discussed in section 2.2 inlet guide vanes are installed upstream of the rotor to increase the total pressure rise obtainable. The mean rotor swirl is simply the average of the (nondimensional) inlet and outlet swirl velocities at the rotor, and generally decreases with the amount of (negative) pre-swirl imparted to the rotor inlet flow. Thus the lower the mean swirl, the higher the number of IGV's required. This is indicated in table IV, where it is shown that as λ decreases from 0.3 to 0.05, V_1 increases from 6 to 35. As might be expected the result of this change on the sound radiation is very significant. Figure 37 illustrates that the first harmonic sound pressure level is reduced by around 20 dB. This is at least in part due to the fact that as less and less inlet swirl is applied, more and more stator vanes are required to recover axial flow downstream of the rotor leading to substantial increases in their modal order mB-kV. Removal of IGV's together with a corresponding increase in the number of stator vanes clearly represents a powerful noise control technique.

4.3.3.5 Effect of Row Separation. — An accepted engineering technique for decreasing the radiated noise is to increase the axial spacing of blade rows. Lowson (ref. 1) discussed this at some length and in particular pointed out that different effects might be expected for rotors and stators. Basically this is becuase for the stator any sound harmonic is generated by airload fluctuations of the same frequency so that increasing row spacing, which preferentially reduces the higher harmonic airloads, should reduce the higher sound harmonics most effectively. On the other hand, rotor blade airload harmonics contribute to all sound harmonics so that a fairly uniform decrease in sound spectrum level might be expected.

To investigate this effect, results have been computed for the baseline fan system for a range of axial spacings between blade rows. The parameter d/c was varied in steps between 1.0 and 4.0 which correspond to clearances of 0 to 10 chord length. The resulting reductions in the harmonic airloads for both rotor and stator are shown in figure 29. The ordinate in both graphs is the harmonic thrust component per blade. It can be seen that the fluctuating load levels decrease very rapidly with row separation.

The effects of this airloading reduction on the first three harmonics are illustrated in figures 38 through 40. The lobed pattern, clearly evident for the first harmonic, is less marked for the higher harmonics. This is a direct result of an increasing number of contributing modes with harmonic numbers. Ignoring the differences in the directivity patterns, however, the most obvious fact indicated by this comparison is that increased row spacing more effectively reduces the higher harmonic sound levels for the complete system.

Some individual variations for the rotor and stator are shown in figure 41, which bear out Lowson's conclusions described above. In each case, results are plotted for three azimuth stations, namely 45°, 90°, and 135° from the fan axis. Sound pressure levels are shown as functions of the separation parameter d/c and are referred to the value dor d/c = 1. Each individual graph therefore compares the decay rates for the first, second, and third sound harmonics.

The stator results are similar for all azimuth positions, and very approximately, a doubling of the separation distance between rotor and stator reduces the first harmonic sound by 6 dB, the second by 12 dB, and the third by 15 dB. The rotor results on the other hand vary considerably with azimuth location although in general the sound pressure level reductions achieved

are not so significant. The first harmonic is reduced by about 4 dB per separation doubling, the second by about 5 dB and the third by between 4 and 8 dB.

Thus, it seems reasonable to conclude that if the stator noise dominates, which it will do in the absence of IGV's increasing row separation will be very effective in reducing noise. Rotor noise can be reduced by the same technique but the benefits (in dB) are only about half as great.

5.0 CONCLUSIONS

As a result of the current study the following conclusions regarding compressor noise radiation and its reduction have been reached:

1) Lowson's analytical results can be utilized in a simplified model which adequately predicts the first harmonic sound radiation by axial flow fans. The method appears to offer considerable promise for general purpose prediction purposes and can be adapted for studies of multi-stage compressor noise.

2) The method is amenable to hand calculation if results are required for a few field points only, particularly if the number of rotor and stator blades are similar. For detailed study of the sound field, however, computerized methods are recommended.

3) A simple two-dimensional aerodynamic model for estimating both steady and fluctuating blade airloads appears to give sufficiently accurate results for use in the noise prediction method. However, some refinement appears necessary for the second and higher sound harmonics.

4) Neglect of duct propagation effects appear to be justified in the light of other uncertainties.

5) Based on the results of a simplified parameter study in which the effects of design changes on a constant performance fan stage were investigated, the following steps appear to offer the most promise for noise reduction purposes:

- Reduction in the number, or elimination, of the inlet guide vanes (along with an associated increase in the number of stator vanes).

- An increase in the axial separation between blade rows.

6) In the same study the following steps did not appear to offer much noise reduction.

- Reduction of tip speed.

- Variation of the number of rotor blades. (Although variations of the rotor blade/IGV/stator vane ratios can have a profound effect and should always be studied in detail).

7) Further development of the theoretical prediction method is desirable, but will be difficult until more accurate, comprehensive experimental data are available.

6.0 REFERENCES

1. Lowson, M. V., "Theoretical Studies of Compressor Noise," Wyle Laboratories Research Staff Report No. WR 68-15, August 1968.

2. Gutin, L. Ya., "On the Sound Field of a Rotating Propeller, " from Physiks Zeitschrift der Sovietunion, Band A Haff 1, (1936) pp. 56-71, Translated as NACA TM 1195, 1948.

3. Tyler, J. M. and Sofrin, T.B., "Axial Flow Compressor Noise Studies," SAE Transactions, pp. 309-332, 1961.

4. Crigler, J.L. and Copeland, W.L., "Noise Studies of Inlet Guide Vane-Rotor Interaction of a Single Stage Axial Flow Compressor," NASA TN D-2962, 1965.

5. Lighthill, M.J., "On Sound Generated Aerodynamically," Proc. Roy. Soc., A211, pp. 564-587, 1952.

6. Ffowcs Williams, J.E. and Hawkings, D.L., "Theory Relating to the Noise of Rotating Machinery," Aeronautical Research Council ARC 29 821, January 1968.

7. Lowson, M.V. and Ollerhead, J.B., "A Theoretical Study of Helicopter Rotor Noise," J. Sound Vib., Vol. 9, No. 2, pp. 197-222, 1969.

8. Betz, A., Introduction to the Theory of Flow Machines, Pergamon Press (1968).

9. Kemp, N.H. and Sears,W.R., "Aerodynamic Interference Between Moving Blade Rows," J. Aerospace Sci., Vol. 20, No. 9, pp. 585-598, 1963.

10. Kemp, N.H. and Sears, W.R., "The Unsteady Forces due to Viscous Wakes in Turbomachines," J. Aerospace Sci., Vol. 22, pp. 478-483, 1955.

11. Sears, W.R., "Some Aspects of Non-Stationary Airfoil Theory and its Practical Applications," J. Aerospace Sci., Vol. 8, pp. 104-188, 1941.

12. Silverstein, A., Katzoff, S. and Bullivant, W.K., "Downwash and Wake Behind Plain and Flapped Airfoils," NACA Report 651, 1939.

13. Olver, F.W.J., "Bessel Functions of Integral Order," Chapter 9, Handbook of Mathematical Functions with Formulas, Graphs, and Mathematical Tables, Abramowitz, M. and Stegun, I.A., editors, U.S. Govt. Printing Office, 1968.

14. Morfey, C.L., "Rotating Pressure Patterns in Ducts: Their Generation and Transmission," J. Sound. Vib., Vol. 1, No. 1, pp. 60-87, 1964.

15. Ollerhead, J.B. and Munch, C.L., "An Application of Theory to Axial Compressor Noise. Appendix C: Bessel Functions of the First Kind: A Table of Values for Orders to 179 and Arguments to 211," NASA CR-66859, July 1969.

For a complete bibliography, the reader is directed to reference 1 of this report.

APPENDIX A

RECURRENCE METHOD TO CALCULATE BESSEL FUNCTION VALUES

The recurrence method mentioned in section 3.0 for the calculation of Bessel function values has been found to be the fastest method when a number of functions having the same argument but different orders are needed. It is particularly well suited to calculation of functions of large numerical order and/or agreement.

The method basically derives from two fundamental relationships for Bessel functions given by Olver (ref. 13) as the following:

$$J_{n-1}(x) + J_{n+1}(x) = \left(\frac{2n}{x}\right) J_n(x) \tag{A-1}$$

$$J_0(x) + 2J_2(x) + 2J_4(x) + \ldots = 1 \tag{A-2}$$

Or, rewriting equation (A-1)

$$J_{n-1}(x) = \left(\frac{2n}{x}\right) J_n(x) - J_{n+1}(x) \tag{A-3}$$

Thus, if $J_n(x)$ and $J_{n+1}(x)$ are known, $J_{n-1}(x)$ can be calculated and likewise $J_{n-2}(x)$, $J_{n-3}(x)$, etc. The problem obviously is one of determining the values of $J_{n+1}(x)$ and $J_n(x)$ for which to start the process.

For a given argument x there is a number q such that $J_q(x) = 0.00$ to any number of significant digits. If we then start the recursion at this point and assume that $J_{q-1}(x) = 1$, equation (A-3) can be written as the relation,

$$J_{q-2}(x) = \frac{2(q-1)}{x} J_{q-1}(x) - J_q(x) \tag{A-4}$$

or

$$J_{q-2}(x) = \frac{2(q-1)}{x} \tag{A-5}$$

and then

$$J_{q-3}(x) = \frac{2(q-2)}{x} \cdot \frac{2(q-1)}{x} - 1 \tag{A-6}$$

In this manner all the functions down to $J_0(x)$ can be calculated.

Since the calculated values must meet the requirements imposed by equation (A-2) they must be normalized by dividing each value by the factor $1/(J_0(x) + 2J_2(x) + \ldots)$ where the values in the denominator are the values calculated by the recursions of equations (A-4), (A-5), and (A-6). At this stage all Bessel function values from $J_0(x)$ to $J_q(x)$ are available. The problem of calculating function values up to $J_n(x)$ is one of determining the value of $q > n$ at which to start the recursion. If q is too small, inaccurate values are obtained; if q is too large unnecessary calculations are performed. The criteria developed for the selection of q is that the error in the function value be less than approximately 10^{-5} after the first recursion. This is done by selecting q to be:

$$q = \left\{ \begin{array}{ll} |x| + 5x^{1/3} & , \quad x \leqslant 8 \\ |x| + 10 & , \quad x > 8 \end{array} \right\} \quad x \geqslant n$$

$$q = \left\{ \begin{array}{ll} n + 5x^{1/3} & , \quad x \leqslant 8 \\ n + 10 & , \quad x > 8 \end{array} \right\} \quad x < n$$

(A-7)

To illustrate the method an example is presented.

It is desired to calculate the value of $J_0(x)$, $J_1(x)$, . . . $J_5(x)$ where $x = 3$. From equation (A-7) the value of q is given as:

$$q = 5 + 5(3)^{1/3} = 13$$

Then,

$$J_{13}(3) = 0, \quad J_{12}(3) = 1$$

$$J_{11}(3) = \frac{2(12)}{3}(1) - 0 \approx 8$$

$$J_{10}(3) = \frac{2(11)}{3}(8) - 1 \approx 58$$

.

.

.

$$J_0(3) = -1160994$$

Now the normalizing factor becomes

$$1/(-1160994 + 2(2168733) + 2(591337) + \ldots + 2(1)) = 1/4465876$$

46

The resulting function values are given by:

Function	Not Normalized	Normalized	Tabulated Values (Ref. 13)
$J_1(3)$	0	0.000000	
$J_{12}(3)$	1	0.000000	
$J_{11}(3)$	8	0.000001	
$J_{10}(3)$	58	0.000012	
$J_9(3)$	379	0.000084	0.000084
$J_8(3)$	2216	0.000496	0.000493
$J_7(3)$	11439	0.002561	0.002547
$J_6(3)$	51090	0.011440	0.011394
$J_5(3)$	192921	0.043198	0.043028
$J_4(3)$	591337	0.132412	0.13203
$J_3(3)$	1380035	0.309017	0.30906
$J_2(3)$	2168733	0.485623	0.486091
$J_1(3)$	1511609	0.338479	0.339059
$J_0(3)$	-1160994	-0.259970	-0.260052

Thus it can be seen that the calculated values are within about 10^{-4} or 10^{-5} of the tabulated values from reference 13. If closer accuracy is desired the recursion can be calculated again but starting with $q = 21$ which gives results with the error approximately 10^{-9} or 10^{-10}.

Note that the value for, in this case $J_{12}(3)$ need not have been 1; indeed, any convenient value can be chosen. This can become a necessity if the un-normalized numbers become larger than computer size limitations allow.

One additional factor to take into consideration is the calculation of Bessel function values is that of case of negative order or argument. In this case, the values can be calculated knowing the relationships:

$$J_{-n}(x) = (-1)^n J_n(x)$$

$$J_n(-x) = (-1)^n J_n(x)$$

(A-8)

47

APPENDIX B

EXAMPLE OF HAND CALCULATION METHOD

For the purposes of demonstrating the use of the hand calculation method described in section 3.3, the parameter study baseline case will be used as an example. It should be noted that when using this method, it is advisable to calculate a few points in the immediate vicinity of the location desired to be certain that the point selected did not happen to fall on one of the minima of the lobal structure. The calculation will be performed at an azimuth location (θ) of 45° and radial distance of 100 ft. Auxiliary points will be taken at 43° and 48°.

(1) Parameters:

$$B = 40 \qquad V = 35 \qquad s = 47$$

$$R = 2.0 \text{ ft} \qquad r_1 = 100 \text{ ft} \qquad \theta = 45^\circ$$

$$m = 1 \qquad M = 0.7 \qquad (D/T)_r = 0.615$$

$$(D/T)_s = 1.492$$

(2) Range of significant modes "k":

Rotor: $\quad k_{min} = \dfrac{mB}{V_v} \ (1 - M \sin \theta) = \dfrac{1.40}{35} \ (1 - 0.7\,(.707)) = 0^*$

$\quad\quad\quad\quad k_{max} = \dfrac{mB}{V_v} \ (1 + M \sin \theta) = \dfrac{1.40}{35} \ (1 + 0.7\,(.707)) = 2^{**}$

Stator: $\quad k_{min} = \dfrac{mB}{V_s} \ (1 - M \sin \theta) = \dfrac{1.40}{47} \ (1 - 0.7\,(.707)) = 0^*$

$\quad\quad\quad\quad k_{max} = \dfrac{mB}{V_s} \ (1 + M \sin \theta) = \dfrac{1.40}{47} \ (1 + 0.7\,(.707)) = 2^{**}$

(3) Using the methods of section 2.2 of the text, required force harmonics are calculated to be:

Rotor: $\quad T_0 = 237.5 \text{ lb/blade}$

$\quad\quad\quad\quad T_1 = 3.81 \text{ lb/blade}$

$\quad\quad\quad\quad T_2 = 2.59 \text{ lb/blade}$

Stator: $\quad T_1 = 2.42 \text{ lb/blade}$

48

(4) The constant terms become:

Rotor: $\dfrac{B}{2\pi R r} = \dfrac{40}{2\pi (2)(100)} = 3.18 \times 10^{-2}$ ft^{-2}

Stator: $\dfrac{S T_1}{2\pi R r} = \dfrac{(47)(2.42)}{2\pi (2)(100)} = 9.05 \times 10^{-2}$ ft^{-2}

Both: $mBM \sin\theta = 1.(40)(0.7)(0.707) = 19.8$

$mBM \cos\theta = 1.(40)(0.7)(0.707) = 19.8$

(5):

Rotor ←——————————————— Step 5 ————————————————→

k	$mB - kV_v$	$(mB - kV_v)\left(\dfrac{F}{T}\right)_r$	$mBM\cos\theta -$ $(mB-kV)\left(\dfrac{F}{T}\right)_r$	T_k	$\dfrac{B T_k}{2\pi R r}\{mBM\cos\theta -$ $(mB-kV)(D/T)_r\}$	$20\log_{10}\left\|\{\ \}\right\|$
0	40	24.6	−4.8	237.5	−36.2	31.2
1	5	3.18	16.6	3.81	2.01	6.06
2	−30	−18.5	38.3	2.59	3.15	9.96

Stator

k	$mB - kV_s$	$(mB - kV_v)\left(\dfrac{F}{T}\right)_s$	$mBM\cos\theta -$ $(mB-kV_s)\left(\dfrac{F}{T}\right)_s$		$\dfrac{V_s T_m}{2\pi R r}\{mBM\cos\theta -$ $(mB-kV_s)(F/T)_s\}$	$20\log_{10}\left\|\{\ \}\right\|$
0	40	59.6	−39.8		3.60	11.1
1	−7	−10.4	30.2		2.74	8.8
2	−54	−80.5	100.3		9.08	19.2

(6, 7, 8):

Rotor

10 $\log_{10}$ $J_{mB-k\sqrt{}}($)	20 $\log_{10}$ J	20 $\log_{10}$ C_{mkr}	SPL_{rk}
	← Step 6 →	← Step 7 →	Step 8
-91.6	-183.2	-152.0	-24.5
-8.9	-17.8	-11.7	115.8
-40.1	-80.2	-70.2	57.3

Stator

10 $\log_{10}$ J	20 $\log_{10}$ J	20 $\log_{10}$ C_{mks}	SPL_{sk}
-91.6	-183.2	-172.1	-44.6
-7.4	-14.8	-6.0	121.5
-183.9	-367.8	-348.6	-221.1

(9) The values of C_{ms} and C_{mr} are given by:

C_{mr} = 115.8 dB re: 0.0002 μ bar

C_{ms} = 121.5 dB re: 0.0002 μ bar   since modes other than k = +1 are negligible.

(10) The total sound pressure level is then calculated:

C_{mT} = 10 $\log_{10}$ [antilog (12.15) + antilog (11.58)]

C_{mT} = 122.4 dB re: 0.0002 μ bar

The total rotor and stator sound pressure level at an angle of 45° to the intake and 100 ft away is, then 122.4 dB. Since it is apparent that this field point is not located at a minima of the lobal pattern, where the level would be very small, it is probably not necessary to calculate the two auxiliary points at 43° and 48°. However, it might be advisable to check at least one of the other points.

It is apparent that if the number of significant modes or the number of desired field points is large, the calculation method can become very tedious and time consuming. For these instances the computerized approach appears to be the best solution. As mentioned previously, the method was developed to aid the designer, or operator, in spot checking the expected sound levels at one or two preselected points, not to perform a detailed study of the sound field. For the intended uses, the hand method appears to be more than adequate.

---

* Note that the values are rounded to the next lowest integer (e.g., 1.5→1)
* * Note that the values are rounded to the next highest integer (e.g., 1.5→2)
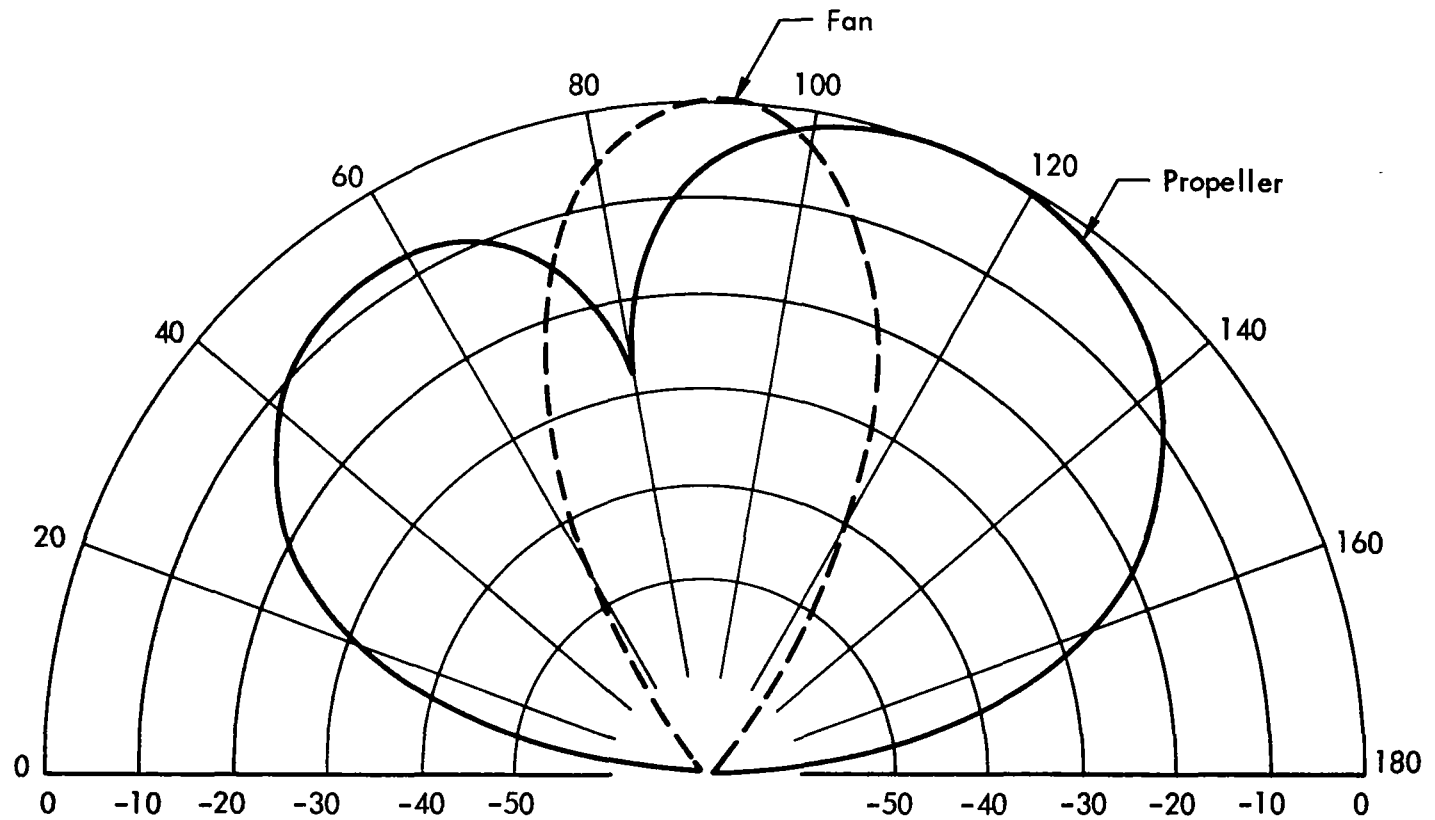
Figure 1. Comparison of First Harmonic Radiation Patterns for a Fan and a Propeller Due to Steady Loading Only and Operating in Free Air. Tip Speed = Mach 0.5 and Static Thrust of 1000 Pounds. Four Blade Propeller of 5-Foot Radius and D/T of 0.1. Forty-Blade Fan of 2.5-Foot Radius and D/T of 1.0.
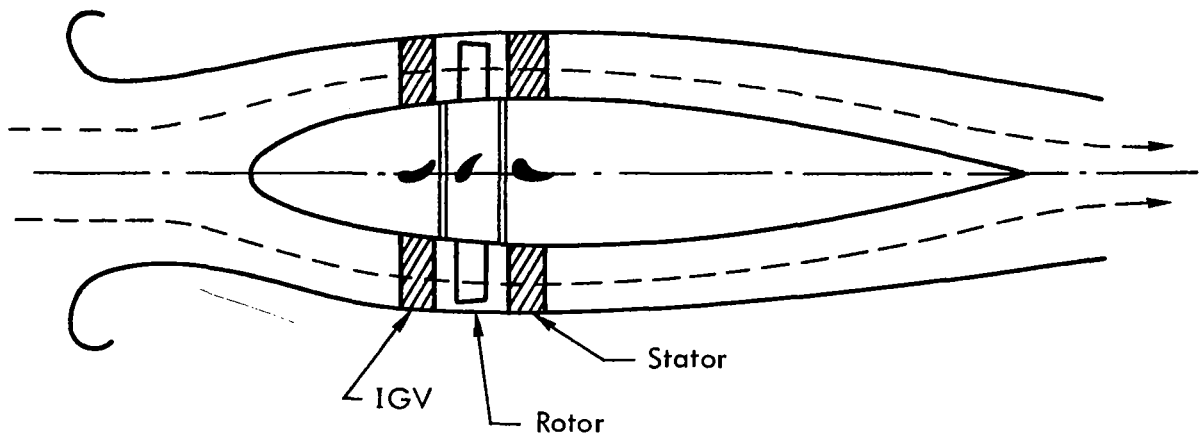
Figure 2. Fan System Geometry
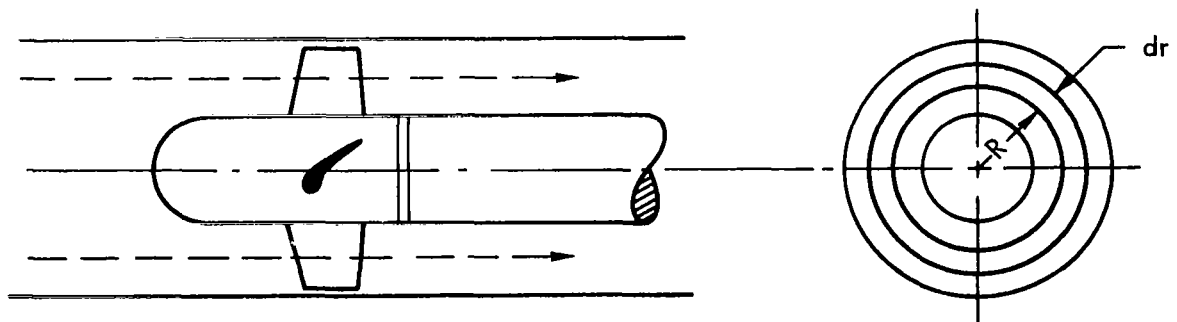
Figure 3. A Simple Axial Flow Fan
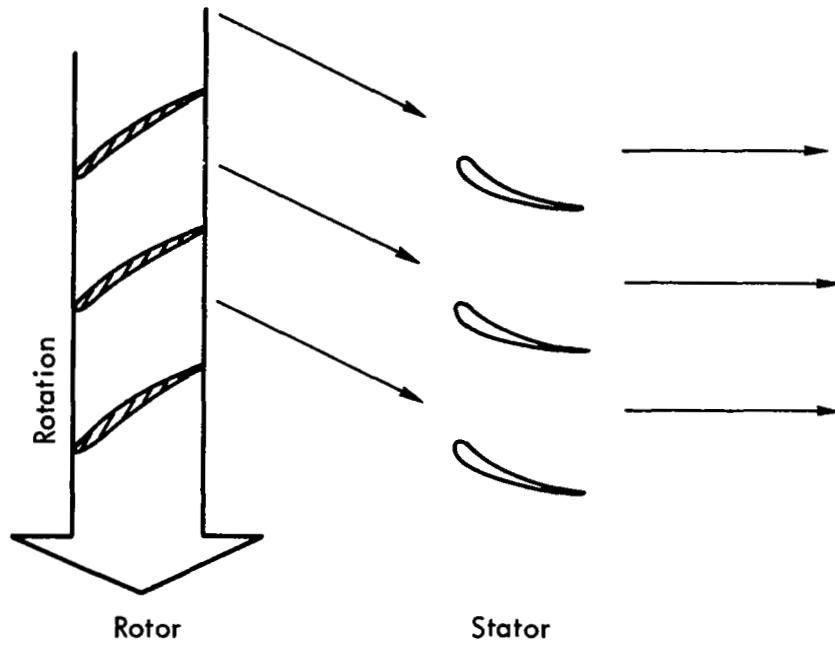
Figure 4. Effect of Stator Vanes on Flow
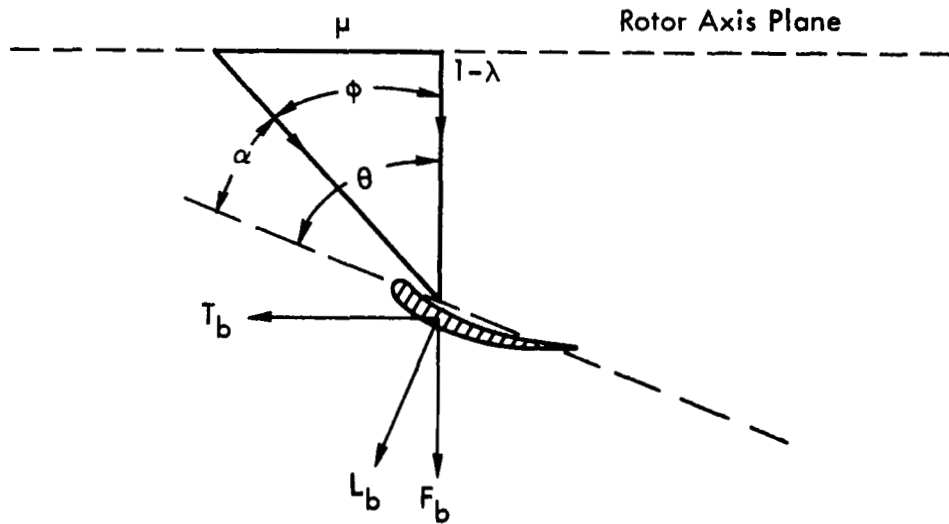
Figure 5. Rotor Blade Flow Geometry
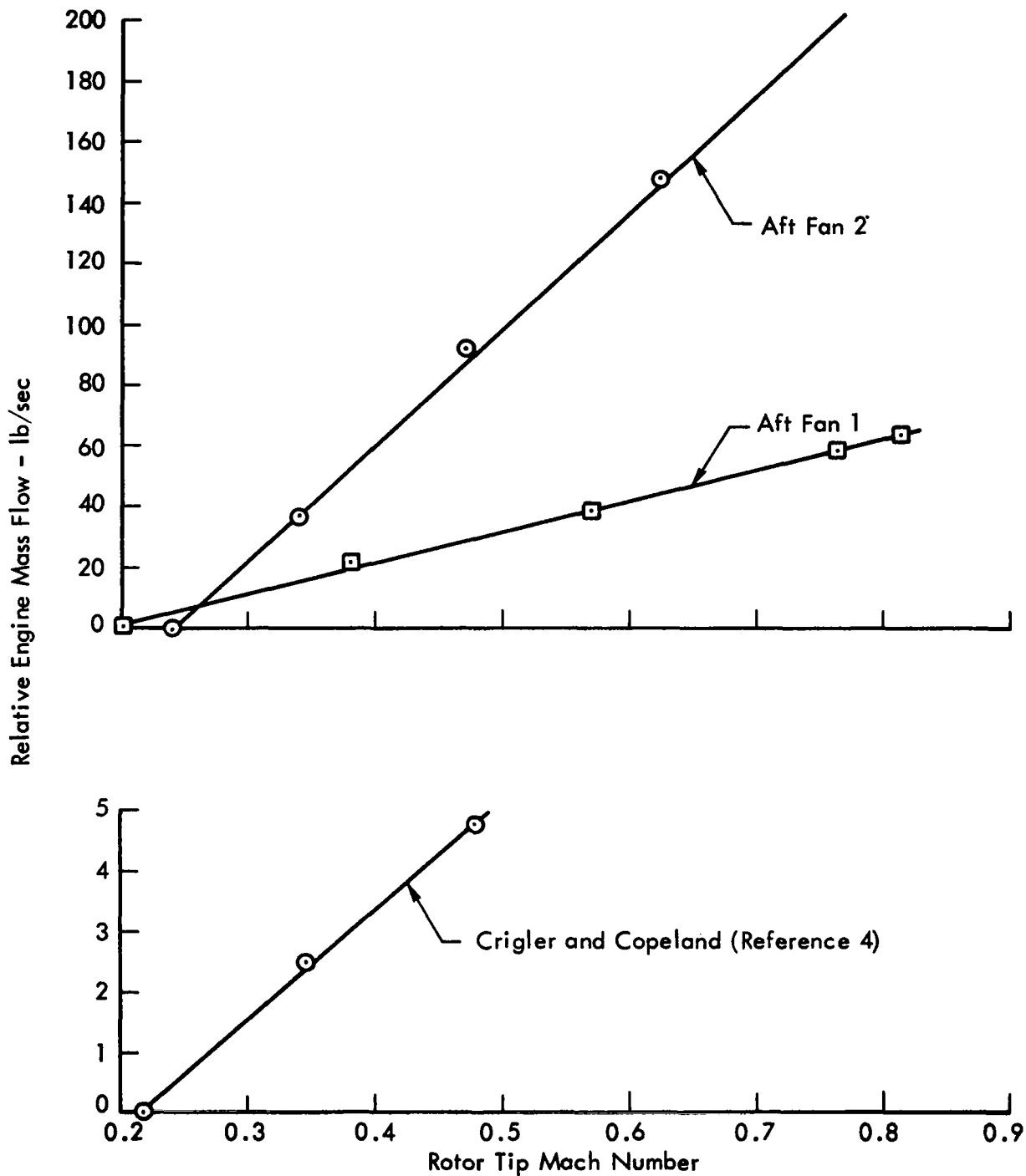
Figure 6. Measured Variation of Engine Mass Flow Rate
with Rotor Tip Speed
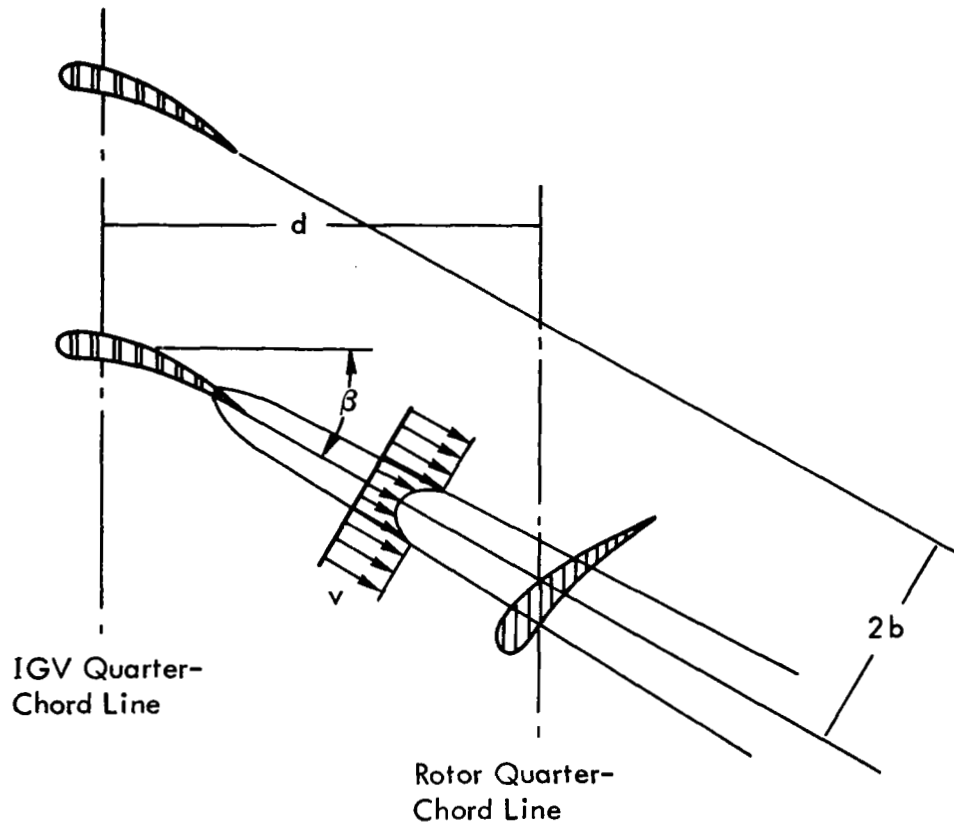
Figure 7a. Wake Intersection Geometry
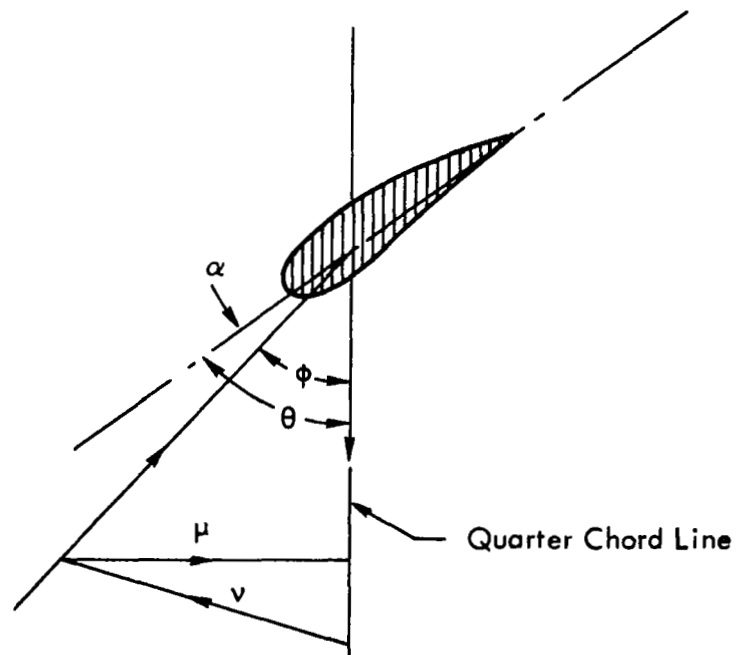
Figure 7b. Flow Velocity Diagram
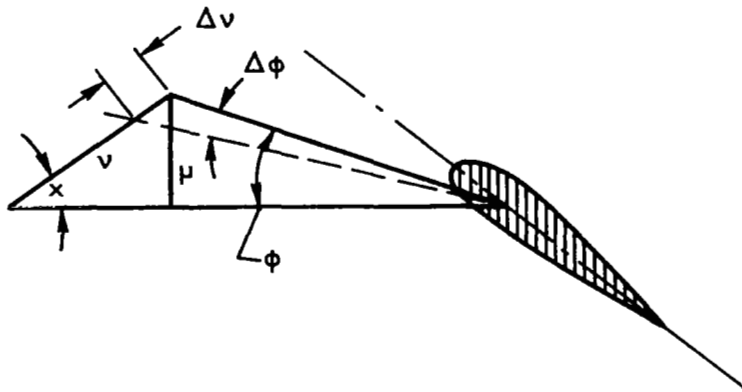
Figure 8. Rotor Blade Velocity Diagram
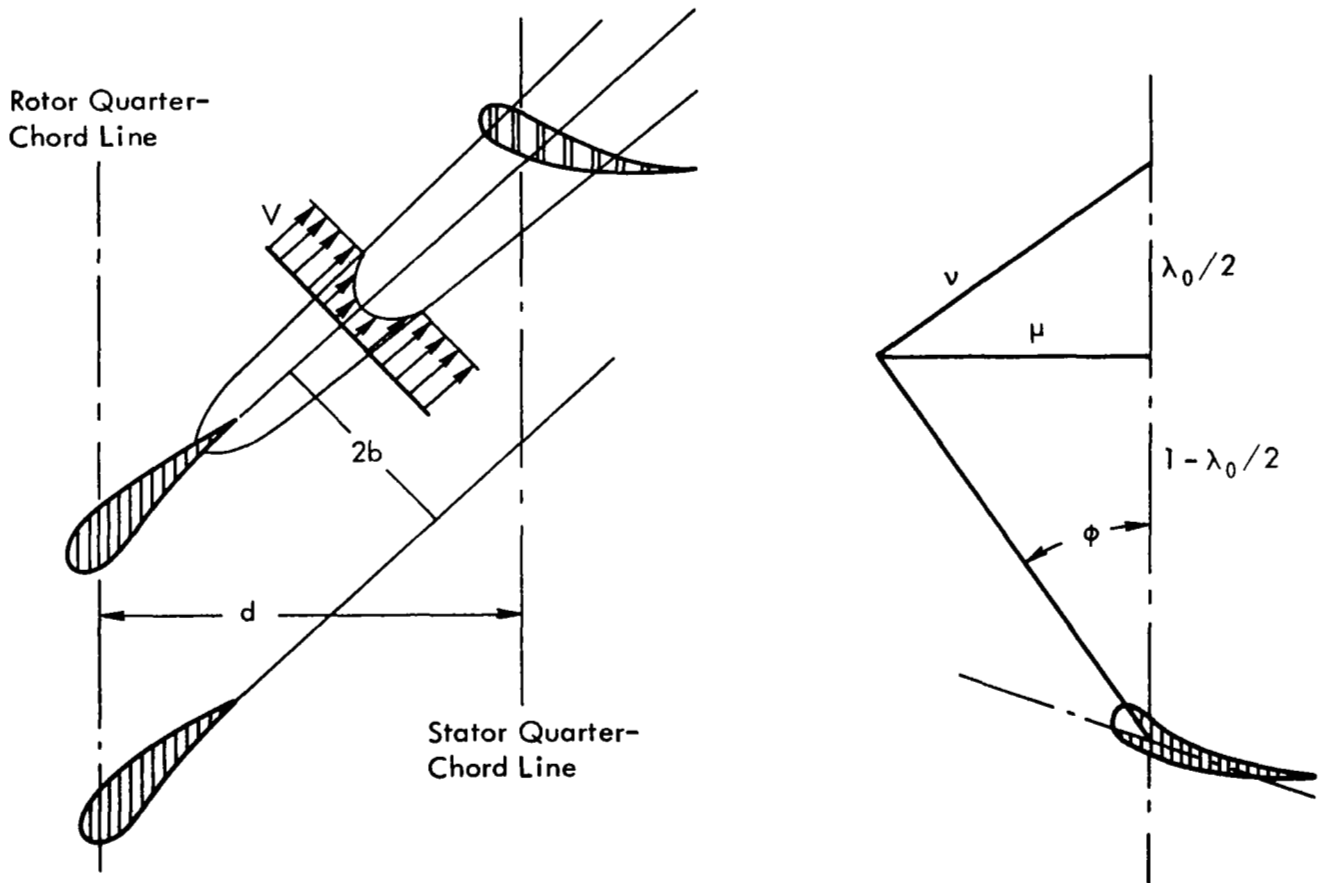
Figure 9. Stator Blade Equivalent Wake Geometry
and Velocity Diagram
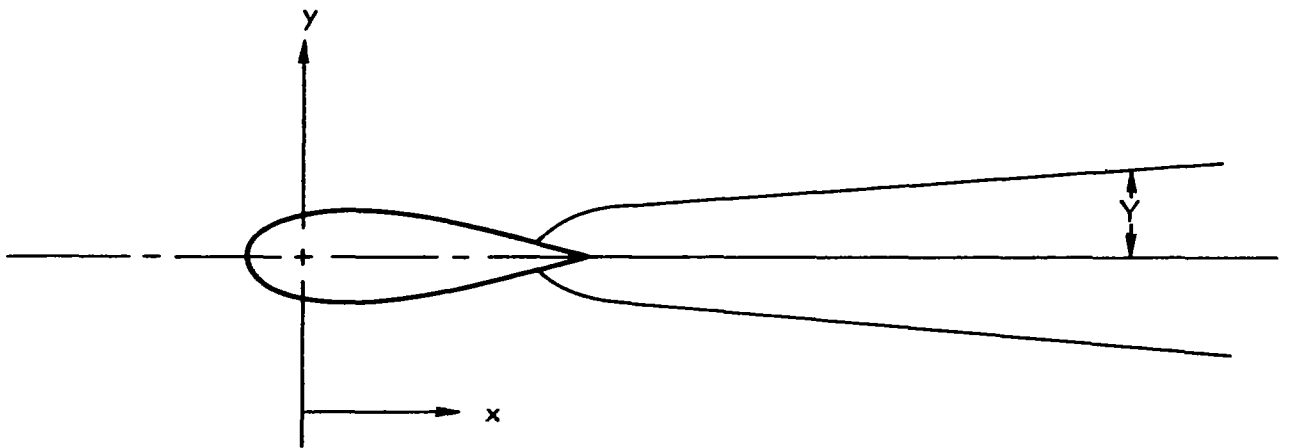
Figure 10. Airfoil Wake Thickness Diagram

58
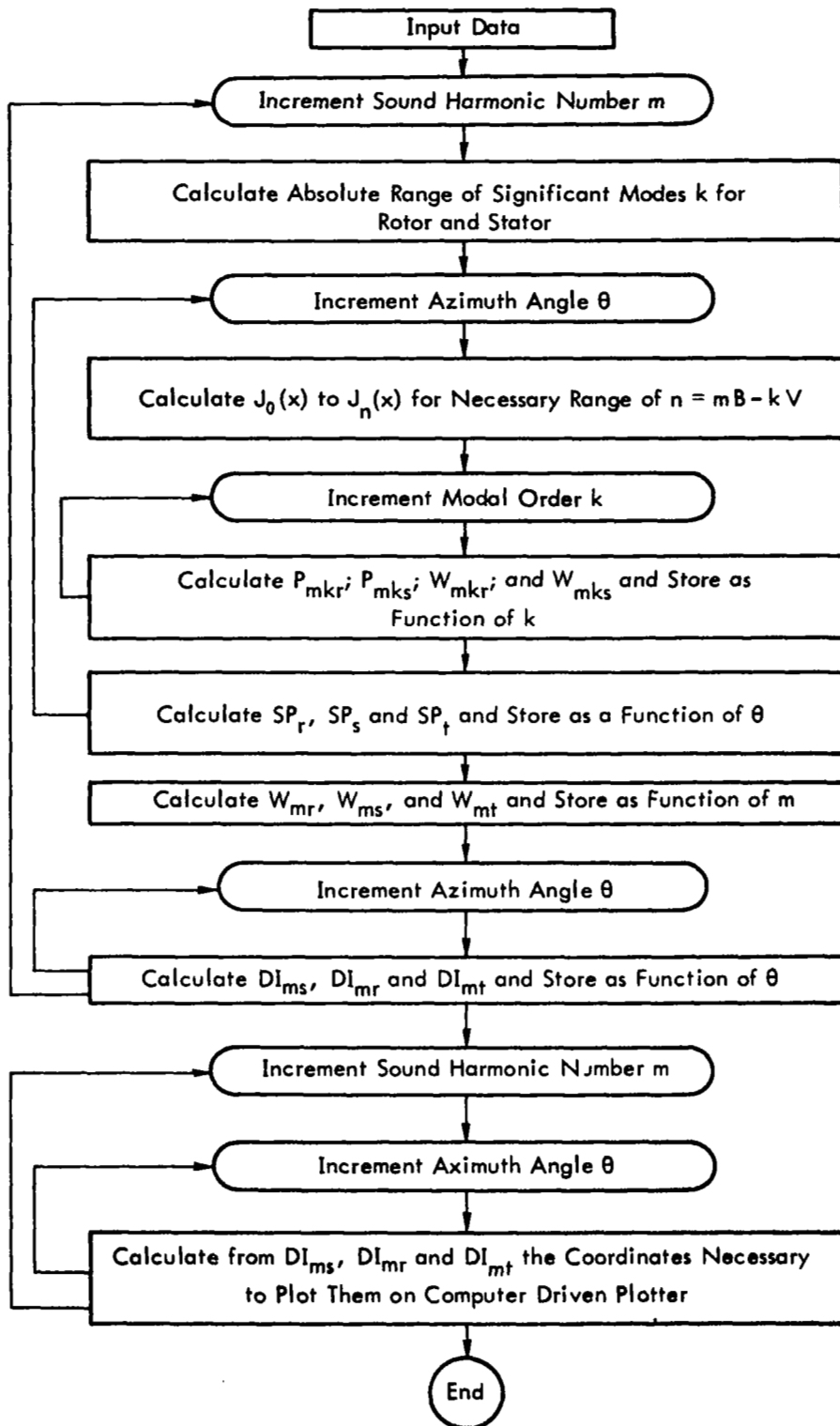
Figure 11. Computer Program Flow Diagram

ROTOR LOADING:
    237.5000   3.8100   2.5900   1.9600   1.5450   1.2100   .0000
       .0000   .0000   .0000   .0000   .0000   .0000   .0000
       .0000   .0000

STATOR LOADING:
      2.4200   .0000   .0000   .0000   .0000
   NUMBER OF ROTOR BLADES (B) = 40   THRUST LOADING (TI) = 3.810 LB/BL
   NUMBER OF STATOR VANES (V) = 47   ROTOR RADIUS   (R) = 2.000 FT.
   TIP MACH NUMBER   (RM) = .70   INLET GUIDE VANES   = 35

```
┌─────────────────────────────────────────┐
│         INTEGRATED POWER LEVEL (DB)      │
├─────────────────────────────────────────┤
│                                          │
│                        (M)               │
│                                          │
│                ***    1      159.5       │
│        ROTOR    *     2         .0       │
│        POWER    *     3         .0       │
│                ***    4         .0       │
│                                          │
│                ***    1      172.4       │
│        STATOR   *     2         .0       │
│        POWER    *     3         .0       │
│                ***    4         .0       │
│                                          │
│                ***    1      172.7       │
│        TOTAL    *     2         .0       │
│        POWER    *     3         .0       │
│                ***    4         .0       │
│                                          │
└─────────────────────────────────────────┘
```

Figure 12. Sample Output

60

DIRECTIVITY INDEXES (DB'S)

THRUST LOADING   (Tl) = 3.810 LB/B   ROTOR RADIUS   = 2.000 FT
INLET   GUIDE   VANES   = 35   SOUND HARMONIC NUMBER   = 1
NUMBER OF ROTOR BLADES = 40   NUMBER OF STATOR VANES = 47

PSI	STATOR DMS	ROTOR DMR	TOTAL DMT
.0	-500.0	-500.0	-500.0
4.0	-63.1	-18.9	-32.0
8.0	-24.3	6.7	-6.4
12.0	-5.6	15.8	3.3
16.0	2.8	12.5	4.3
20.0	1.9	9.4	2.8
24.0	-11.2	9.8	-2.7
28.0	.2	7.7	1.1
32.0	-37.5	7.3	-5.8
36.0	-1.6	5.5	-.8
40.0	-13.9	6.3	-6.1
44.0	-4.2	-.0	-3.9
48.0	-6.8	5.9	-4.1
52.0	-12.8	-11.6	-12.7
56.0	-5.4	2.0	-4.5
60.0	-10.4	1.5	-8.1
64.0	-20.1	-9.4	-18.2
68.0	-9.3	-5.5	-9.1
72.0	-8.7	-2.7	-8.1
76.0	-11.2	-3.2	-10.2
80.0	-15.8	-3.6	-13.4
84.0	-21.7	-3.5	-15.5
88.0	-27.3	-3.6	-16.4
92.0	-29.0	-3.9	-16.8
96.0	-26.7	-3.5	-16.2
100.0	-24.5	-1.5	-14.2
104.0	-24.7	1.0	-11.9
108.0	-29.3	1.8	-11.2
112.0	-62.7	-2.2	-15.3
116.0	-41.9	-6.7	-19.9
120.0	-27.1	5.4	-7.7
124.0	-19.3	5.5	-7.4
128.0	-25.0	-8.5	-20.0
132.0	-17.8	8.8	-4.2
136.0	-14.2	2.7	-9.0
140.0	-23.1	8.8	-4.2
144.0	-10.3	7.9	-4.1
148.0	-45.7	9.6	-3.5
152.0	-7.7	9.9	-2.0
156.0	-18.7	11.9	-1.2

Figure 12. Continued.

61

DIRECTIONAL SOUND PRESSURE LEVELS   (DB)

CALCULATED AT 100.0 FOOT RADIUS

* CASE P4 -- BASELINE CASE *
   TR(I)
   237.5000   3.8131   2.5872   1.9706   1.5456

      1.2134   .9394   .7099   .5185   .3616

       .2367   .0000   .0000   .0000   .0000

       .0000
   TS(I)
      2.4209   1.4766   .9322   .5482   .2795

NUMBER OF ROTOR BLADES =40   THRUST   LOADING   = 3.813 LB/B
NUMBER OF STATOR VANES =47   ROTOR   RADIUS   = 2.000 FT
TIP MACH NUMBER   =   .700   ROTOR DRAG/THRUST   =   .615
STATOR DRAG/THRUST   = 1.492   INLET GUIDE VANES   =35
STEADY THRUST - ROTOR =237.500

SOUND HARMONIC NUMBER = 1
TOTAL SOUND PRESSURE LEVEL OVER ALL MODES K FROM -1 TO   2 FOR THE ROTOR
AND ALL MODES K FROM -1 to   2 FOR THE STATOR

PSI	STATOR SPL	ROTOR SPL	TOTAL SPL
0	-500.0	-500.0	-500.0
5	74.7	101.9	101.9
10	111.5	124.7	124.9
15	126.4	126.9	129.7
20	126.8	121.4	127.9
25	120.9	116.8	122.4
30	121.0	122.6	124.9
35	122.6	111.9	122.9
40	111.0	118.3	119.0
45	121.5	115.9	122.6
50	105.8	114.2	114.8
55	119.2	112.2	120.0
60	114.5	113.5	117.0
65	110.1	99.4	110.4
70	116.4	108.6	117.1
75	114.5	109.0	115.6

Figure 12. Concluded.
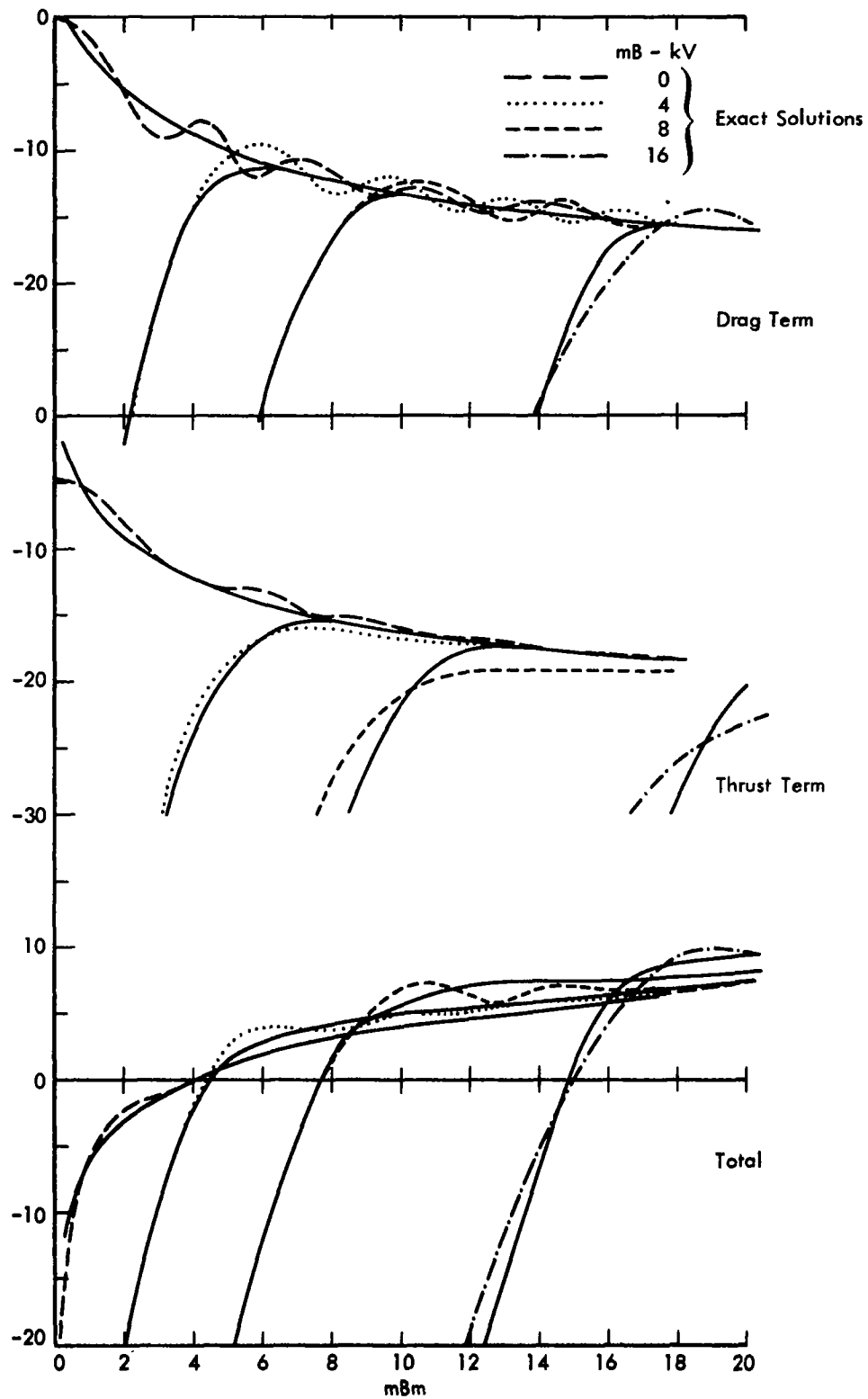
Figure 13. Comparison of Exact and Approximate Solutions for Sound Power

Figure 14. Variation of $\left[\cos\theta - \frac{1}{M}\left(1 - \frac{kV}{mB}\right)\right]$ with $\frac{kV}{mB}$ for Rotational Mach Number M of 0.5

64
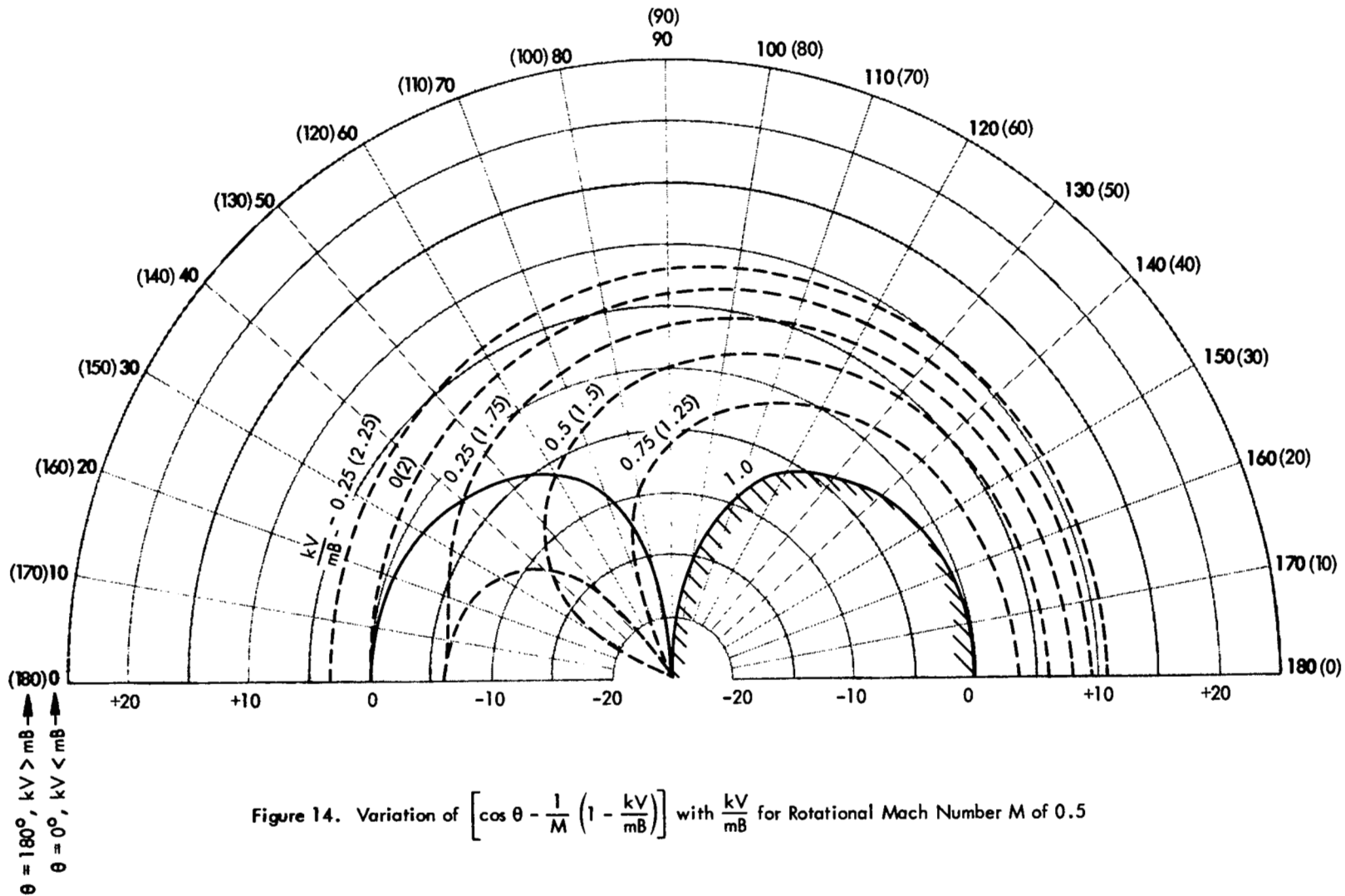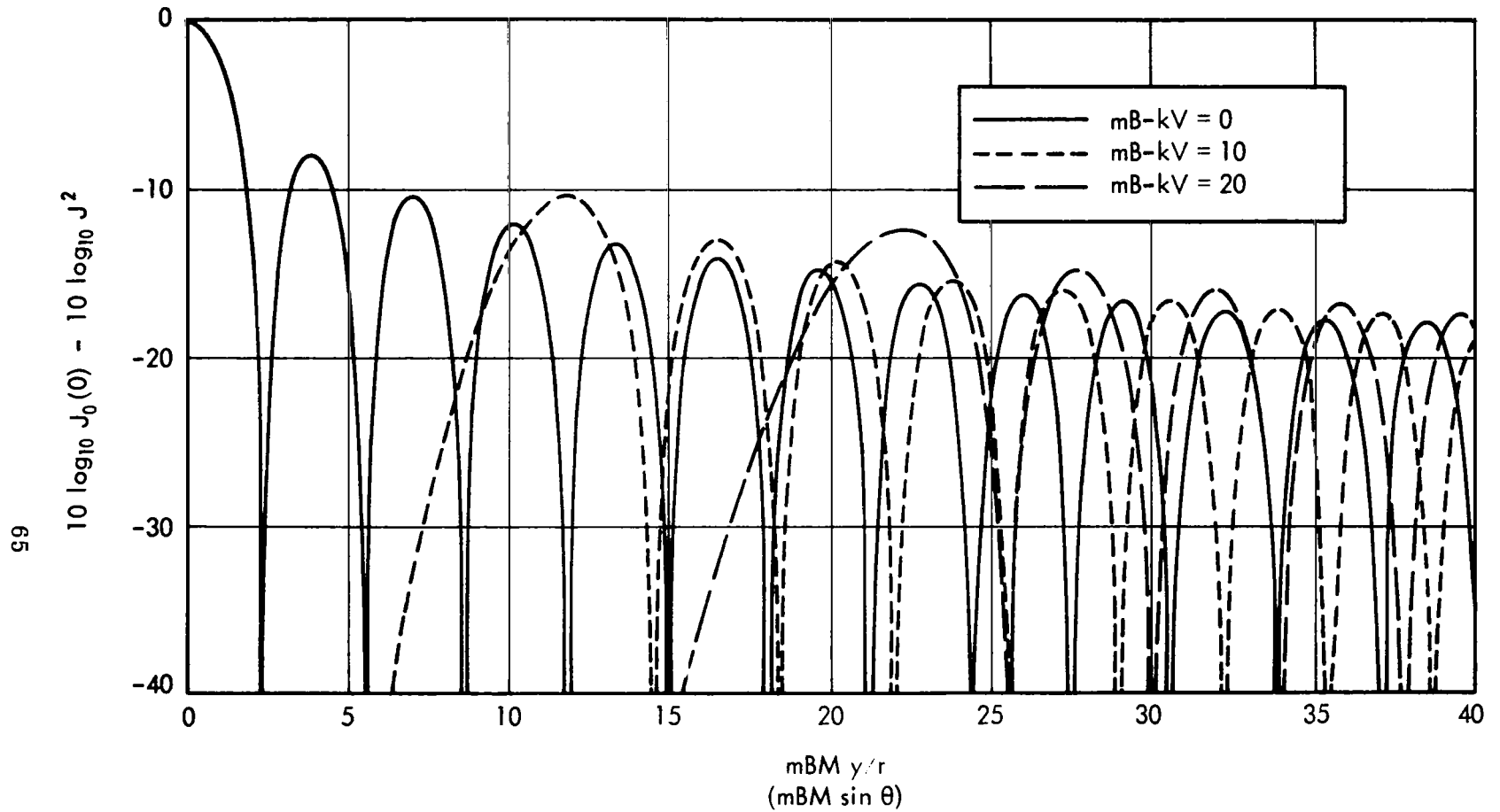
Figure 15. Bessel Function Intensity $[10 \log_{10} (J_n(x))^2]$ as a Function of Argument for Various Orders. Argument = mBM sin θ, Order = mB − kV.

Increasing:

Number of Blades
Tip Mach Number
Sound Harmonic Number

nM = 4   nM = 8   nM = 16   nM = 32

μ = 1

μ = 4

μ = 16

Increasing
Modal Order
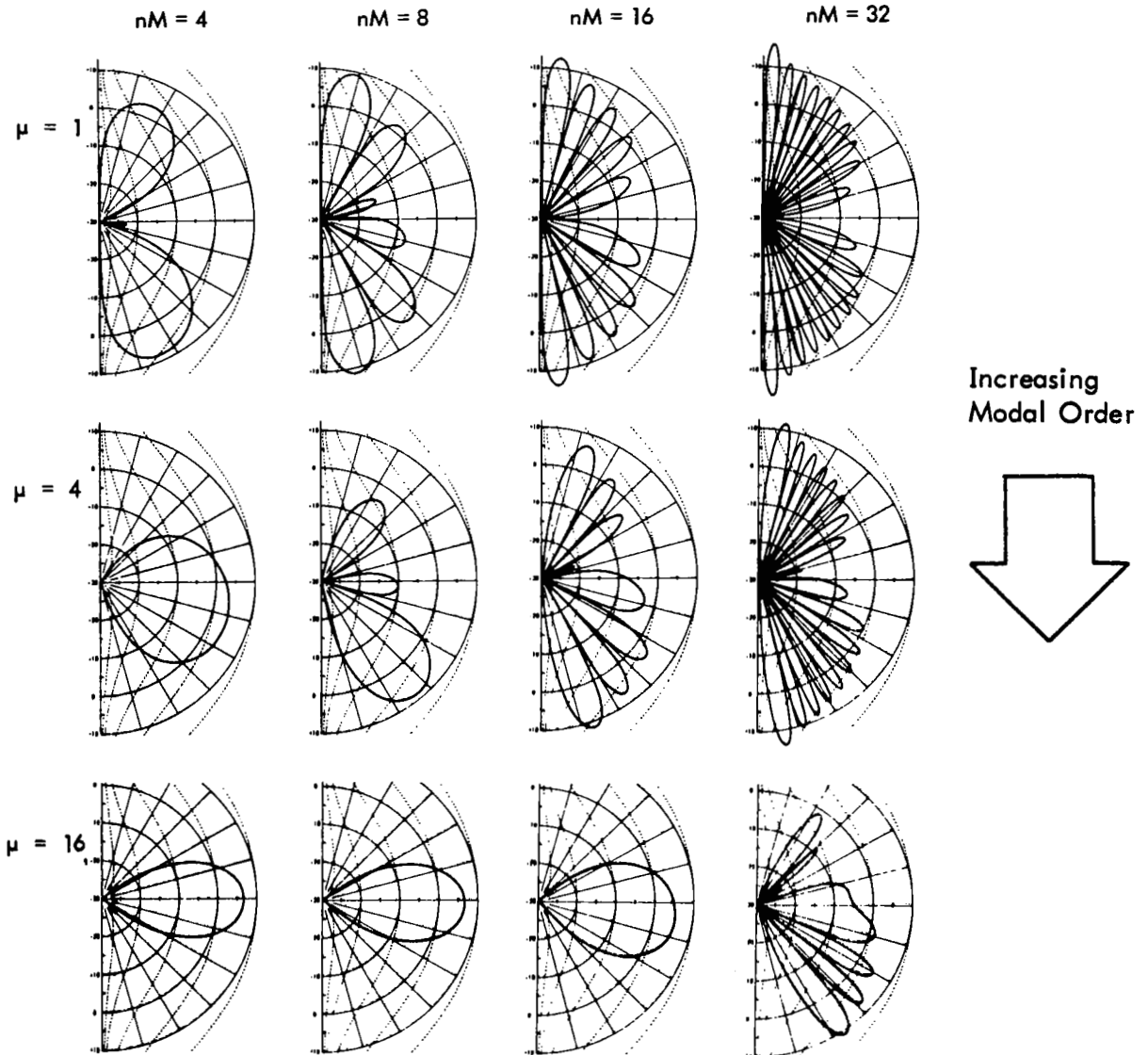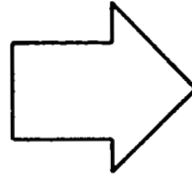
Figure 16. Directivity Patterns for Fluctuating Force Terms in Stator-Rotor Interactions (Reference 1)
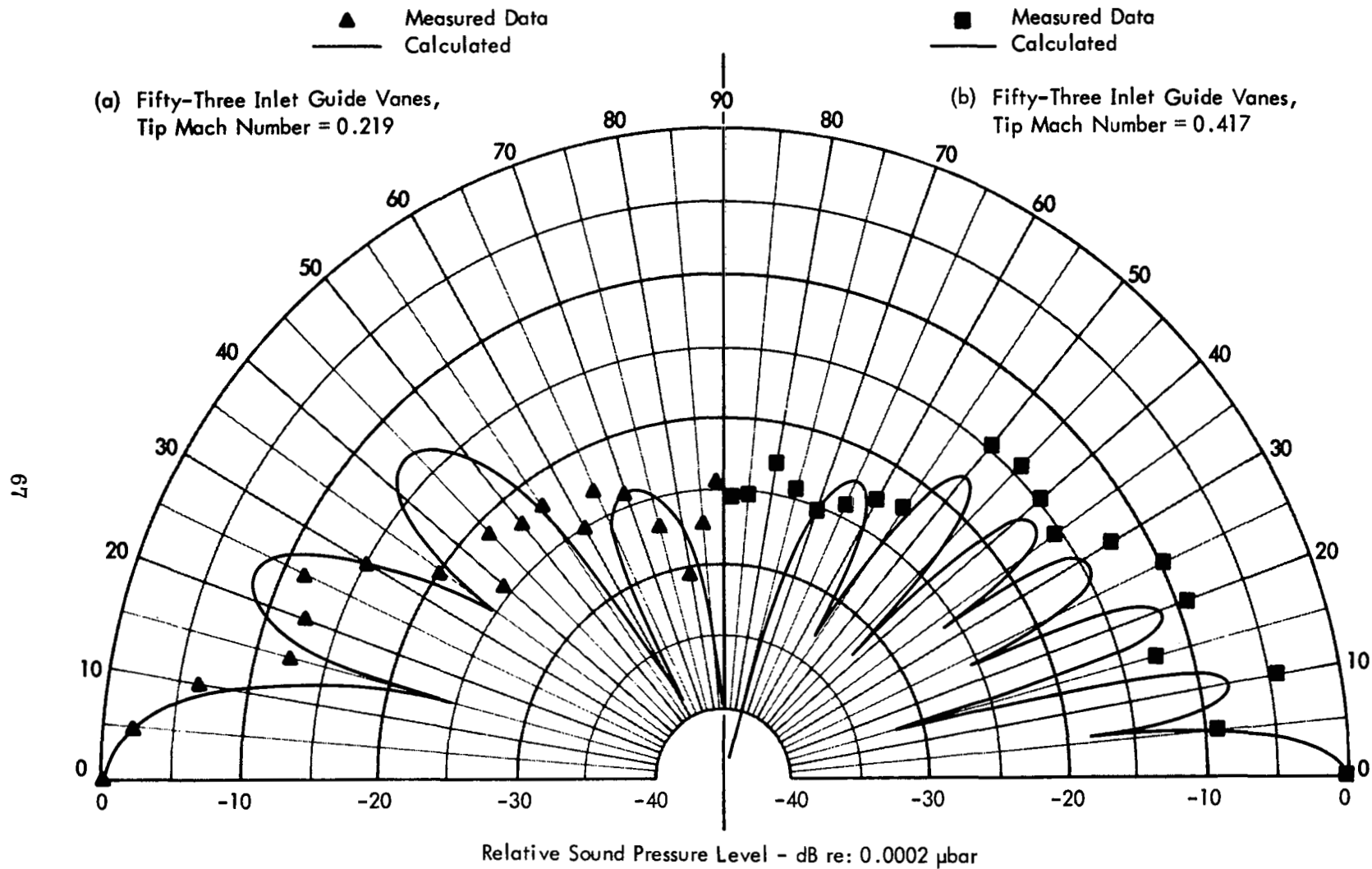
Figure 17. Comparison of Measured and Calculated Directivity Patterns for 12-Foot Radius
(Measured Data from Reference 4)

Legend:
▲ Measured Data
——— Calculated

■ Measured Data
——— Calculated

(a) Sixty-Two Inlet Guide Vanes,
    Tip Mach Number = 0.346

(b) Sixty-Two Inlet Guide Vanes,
    Tip Mach Number = 0.477

Relative Sound Pressure Level – dB re: 0.0002 μbar
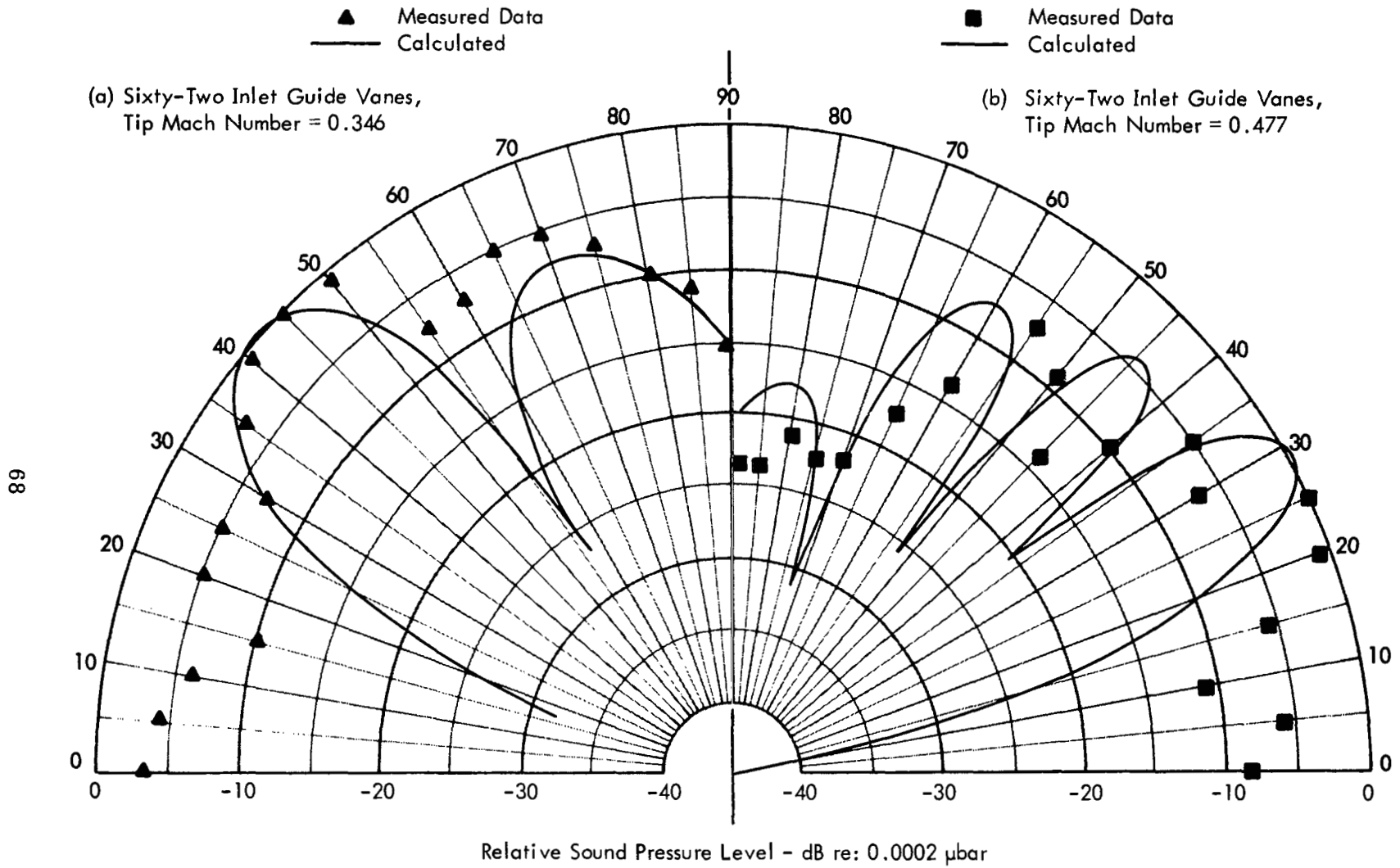
Figure 18. Comparison of Calculated and Measured Directivity Patterns for 12-Foot Radius
(Measured Data from Reference 4)
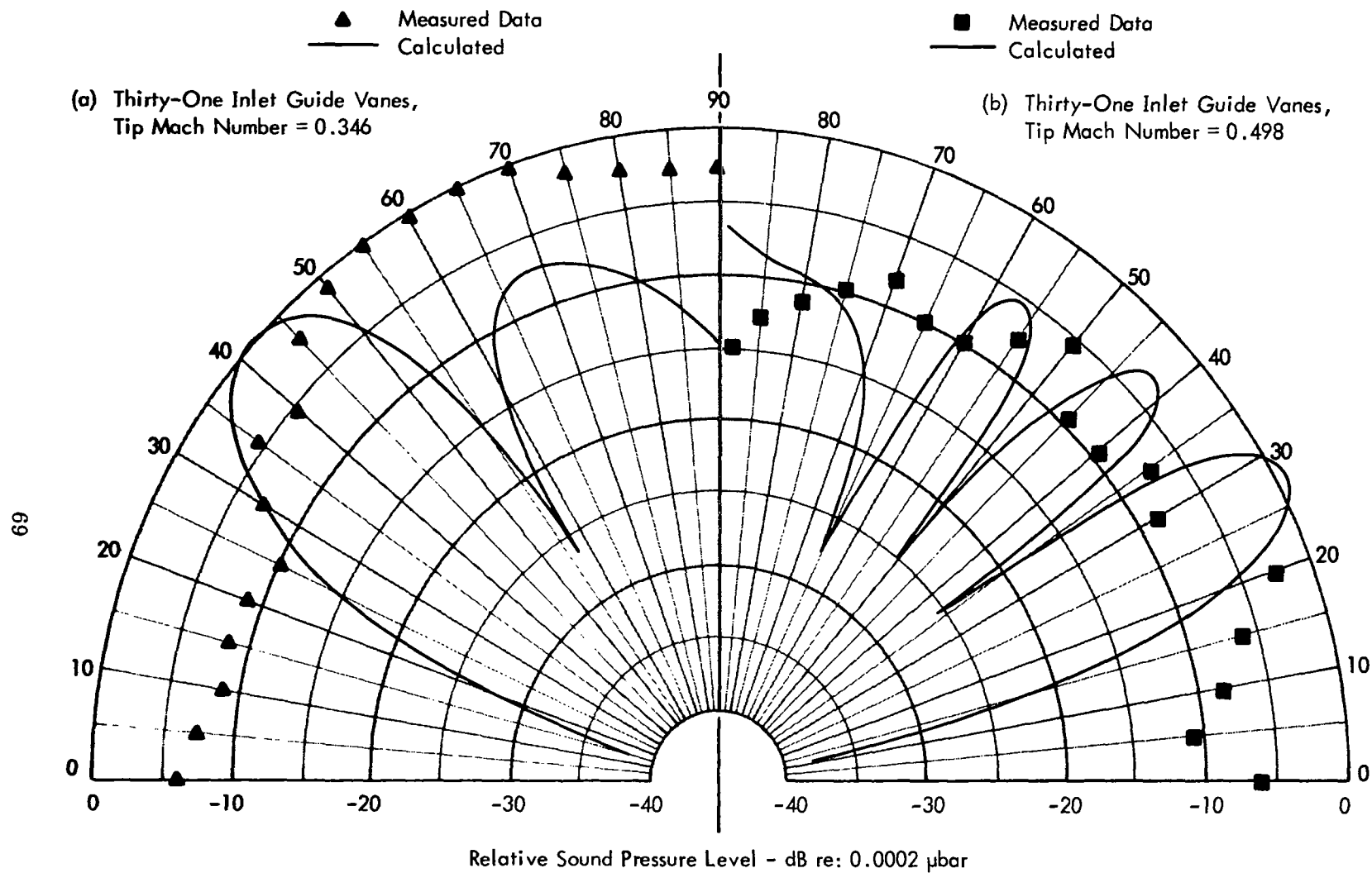
Figure 19. Comparison of Calculated and Measured Directivity Patterns for 12-Foot Radius (Measured Data from Reference 4)
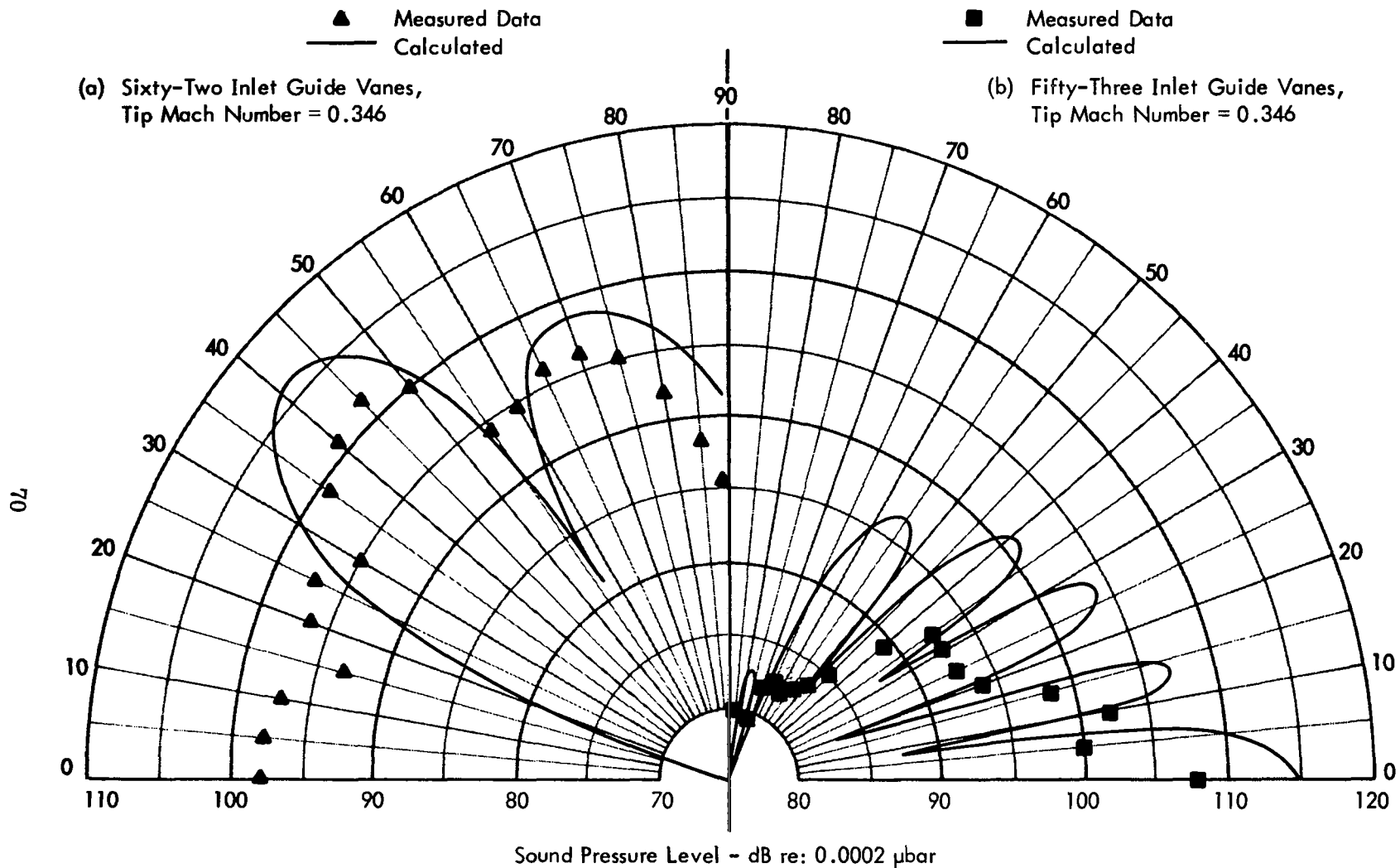
Figure 20. Comparison of Calculated and Measured First Harmonic Noise Level for Various Numbers of Inlet Guide Vanes Measured on 12-Foot Radius (Reference 4)

▲   Measured Data

——— Calculated

(c) Thirty-One Inlet Guide Vanes,
Tip Mach Number = 0.346

Sound Pressure Level – dB re: 0.0002 μbar
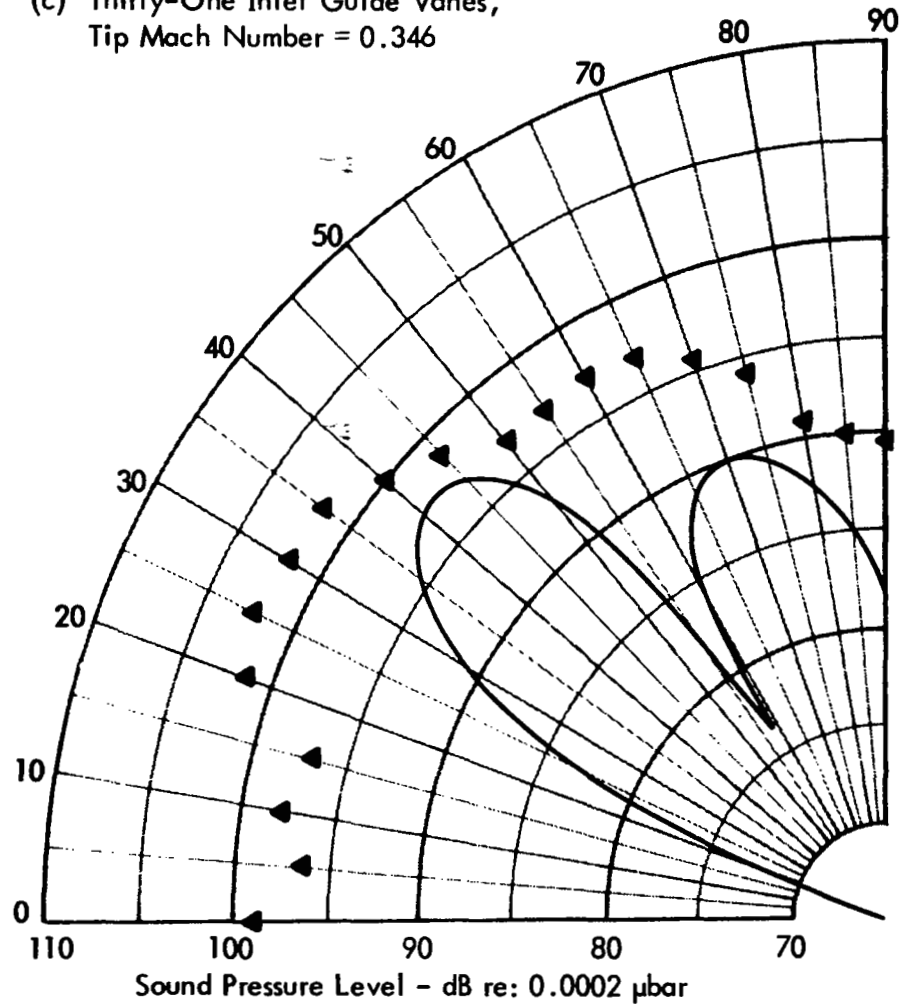
Figure 20. Concluded
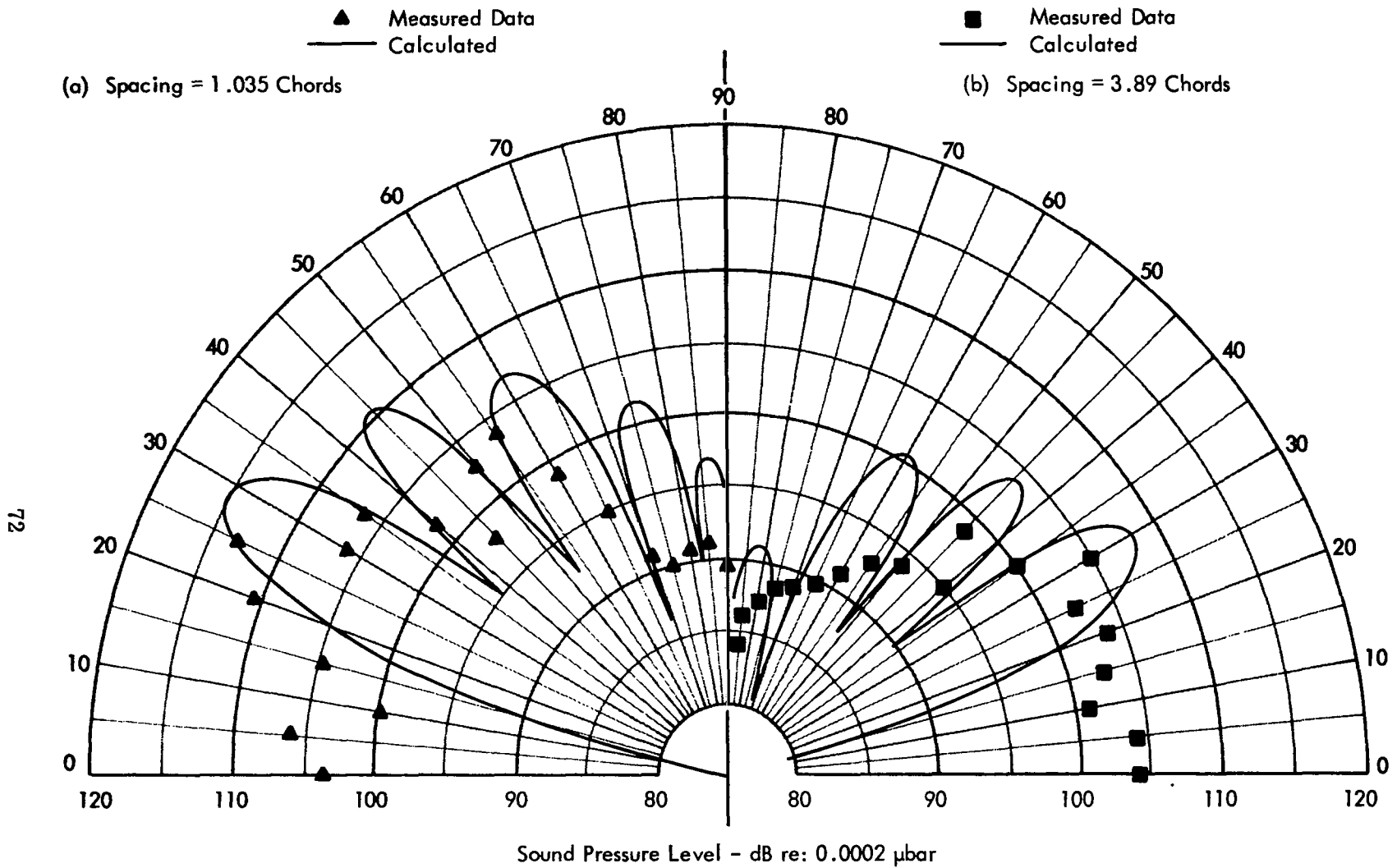
Figure 21. Comparison of Measured and First Harmonic Noise for Various IGV/Rotor Spacings. IGV = 62, M_t = 0.477, Measured on 12-Foot Radius (Reference 4)

Figure 21. Concluded
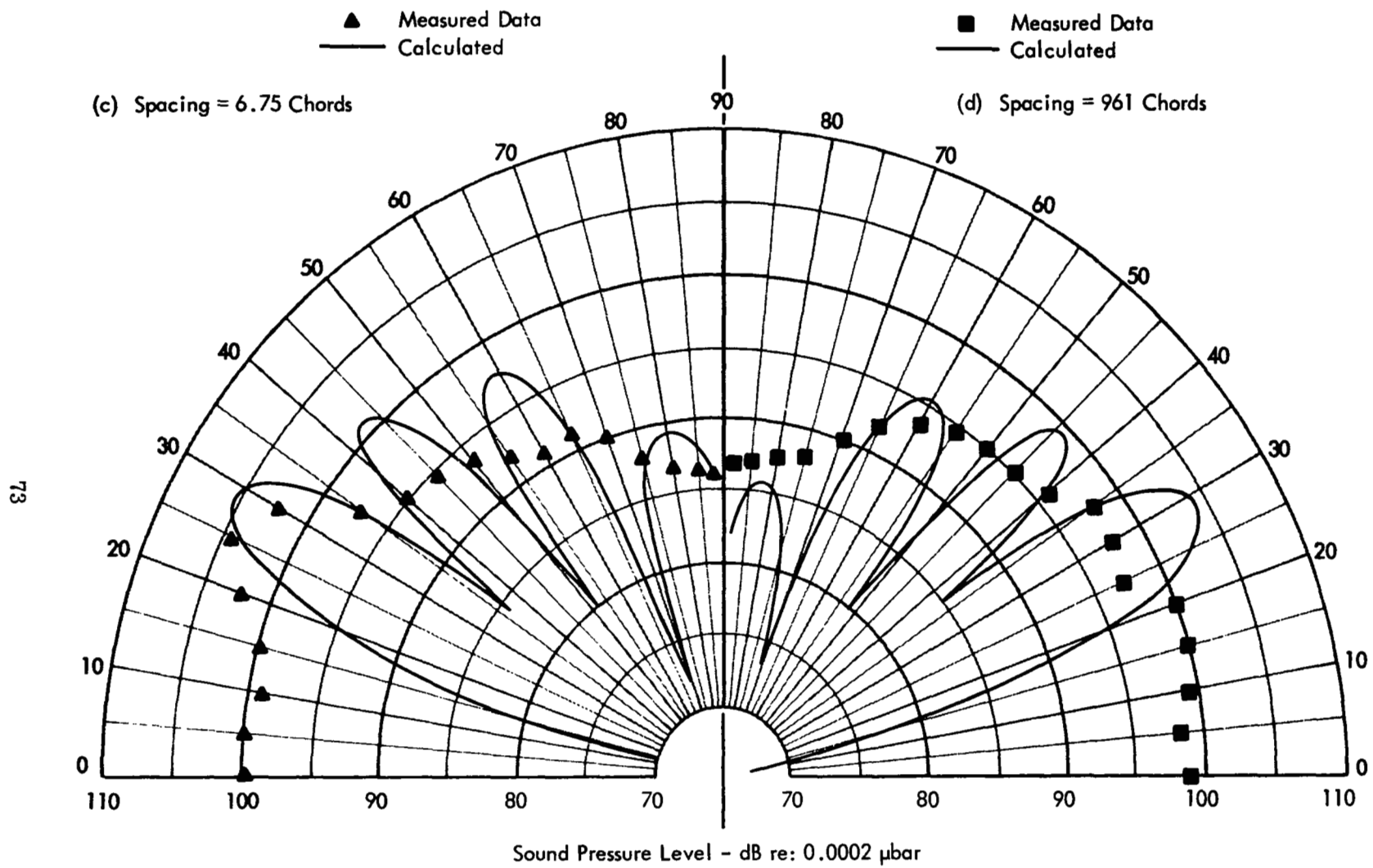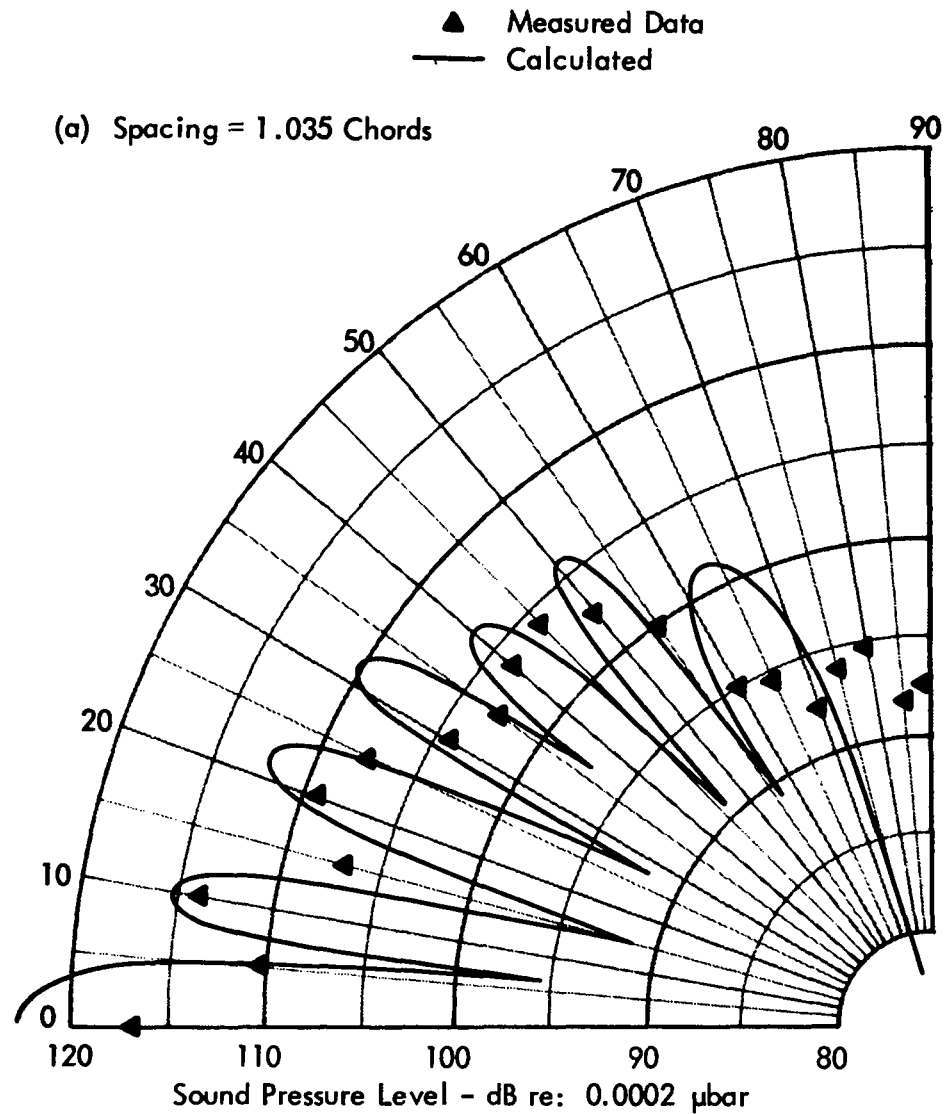
Figure 22. Comparison of Measured and Calculated First Harmonic Noise for Various IGV/Rotor Spacings. IGV = 53, M_t = 0.471, Measured on 12-Foot Radius (Reference 4)

74

▲ Measured Data
——— Calculated

■ Measured Data
——— Calculated

(b) Spacing = 3.89 Chords

(c) Spacing = 6.75 Chords

Sound Pressure Level – dB re: 0.0002 μbar
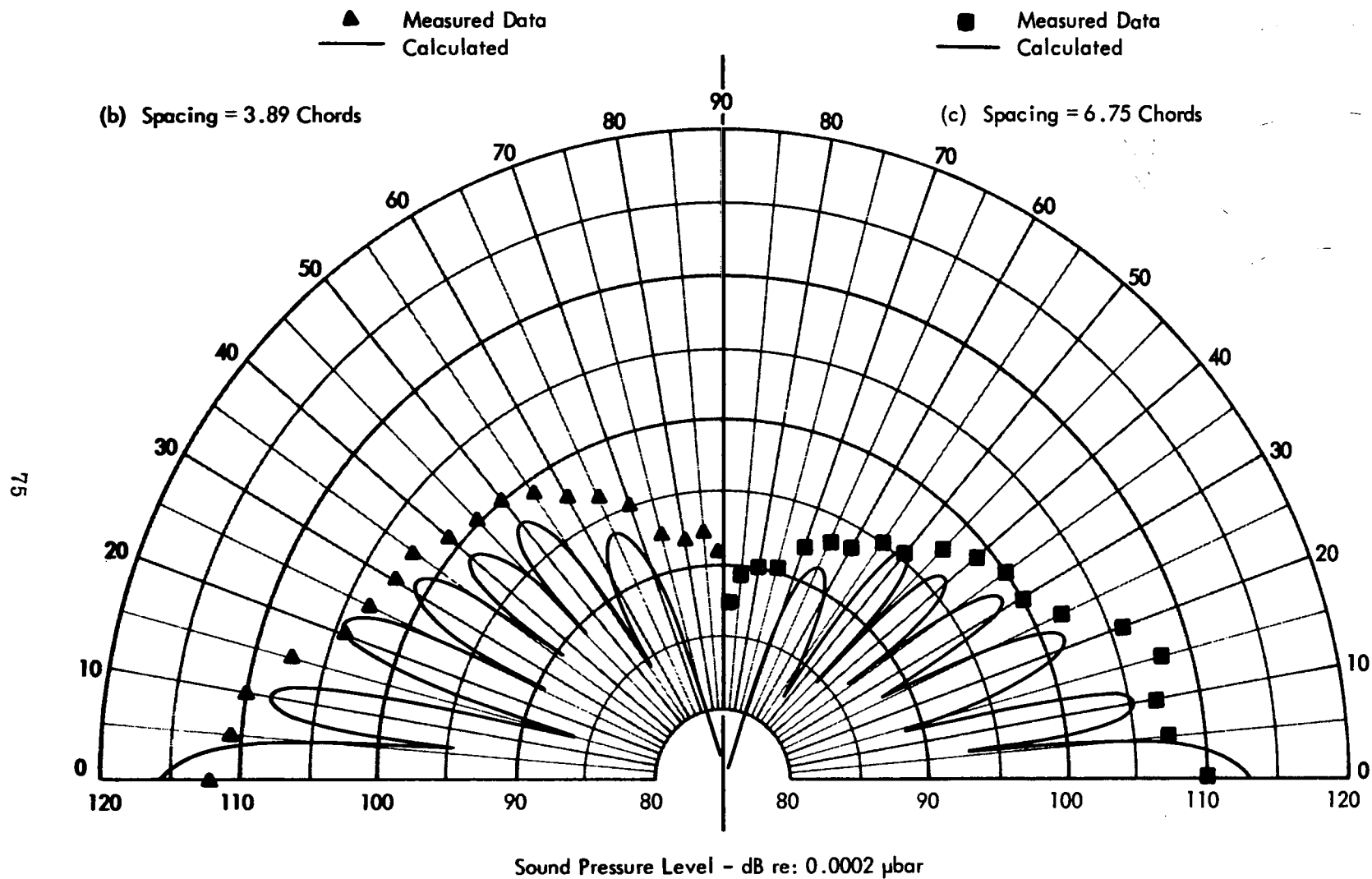
Figure 22. Concluded
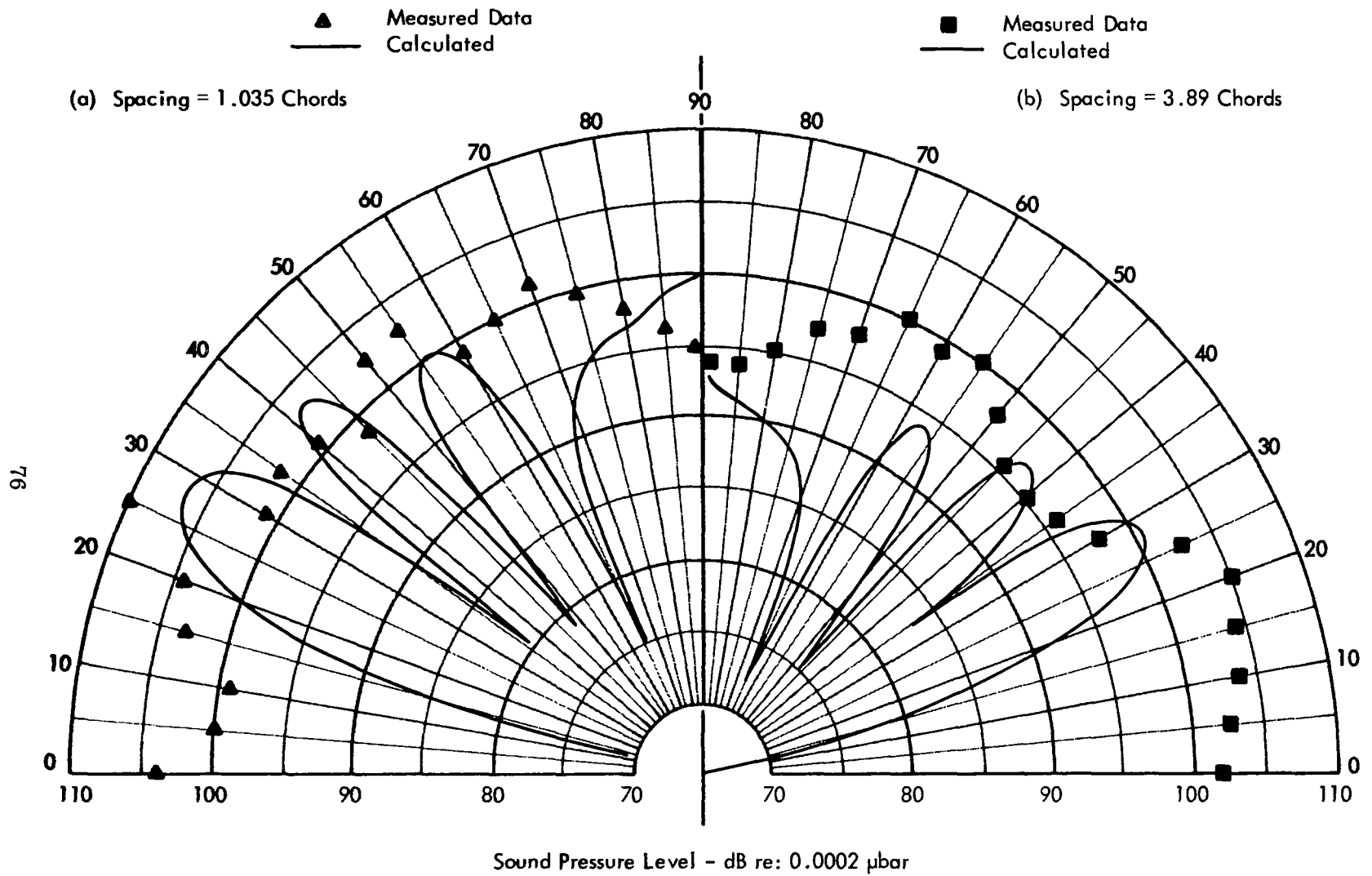
Figure 23. Comparison of Measured and Calculated First Harmonic Noise for Various IGV/Rotor Spacings. IGV = 31, M_t = 0.498, Measured for 12-Foot Radius (Reference 4)

▲ Measured Data
— Calculated

(c) Separation 6.75 Chords

Sound Pressure Level – dB re: 0.0002 μbar
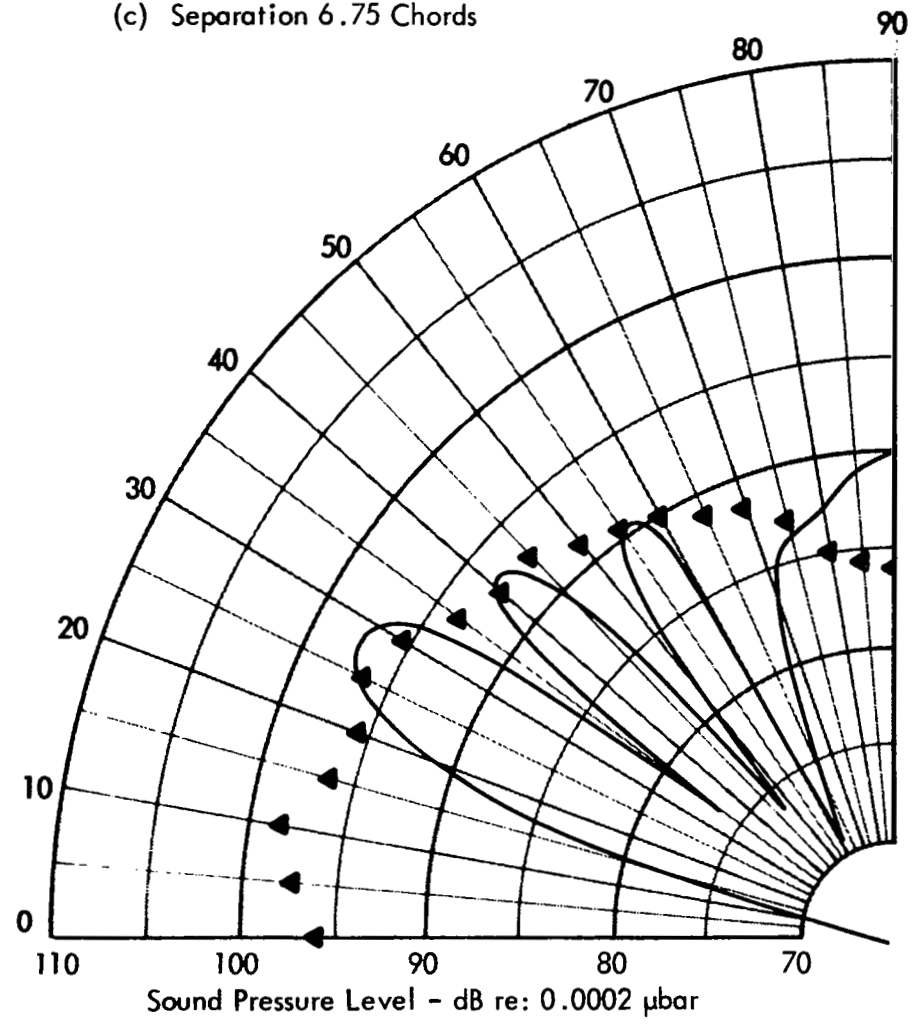
Figure 23. Concluded
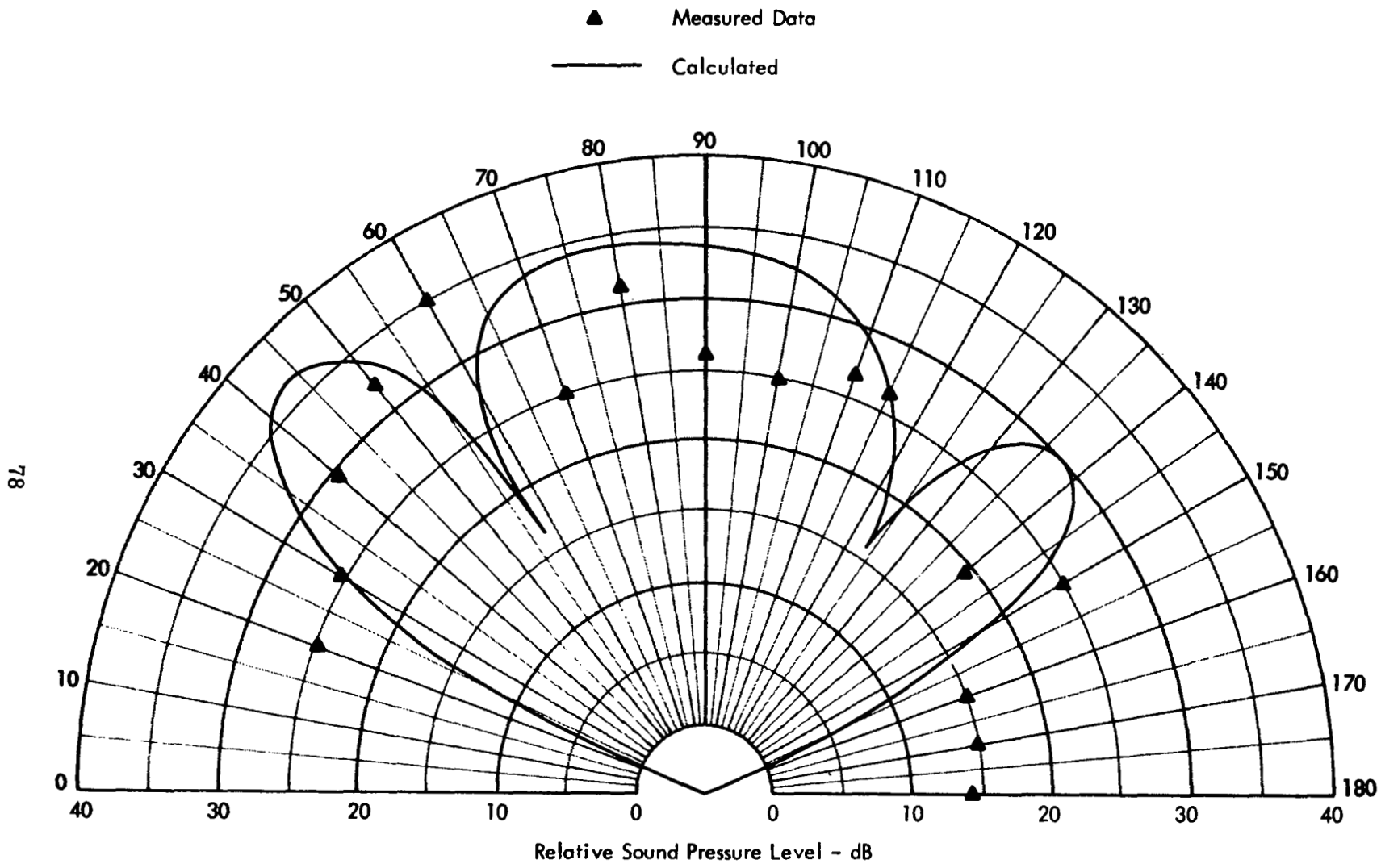
Figure 24. Comparison of Measured and Calculated First Harmonic Noise for Aft Fan Engine 1 at 8550 rpm
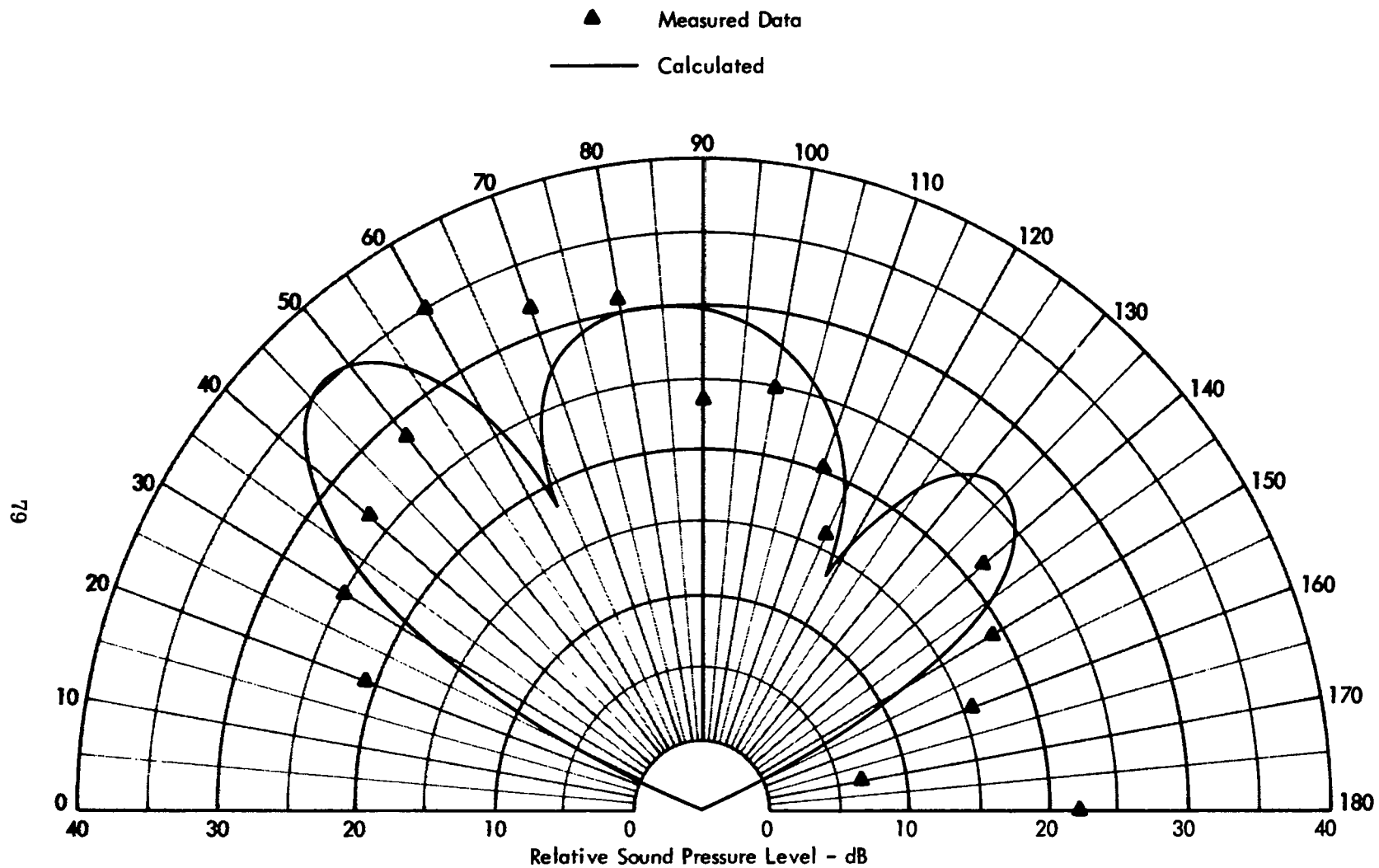
Figure 25. Comparison of Measured and Calculated First Harmonic Noise for Aft Fan Engine 1 at 8000 rpm

Relative Sound Pressure Level – dB
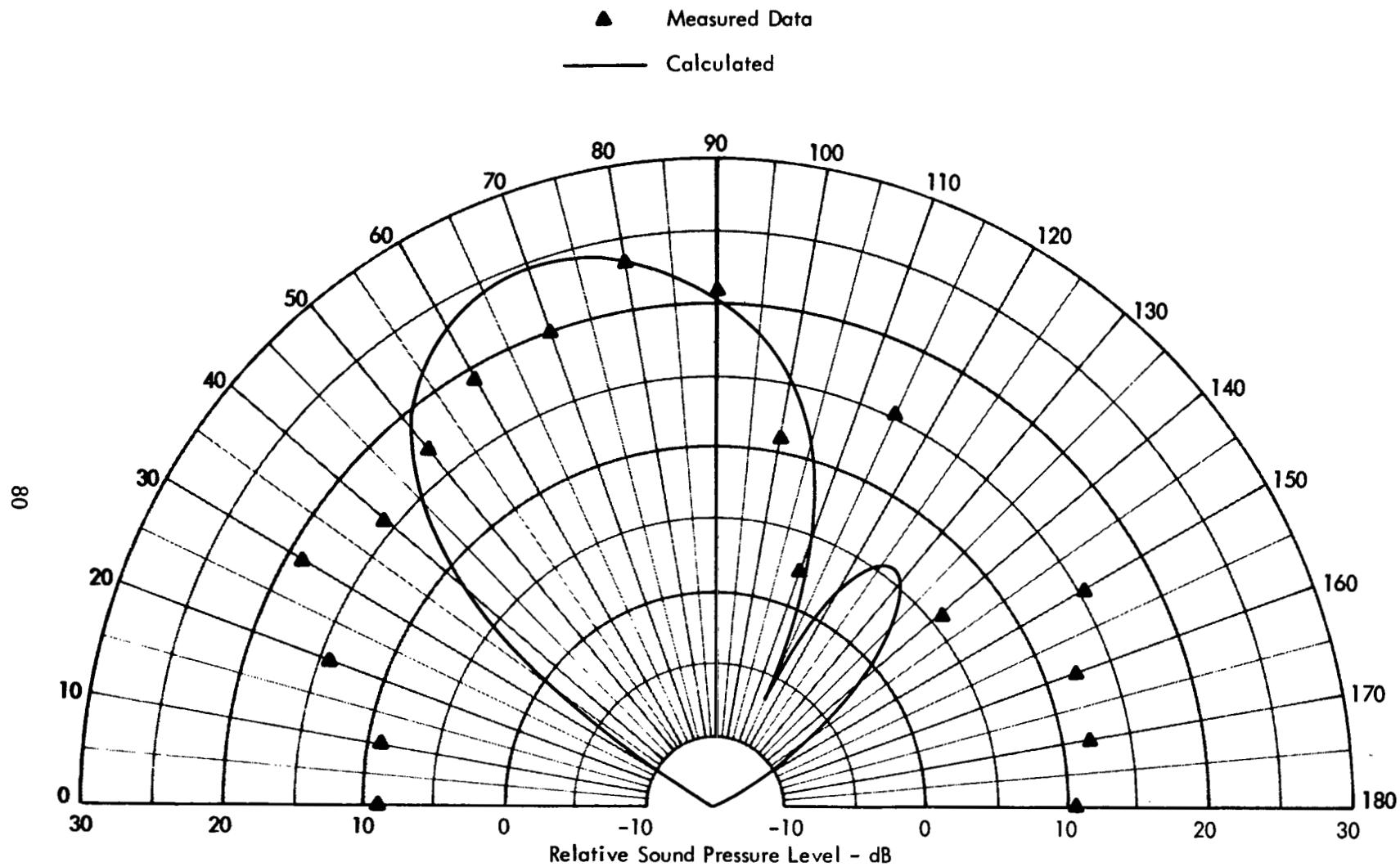
Figure 26. Comparison of Measured and Calculated First Harmonic Noise for Aft Fan Engine 1 at 6000 rpm
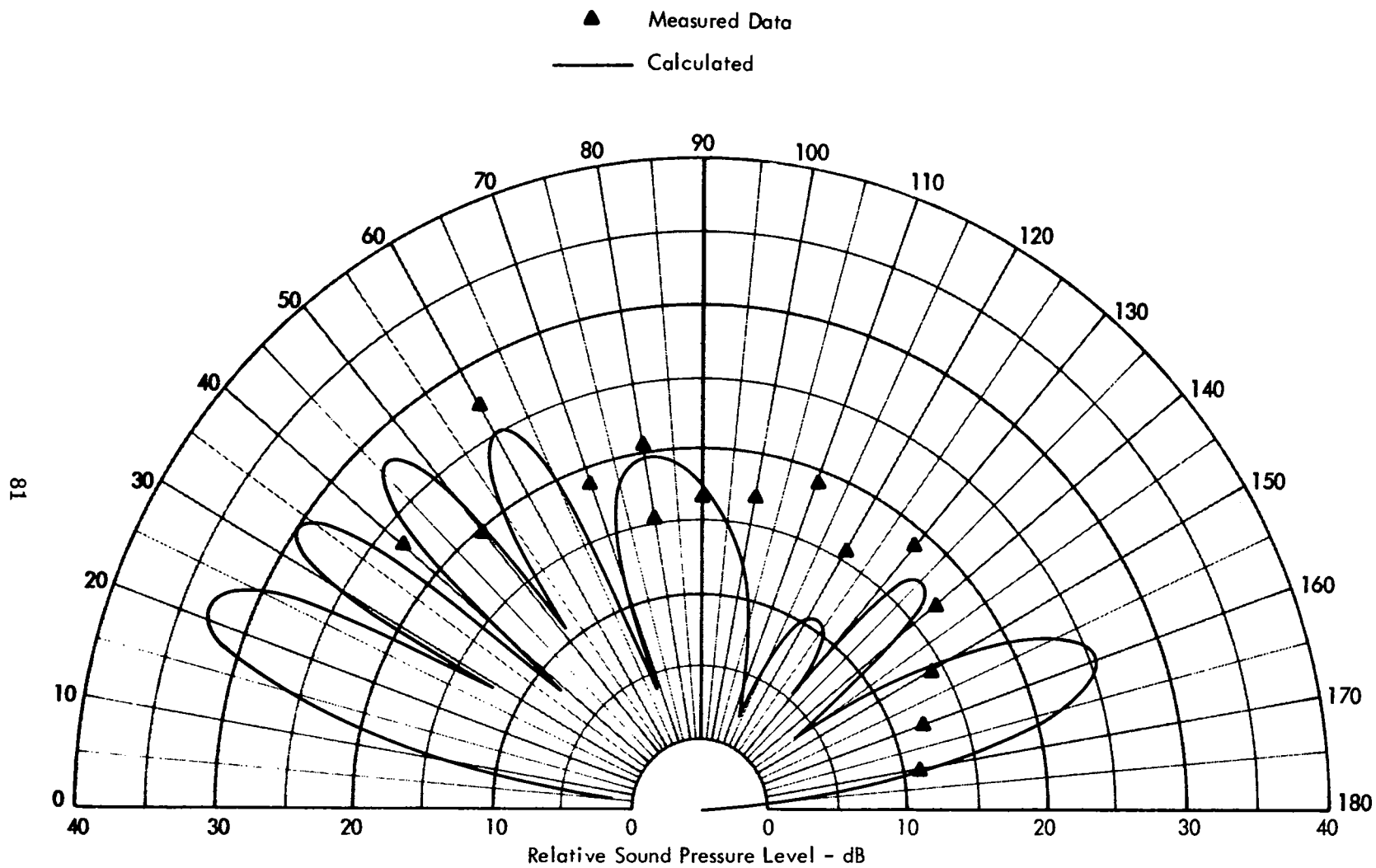
Figure 27. Comparison of Measured and Calculated First Harmonic Noise for Aft Fan Engine 2 at 3217 rpm
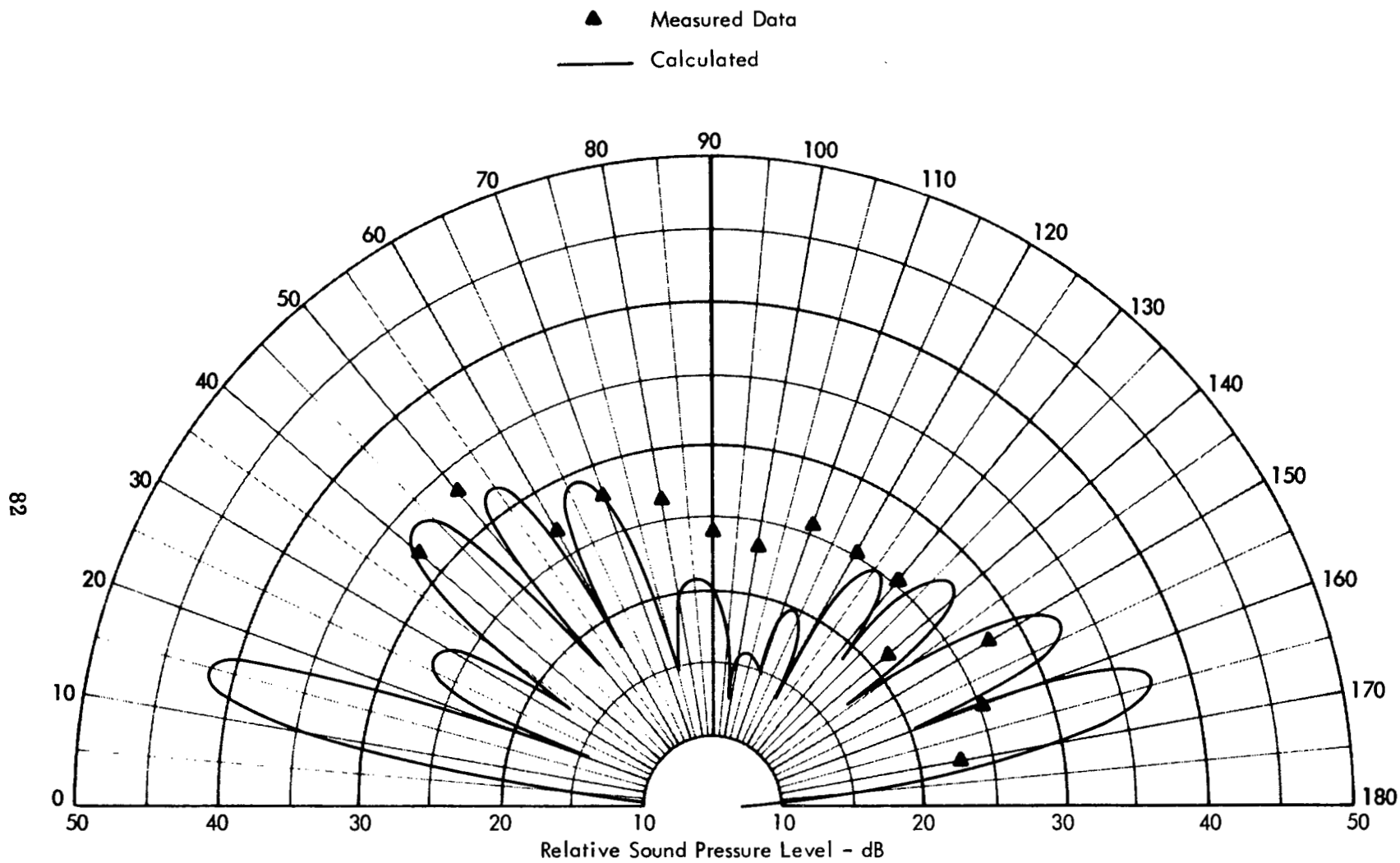
Figure 28. Comparison of Measured and Calculated First Harmonic Noise for Aft Fan Engine 2 at 4449 rpm
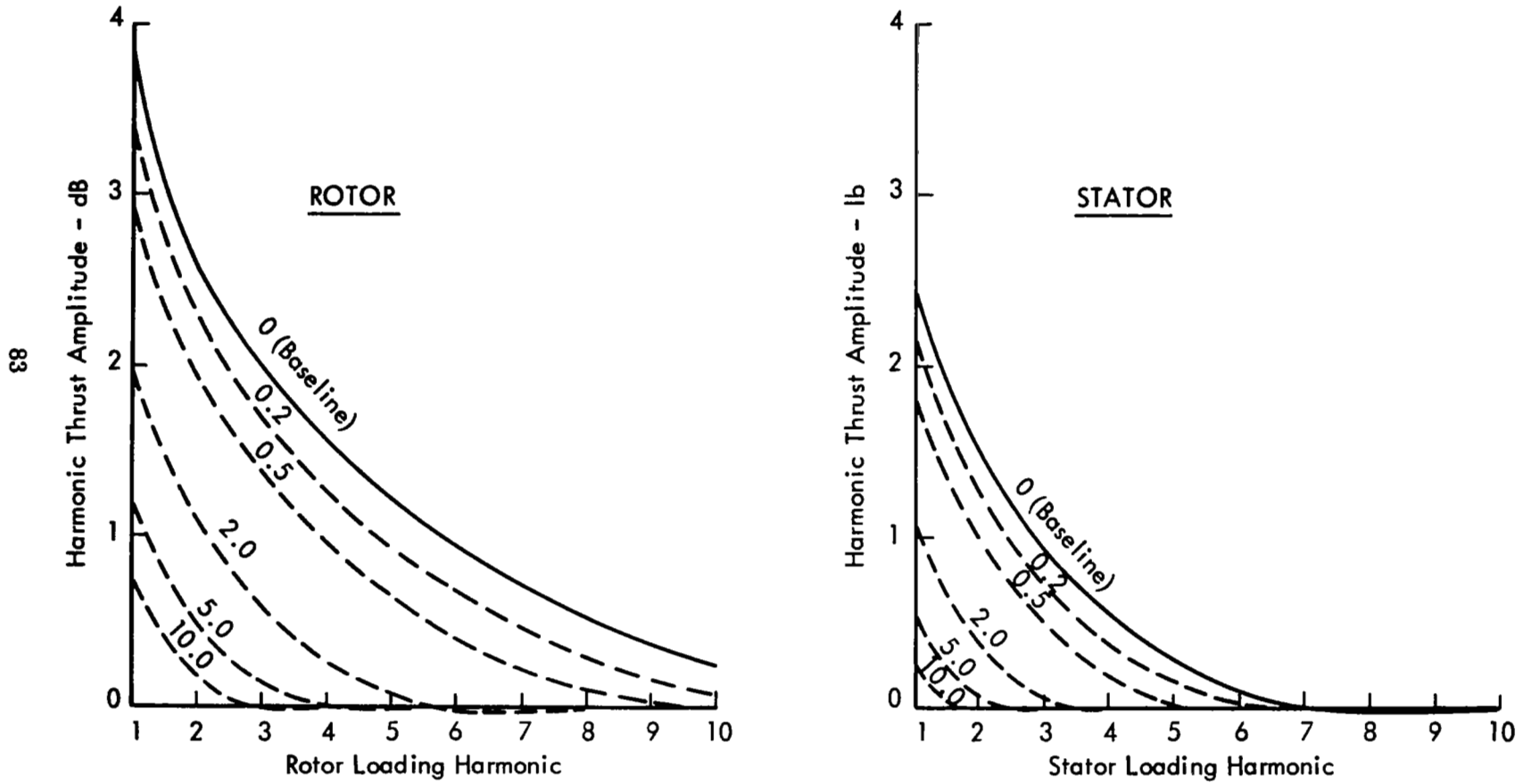
Figure 29. Effect of Rotor/Stator Separation on Harmonic Airloads

83
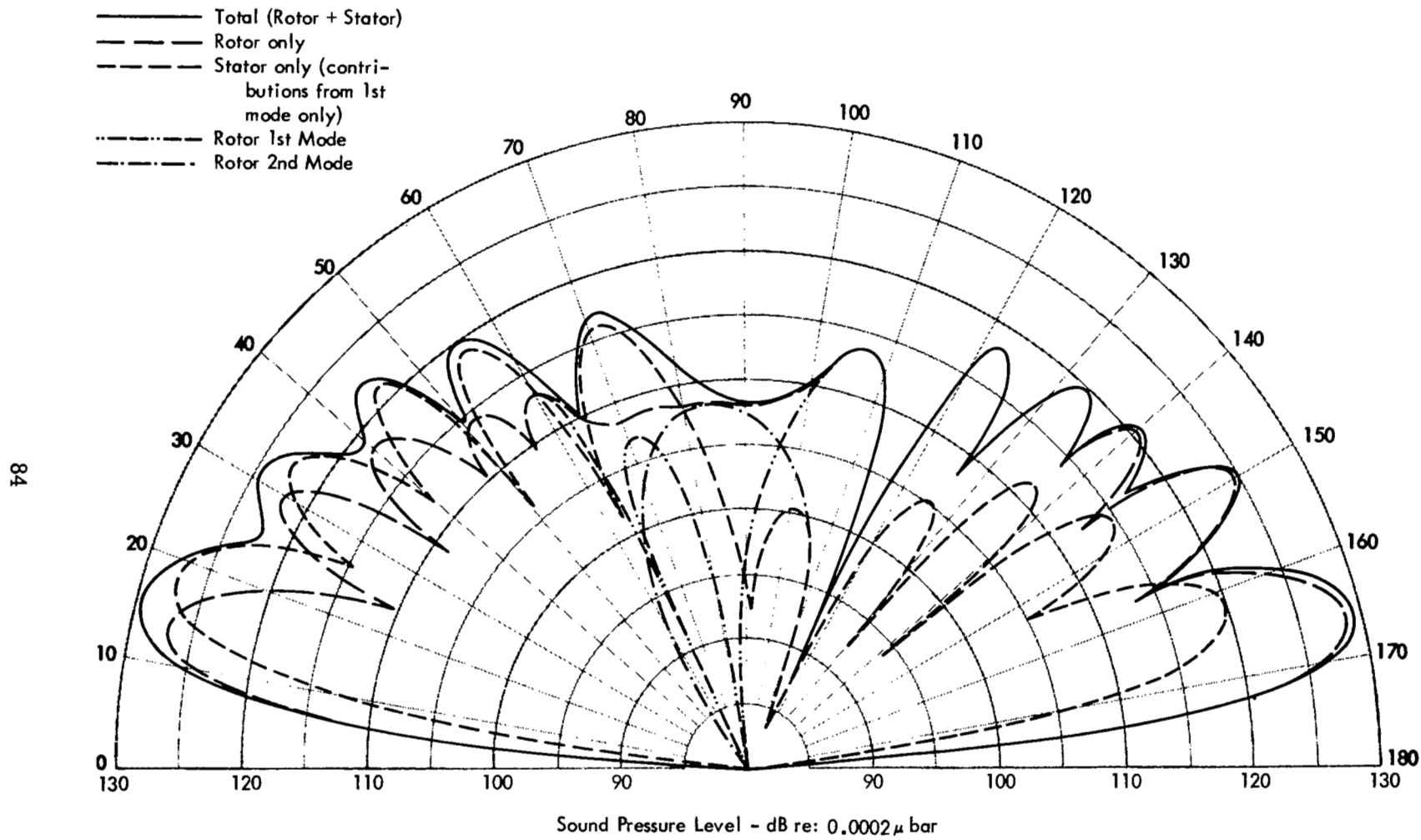
Figure 30. Parameter Study Baseline Case First Harmonic Noise Radiation Indicating
Modal Contributions

Sound Pressure Level – dB re: 0.0002 μ bar
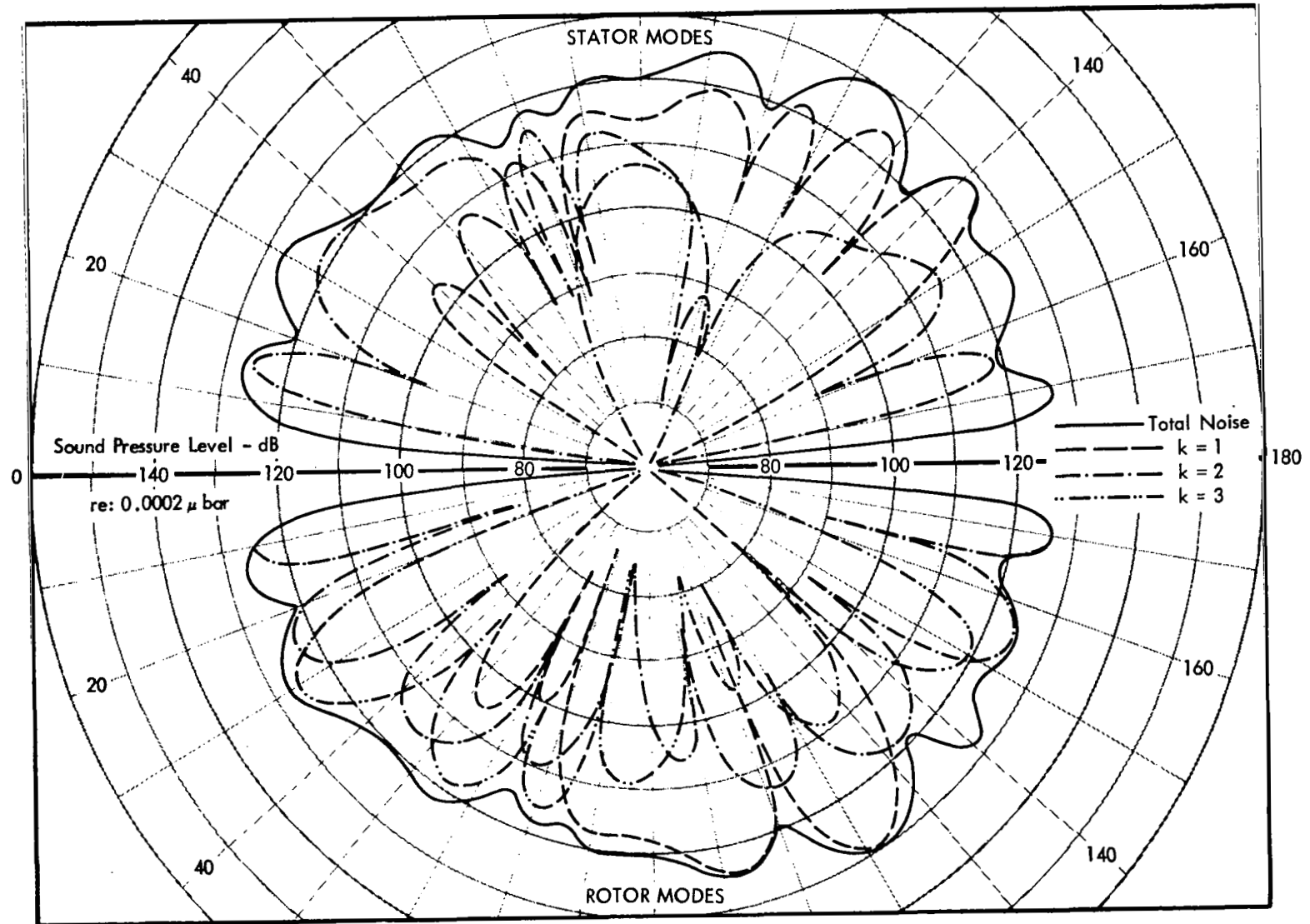
Figure 31. Parameter Study Baseline Case Second Harmonic Noise Radiation Indicating
Modal Contributions
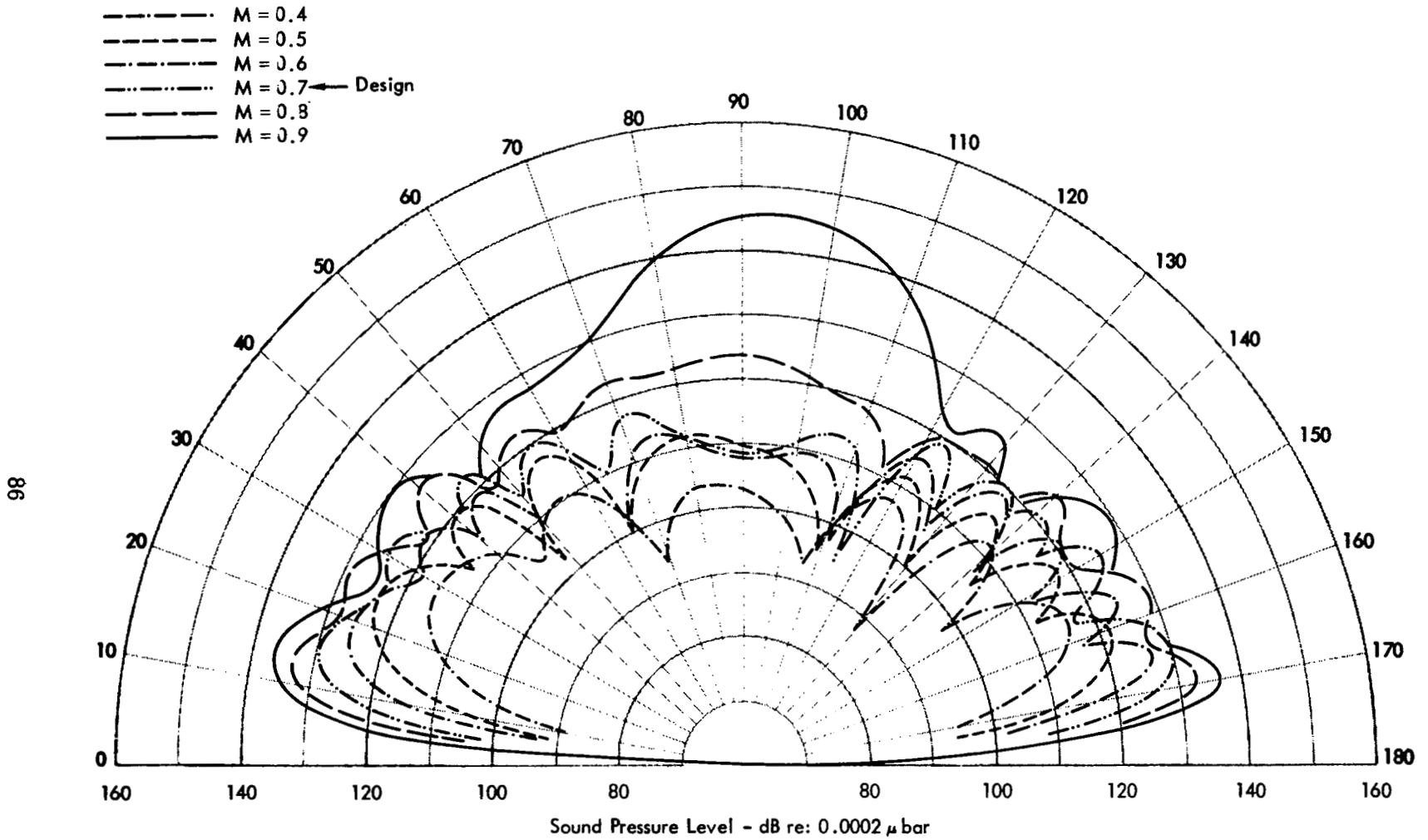
Figure 32. Variation of First Harmonic Compressor Noise with Rotor Tip Speed. Baseline
Compressor Configuration Run "Off Design".
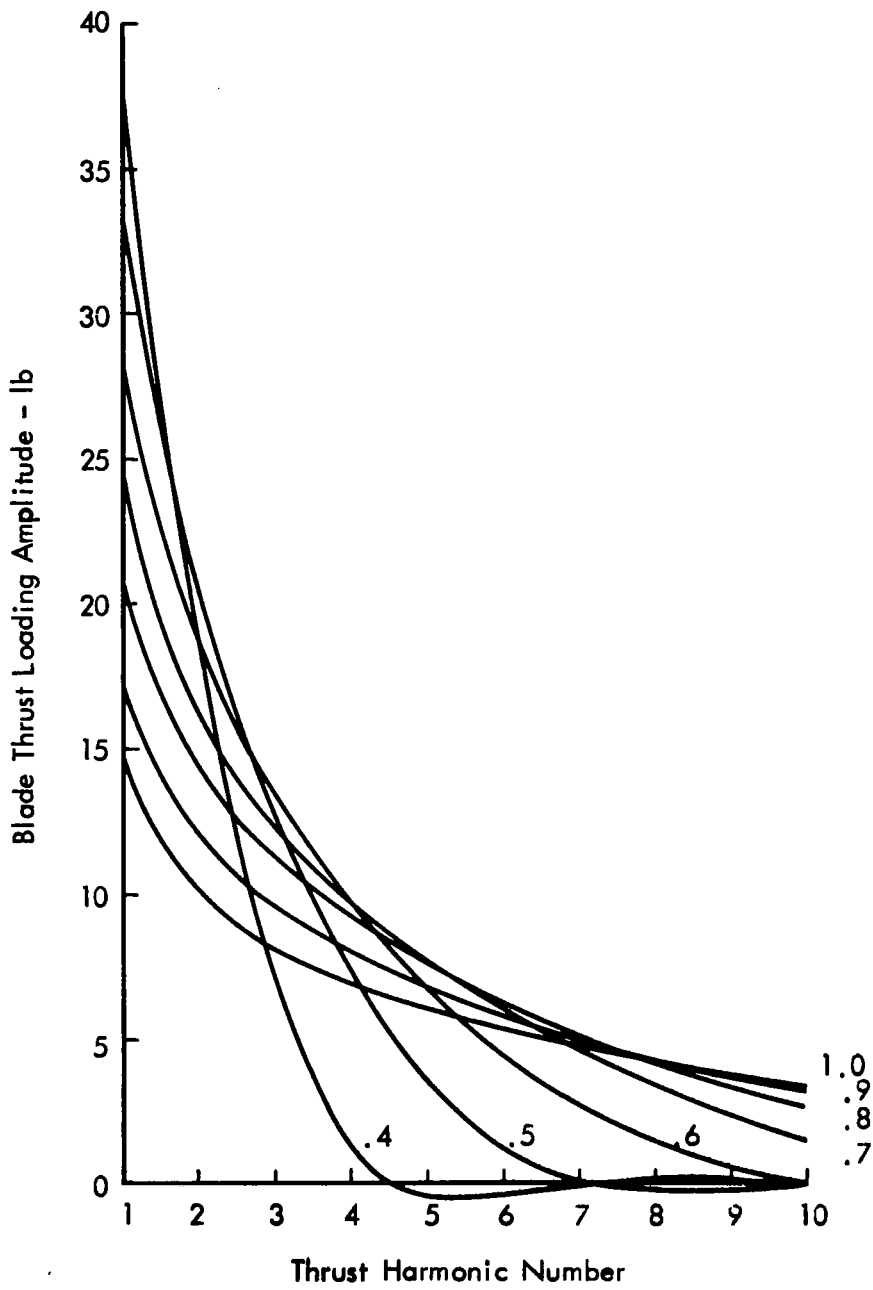
Figure 33. Effect of Rotational Mach Number on Thrust Loading Harmonics
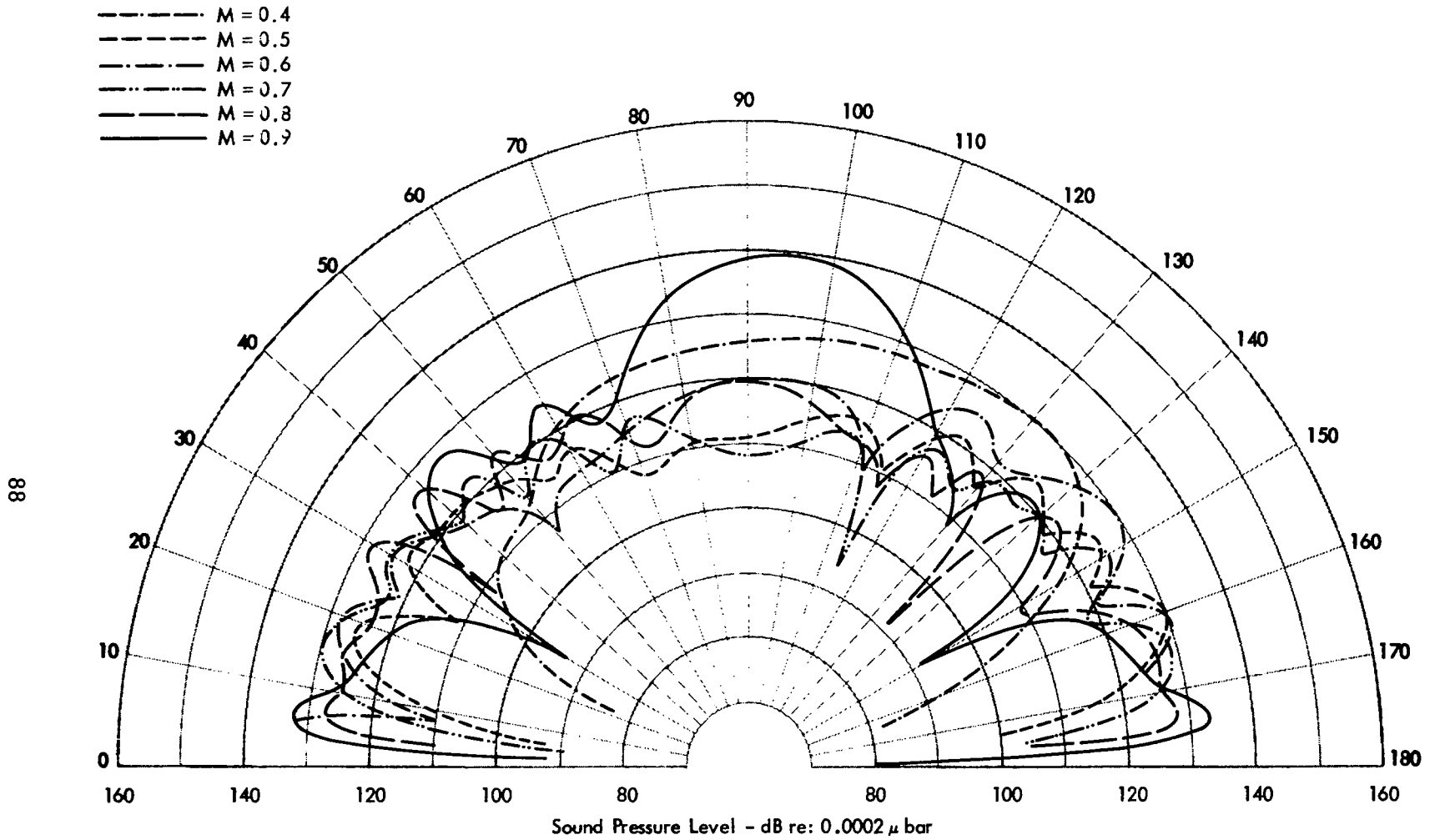
Figure 34. Effect of Tip Speed Variation on First Harmonic Compressor Noise Radiation.
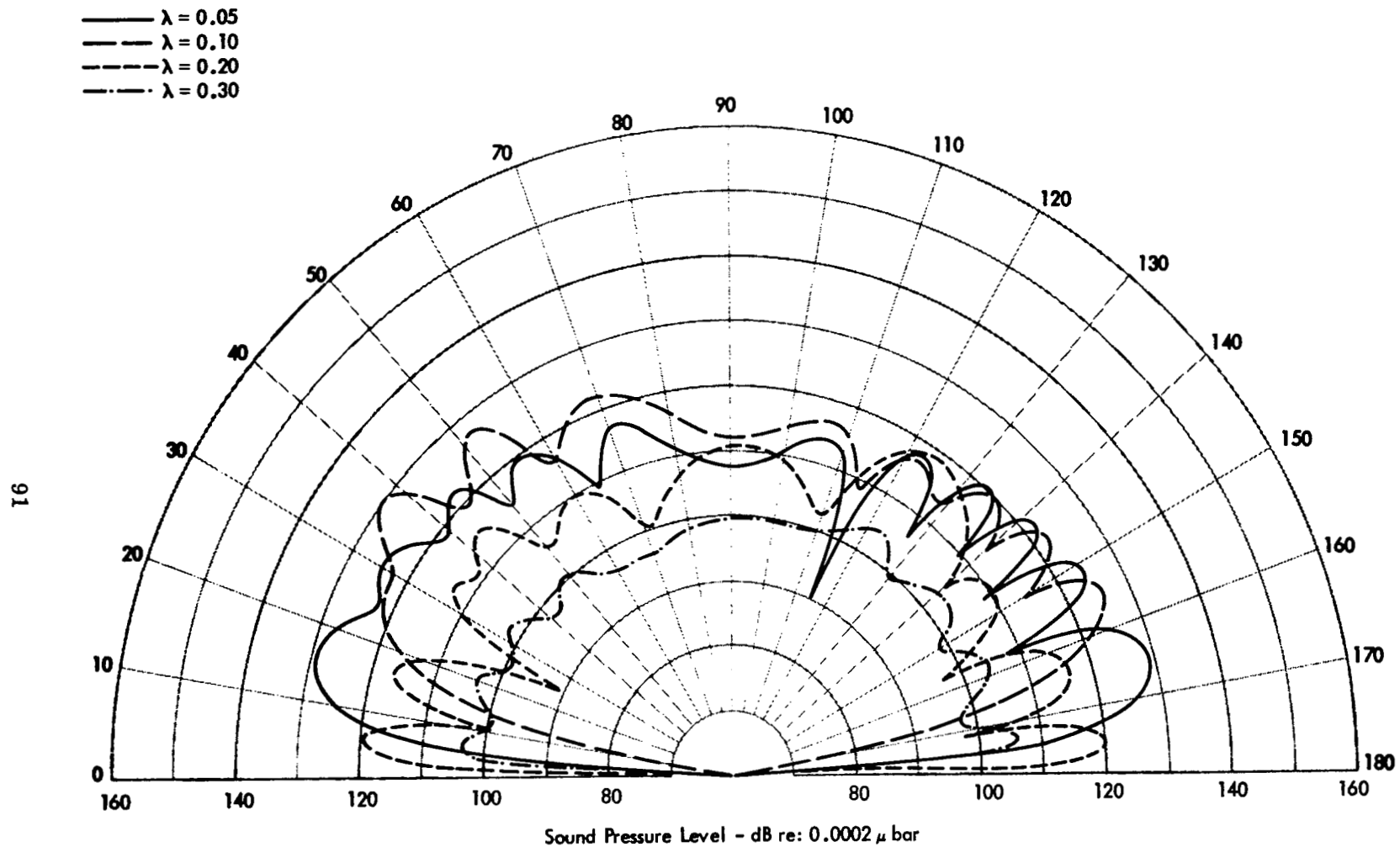Constant Performance Compressor.

88
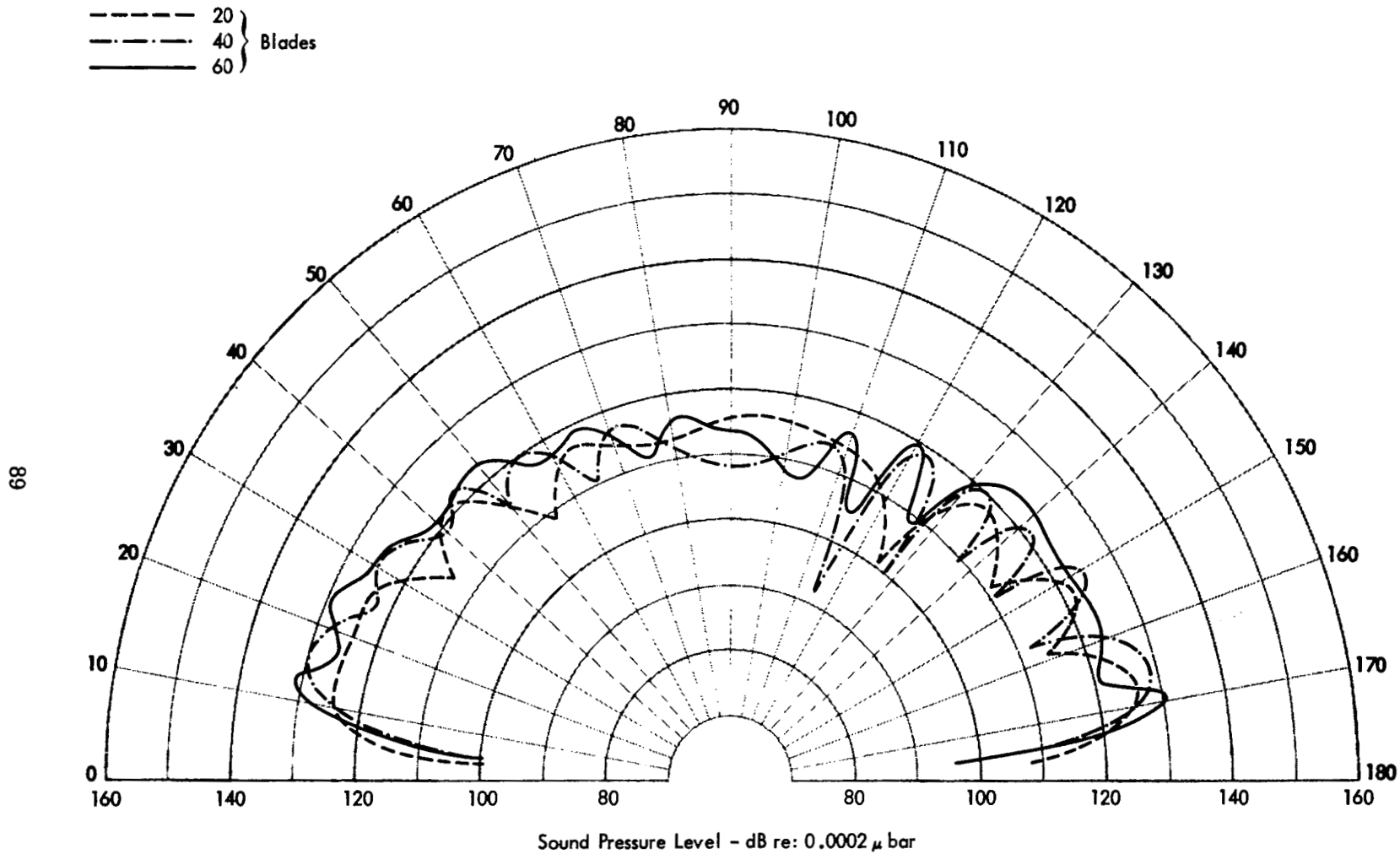
Figure 35. Variation of First Harmonic Compressor Noise with Number of Rotor Blades.
Compressor Maintained at Constant Performance.
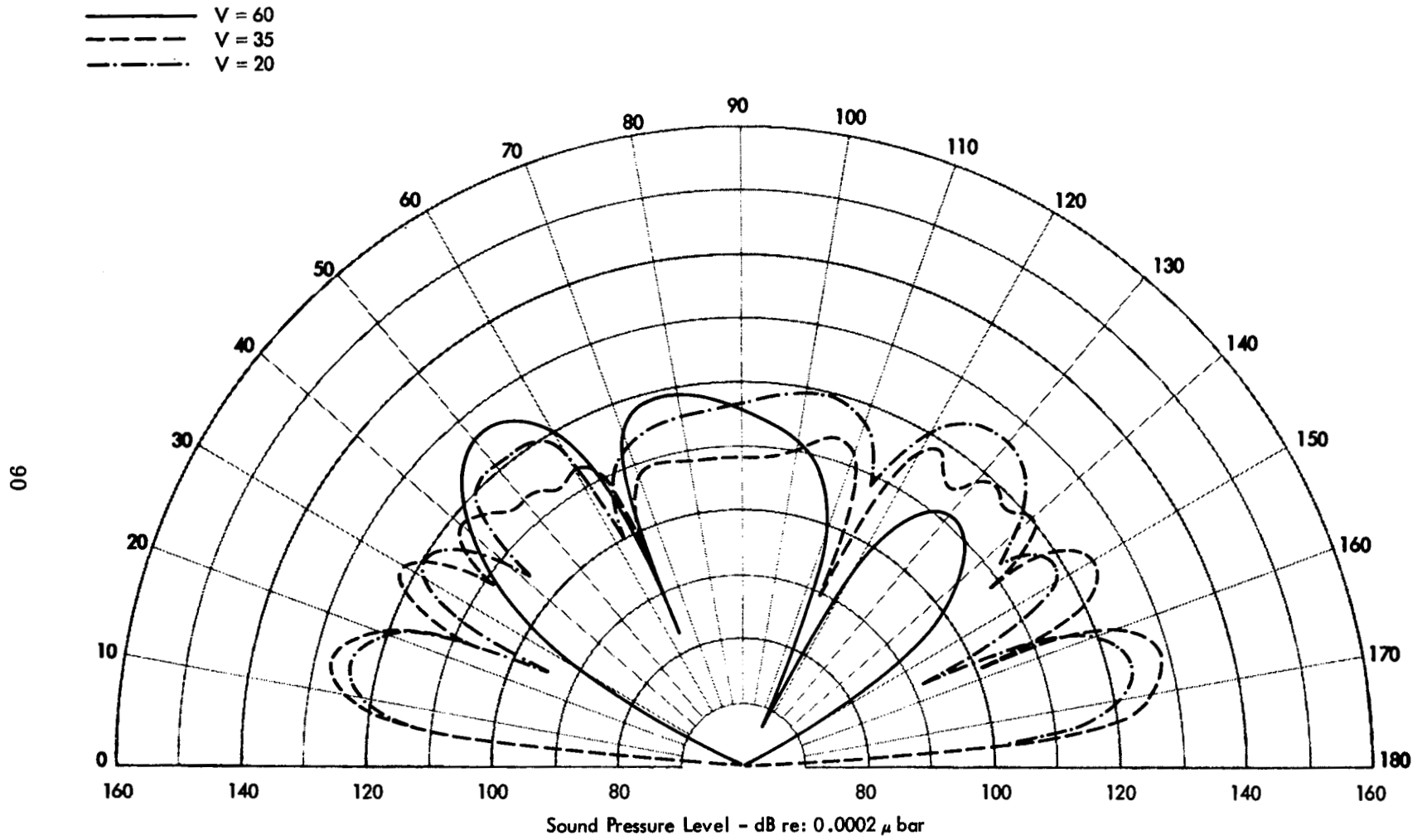
Figure 36. Variation of First Harmonic Rotor Noise with Number of Inlet Guide Vanes
(or First Harmonic Stator Noise with Number of Stator Vanes)

Figure 37. Variation of First Harmonic Compressor Noise with Inlet Swirl. Compressor Maintained at Constant Performance.
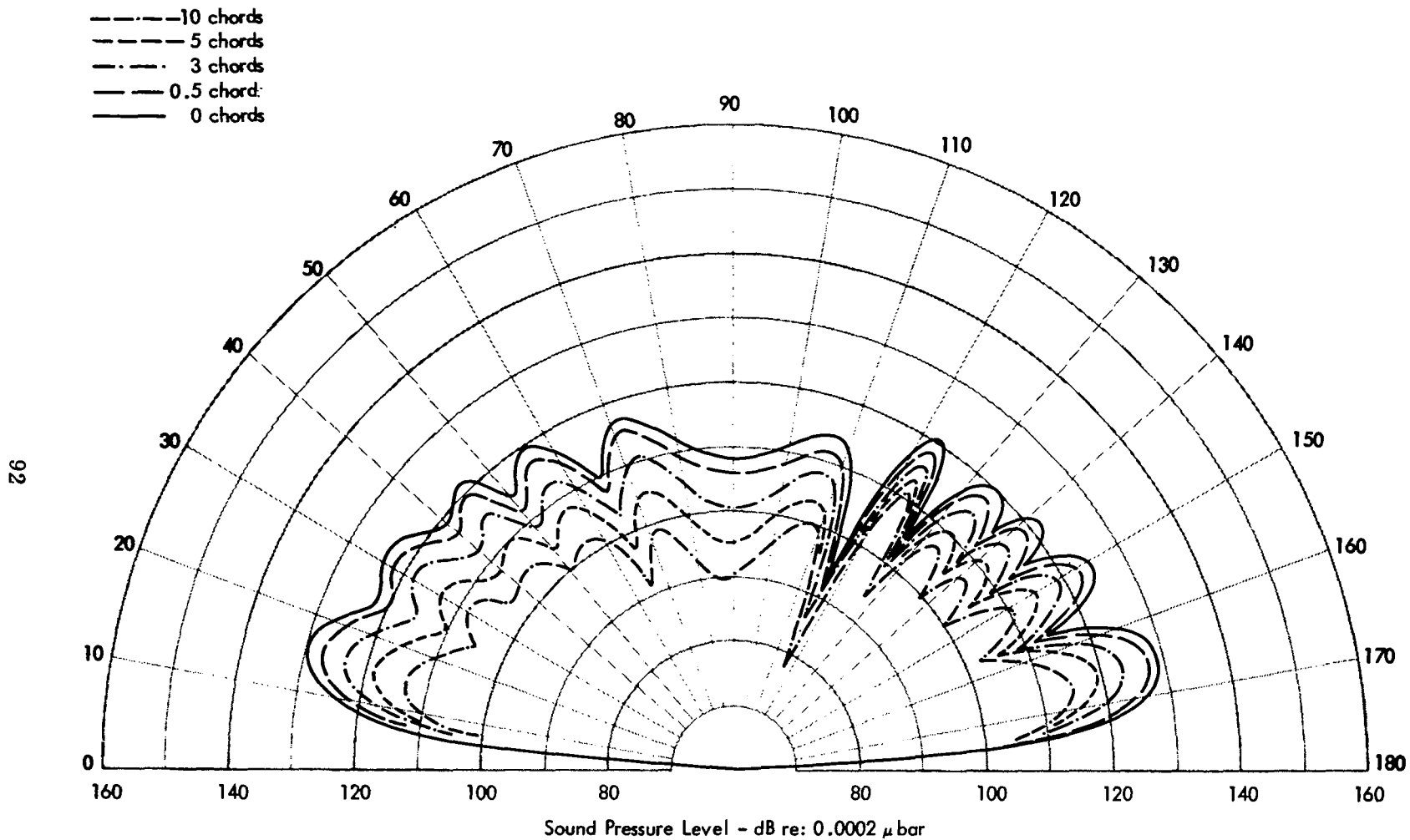
Figure 38. Variation of First Harmonic Compressor Noise with Rotor/Stator Separation.
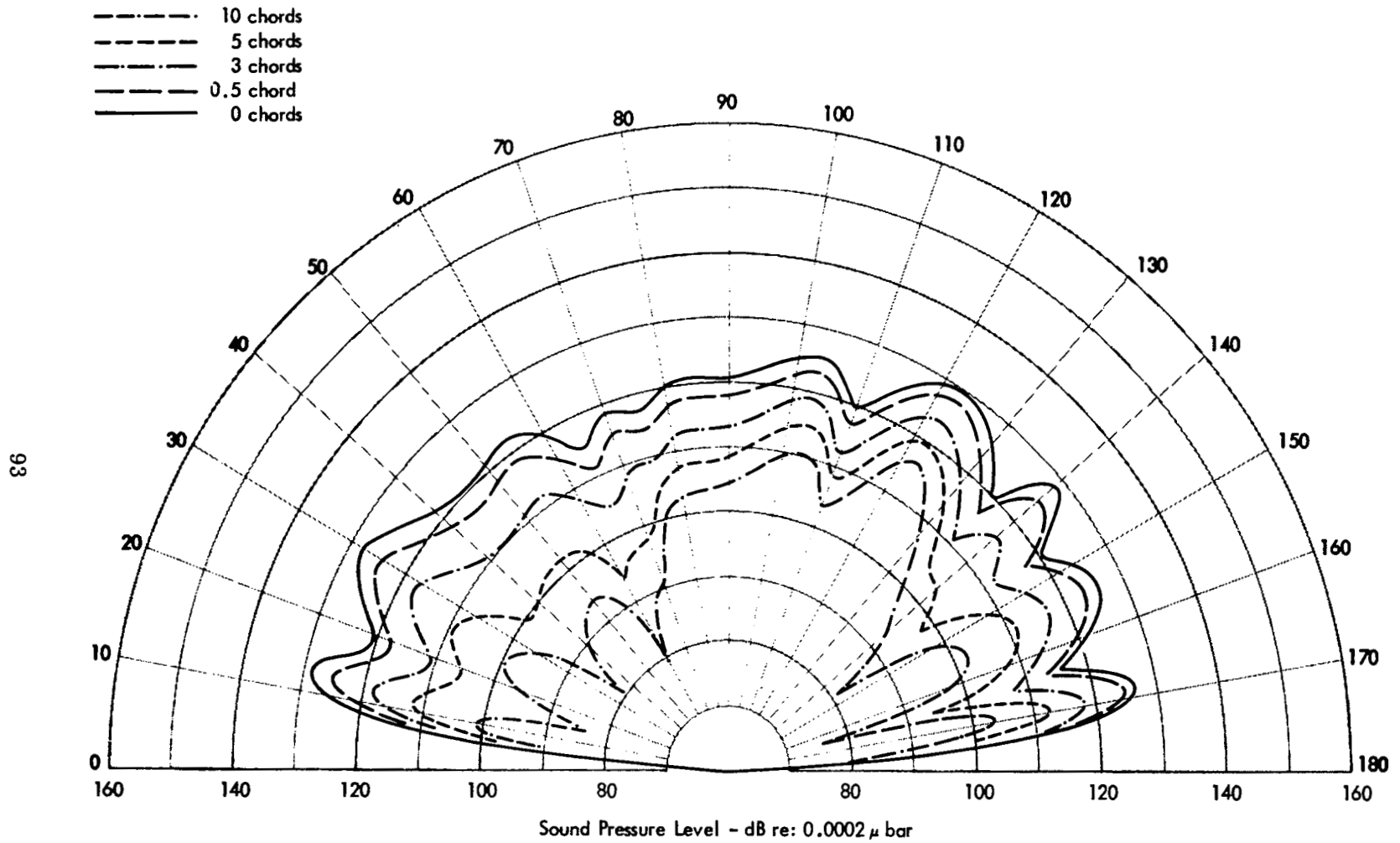Compressor Operated at Constant Performance.

Figure 39. Variation of Second Harmonic Compressor Noise with Rotor/Stator Separation.
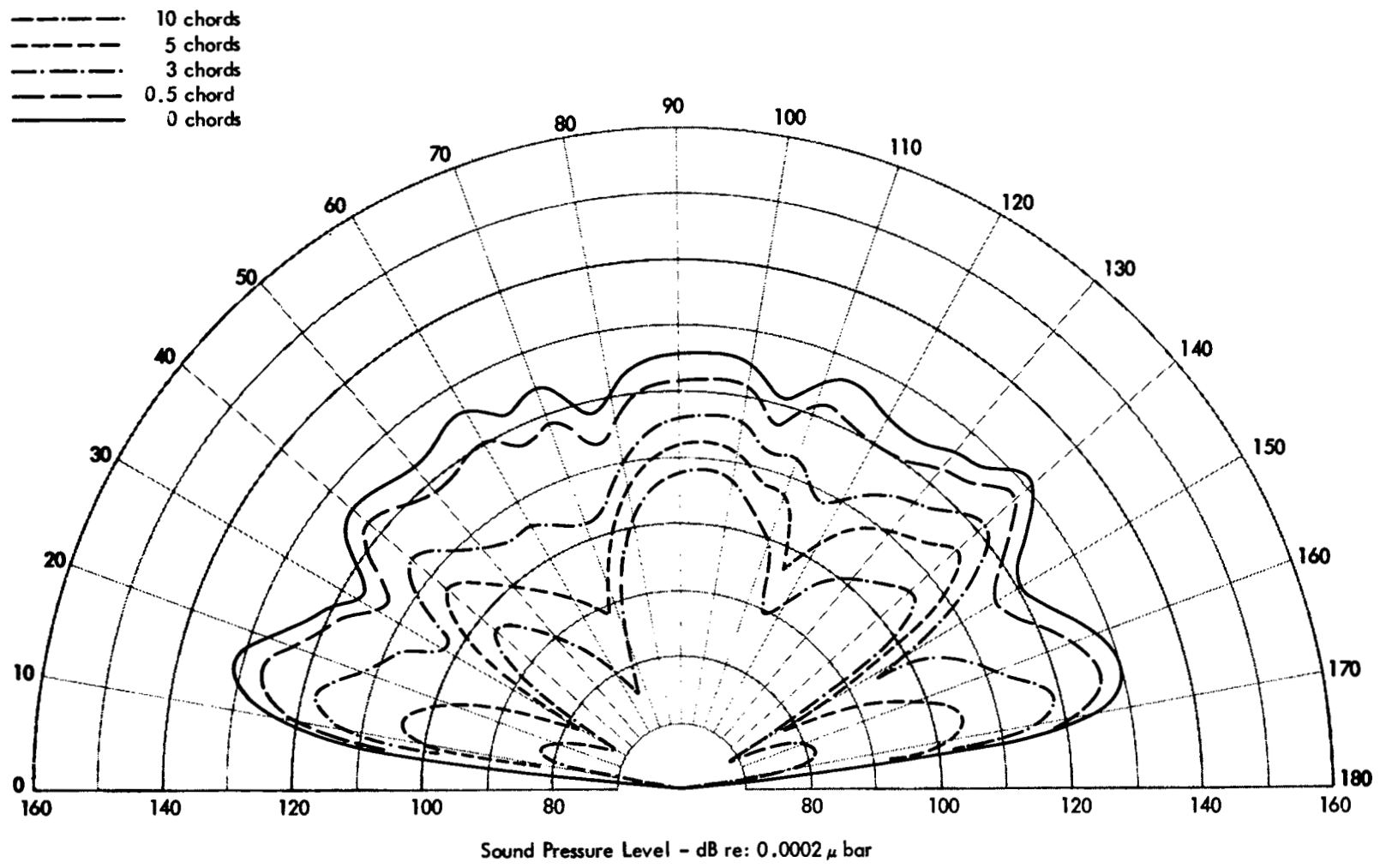Compressor Maintained at Constant Performance.

Sound Pressure Level – dB re: 0.0002 μ bar

Legend:
- — —·— — 10 chords
- — — — — 5 chords
- —·—·—· 3 chords
- — — — 0.5 chord
- ——————— 0 chords

Sound Pressure Level – dB re: 0.0002 μ bar

Figure 40. Variation of Third Harmonic Compressor Noise with Rotor/Stator Separation.
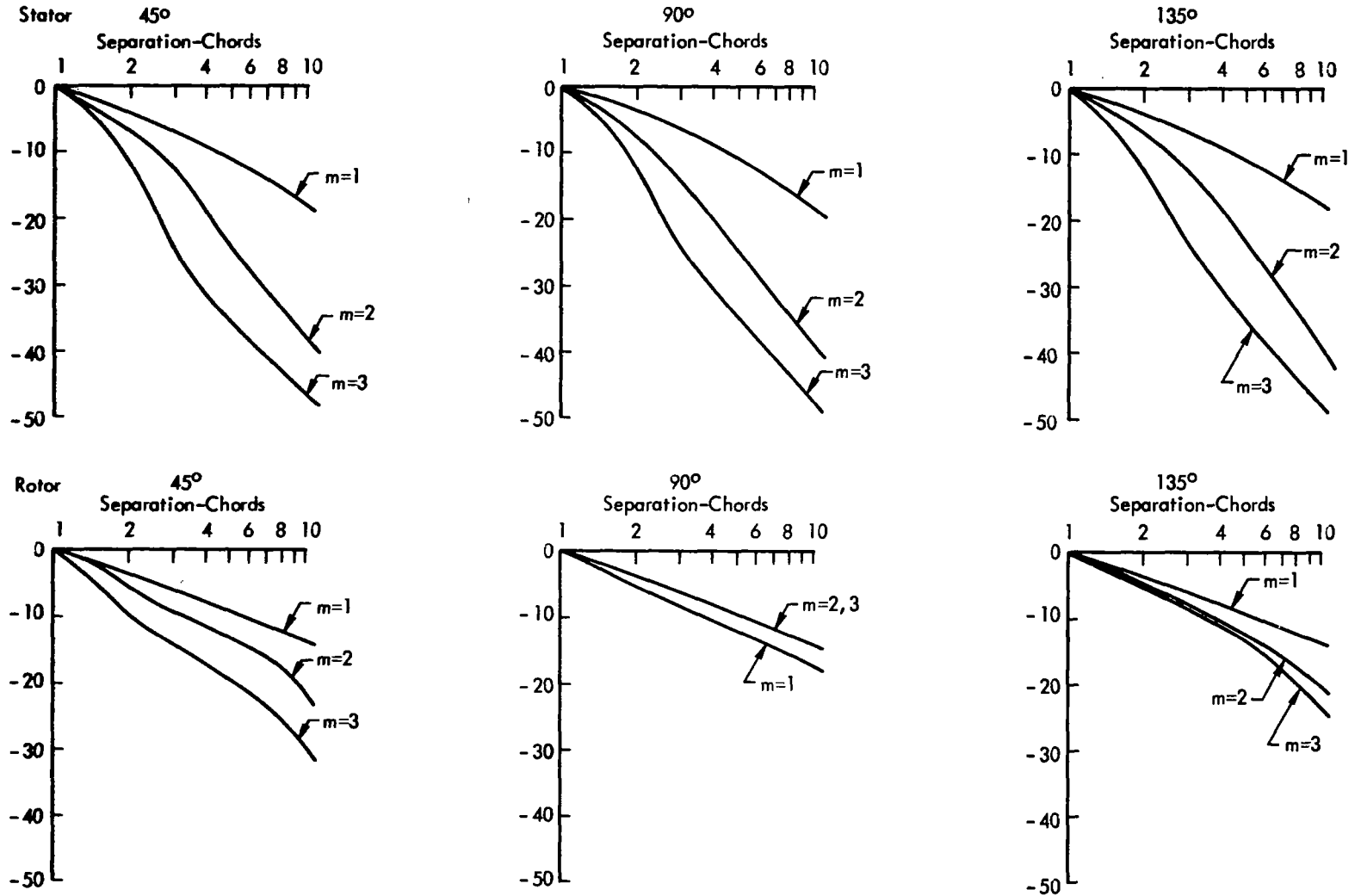Compressor Maintained at Constant Performance.

Figure 41.   Variation of First Three Harmonics of Rotor and Stator Noise with IGV/Rotor and Rotor/Stator Separation at Three Azimuth Locations. Compressor Maintained at Constant Performance.